



Terms and Conditions of Use of Digitised Theses from Trinity College Library Dublin

Copyright statement

All material supplied by Trinity College Library is protected by copyright (under the Copyright and Related Rights Act, 2000 as amended) and other relevant Intellectual Property Rights. By accessing and using a Digitised Thesis from Trinity College Library you acknowledge that all Intellectual Property Rights in any Works supplied are the sole and exclusive property of the copyright and/or other IPR holder. Specific copyright holders may not be explicitly identified. Use of materials from other sources within a thesis should not be construed as a claim over them.

A non-exclusive, non-transferable licence is hereby granted to those using or reproducing, in whole or in part, the material for valid purposes, providing the copyright owners are acknowledged using the normal conventions. Where specific permission to use material is required, this is identified and such permission must be sought from the copyright holder or agency cited.

Liability statement

By using a Digitised Thesis, I accept that Trinity College Dublin bears no legal responsibility for the accuracy, legality or comprehensiveness of materials contained within the thesis, and that Trinity College Dublin accepts no liability for indirect, consequential, or incidental, damages or losses arising from use of the thesis for whatever reason. Information located in a thesis may be subject to specific use constraints, details of which may not be explicitly described. It is the responsibility of potential and actual users to be aware of such constraints and to abide by them. By making use of material from a digitised thesis, you accept these copyright and disclaimer provisions. Where it is brought to the attention of Trinity College Library that there may be a breach of copyright or other restraint, it is the policy to withdraw or take down access to a thesis while the issue is being resolved.

Access Agreement

By using a Digitised Thesis from Trinity College Library you are bound by the following Terms & Conditions. Please read them carefully.

I have read and I understand the following statement: All material supplied via a Digitised Thesis from Trinity College Library is protected by copyright and other intellectual property rights, and duplication or sale of all or part of any of a thesis is not permitted, except that material may be duplicated by you for your research use or for educational purposes in electronic or print form providing the copyright owners are acknowledged using the normal conventions. You must obtain permission for any other use. Electronic or print copies may not be offered, whether for sale or otherwise to anyone. This copy has been supplied on the understanding that it is copyright material and that no quotation from the thesis may be published without proper acknowledgement.

**THE ADSORPTION OF SIMPLE AMINES ON
PLATINUM SURFACES**

A thesis submitted to
THE UNIVERSITY OF DUBLIN
for the degree of
DOCTOR IN PHILOSOPHY

by

ANTHONY IGOE

Department of Chemistry
University of Dublin
Trinity College
Dublin 2
Ireland.

1999

DECLARATION

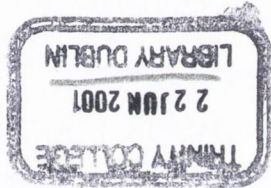
This thesis is submitted by the undersigned to the University of Dublin for examination for the degree of Doctor in Philosophy. This thesis has not been submitted for a degree in this or any other university. Except where acknowledgement is given, the work described herein is original and carried out by the author alone.

Anthony Igoe

Anthony C. Igoe

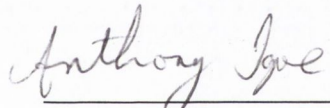


6292
THESIS



DECLARATION

I agree that the Library may lend or copy this thesis upon request.


Anthony C. Igoe

SUMMARY

ACKNOWLEDGEMENTS

This thesis presents the results of an investigation of the adsorption of methylamine, dimethylamine, trimethylamine and ethylenediamine on Pt(111) and Pt(331). The chemical composition and geometric structure of the clean crystals were characterised by Auger electron spectroscopy, low energy electron diffraction, and X-ray photoelectron spectroscopy.

Thermal desorption experiments have shown that, on heating the Pt(111) crystal, methylamine undergoes decomposition into H_2 , HCN and C_2N_2 . A small amount of methylamine decomposes completely to leave carbon and nitrogen residues on the surface. The decomposition of methylamine on Pt(331) produces the same decomposition products as are produced on Pt(111). However, HCN desorption occurs at significantly lower temperatures. On both Pt(111) and Pt(331) a high temperature C_2N_2 peak is observed consistent with previous studies on methylamine, cyanogen and hydrogen cyanide adsorption on platinum.

Dimethylamine decomposes on both Pt(111) and Pt(331) to form H_2 , HCN and CH_4 . No C_2N_2 desorption is observed, in contrast to methylamine decomposition. Methane production is in direct competition to H_2 production. The decomposition pathway involves cleavage of the C-N bond, at which point either decomposition of the methyl group occurs to give H_2 , or the methyl group picks up a hydrogen to form methane. Trimethylamine produces the same desorption products as dimethylamine on platinum and undergoes decomposition in a similar manner. The decomposition processes for both chemicals are essentially the same on both Pt(111) and Pt(331). However, HCN desorbs at lower temperatures on Pt(331) than on Pt(111), as was noted for methylamine decomposition.

Ethylenediamine decomposition on platinum is a dehydrogenation process, forming H_2 and C_2N_2 , with C-C bond cleavage to form HCN providing a competitive process. C_2N_2 desorbs at low temperatures, the result of dehydrogenation. No high temperature C_2N_2 desorption event occurs. XPS results indicate that there are no CN_{ads} species on the surface. Adsorption and decomposition of ethylenediamine on Pt(331) occurs at step sites, producing C_2N_2 at a higher temperature than on Pt(111).

ACKNOWLEDGEMENTS

I would first like to thank my supervisor Dr. M.E. Bridge for his guidance over the years. I would also like to thank Prof. D.R. Lloyd for taking an interest in the work and for his useful suggestions and help. I am particularly grateful to Dr. Tom McCabe, whose help, guidance and friendship over the years has been invaluable.

I would like to thank all of the technical staff for their help.

Thank you to Mario for his help on the methylamine work and Jenny for her help on dimethylamine. Thanks to Dorothy for providing the trimethylamine.

To all my friends, both in college and outside, for their continued friendship and support. To Lionel, Janice, Marika, Keelin, Fiona, Conor, Elise, Evelyn, Damien, Richard, Una, Guillaume, Cecile, Gillian, Phil, Brendan, Andreas, Eileen, Christophe, Mo, José, Dan and Denise. A special thanks to Anne for helping me print my thesis.

I would especially like to thank Demetri, who has been a great friend and colleague.

To my friends outside college, Stephen, Pat, Neil, Dave, Tadhg, Hilda, Bren, Ita, Ronan, John and Aideen, Peter and Linda, Fin and Marge, Dermot and Toni, Padraic, Finbar Murphy and Tim Golden.

Thanks to Lily O'Brien for treating me like a member of the family.

I would also like to thank Prof. J. Kelly and the Kriebel fund for the financial assistance they provided during the last year.

Finally, I would like to thank my parents and sisters, Selena and Katherine, for their love and support.

ABBREVIATIONS

AES	Auger Electron Spectroscopy
ARUPS	Angle-resolved Ultraviolet Photoelectron Spectroscopy
DMA	Dimethylamine
EDA	Ethylenediamine
EELS	Electron Energy Loss Spectroscopy
ESCA	Electron Spectroscopy for Chemical Analysis
FEC	Fast Entry Chamber
HREELS	High Resolution Electron Energy Loss Spectroscopy
L	Langmuir
LEED	Low Energy Electron Diffraction
NEXAFS	Near - Edge X-ray Absorption Fine Structure
RAIRS	Reflection-absorption Infra-red Spectroscopy
SAC	Sample Analysis Chamber
SPC	Sample Preparation Chamber
TDS	Thermal Desorption Spectroscopy
TMA	Trimethylamine
TPD	Temperature Programmed Desorption
UHV	Ultra High Vacuum
UPS	Ultra-violet Photoelectron Spectroscopy
VG	Vacuum Generators
VSU	Vacuum Science Workshop
XPS	X-ray Photoelectron Spectroscopy

CONTENTS

Declaration.....	i
Summary.....	ii
Acknowledgements.....	iii
Abbreviations.....	iv
Contents.....	v

CHAPTER 1 INTRODUCTION 1

1.1 GENERAL INTRODUCTION.....	2
1.2 LOW ENERGY ELECTRON DIFFRACTION.....	5
1.3 AUGER ELECTRON SPECTROSCOPY.....	10
1.4 THERMAL DESORPTION SPECTROSCOPY.....	12
1.5 X-RAY PHOTOELECTRON SPECTROSCOPY.....	15

CHAPTER 2 EXPERIMENTAL TECHNIQUES 18

2.1 THE EXPERIMENTAL SYSTEMS.....	19
2.1.1 The LEED/Auger System.....	19
2.1.2 The ESCA System.....	22
2.2 EXPERIMENTAL TECHNIQUES.....	24
2.2.1 Low Energy Electron Diffraction.....	24
2.2.2 Auger Electron Spectroscopy.....	26
2.2.3 Thermal Desorption Spectroscopy.....	27
2.2.4 X-ray Photoelectron Spectroscopy.....	29
2.3 CRYSTAL PREPARATION.....	31
2.3.1 The Platinum Crystals.....	31
2.3.2 Crystal Mounting.....	31
2.3.3 Crystal Cleaning and Characterization in Vacuo.....	34
2.4 THE ADSORBATES.....	38

CHAPTER 3 METHYLAMINE ON Pt(111) AND Pt(331) 41

3.1	RESULTS.....	42
3.1.1	Methylamine on Pt(111).....	42
3.1.2	Methylamine on Pt(331).....	49
3.2	DISCUSSION.....	55
3.2.1	HCN desorption.....	55
3.2.2	C ₂ N ₂ desorption.....	61
3.2.3	H ₂ desorption.....	63
3.2.4	28 amu desorption.....	64
3.2.5	Minor Products.....	64
3.2.6	XPS Experiments.....	64
3.3	CONCLUSIONS.....	65

**CHAPTER 4 DIMETHYLAMINE AND TRIMETHYLAMINE
ON Pt(111) AND Pt(331)** 68

4.1	RESULTS.....	69
4.1.1	Dimethylamine on Pt(111).....	69
4.1.2	Dimethylamine on Pt(331).....	75
4.1.3	Trimethylamine on Pt(111).....	81
4.1.4	Trimethylamine on Pt(331).....	87
4.2	DISCUSSION.....	93
4.2.1	Trimethylamine on platinum.....	93
4.2.1.1	H ₂ desorption.....	93
4.2.1.2	HCN desorption.....	96
4.2.1.3	CH ₄ desorption.....	96
4.2.1.4	28 amu desorption.....	97
4.2.1.5	XPS experiments.....	97
4.2.2	Dimethylamine on platinum.....	98
4.3	CONCLUSIONS.....	100
4.3.1	Dimethylamine on platinum.....	100
4.3.2	Trimethylamine on platinum.....	101

<u>CHAPTER 5</u>	<u>ETHYLENEDIAMINE ON Pt(111) AND Pt(331)</u>	103
5.1	RESULTS.....	104
5.1.1	Ethylenediamine on Pt(111).....	104
5.1.2	Ethylenediamine on Pt(331).....	111
5.2	DISCUSSION.....	118
5.2.1	C ₂ N ₂ desorption.....	118
5.2.2	H ₂ desorption.....	119
5.2.3	HCN desorption.....	120
5.2.4	XPS experiments.....	121
5.3	CONCLUSIONS.....	123
<u>CHAPTER 6</u>	<u>CONCLUSIONS AND FURTHER WORK</u>	124
6.1	METHYLAMINE ON Pt(111) AND Pt(331).....	125
6.2	DIMETHYLAMINE AND TRIMETHYLAMINE ON Pt(111) AND Pt(331)	125
6.3	ETHYLENEDIAMINE ON Pt(111) AND Pt(331).....	126
<u>REFERENCES</u>		127
<u>BIBLIOGRAPHY</u>		133

CHAPTER ONE

INTRODUCTION

CHAPTER 1 INTRODUCTION

1.1 GENERAL INTRODUCTION

In order to develop a clear understanding of the fundamental processes involved in catalysis and corrosion it is necessary to study the chemical composition and atomic arrangement of solid surfaces and to investigate the mechanisms of adsorption and reaction on these surfaces. In the case of catalysis, for example, more active and selective catalysts may be designed once a detailed knowledge of the interaction of the reacting species with the surface of the metal catalyst can be ascertained.

The development of ultra-high vacuum technology made possible the preparation and maintenance of clean surfaces on a time scale sufficient to carry out surface characterisation and surface-adsorbate interaction experiments. The adaptation of Auger electron spectroscopy [1-4] and X-ray photoelectron spectroscopy [5] to surface studies in the late 1960's provided a reliable means of determining the surface composition of clean and adsorbate-covered surfaces. Over the intervening years numerous techniques have been developed or adapted to probe the geometry and electronic structure of surface systems, including low energy electron diffraction [6-9], ultraviolet photoelectron spectroscopy [5, 10, 11], high resolution electron energy loss spectroscopy [12], reflection absorption infrared spectroscopy [13-15], molecular beam studies [16, 17], secondary ion mass spectrometry [18], photoelectron diffraction [19] and normal incidence X-ray standing waves [20]. Thermal desorption spectroscopy [21-23], or temperature programmed desorption as it is also known, provides information on the number and nature of adsorbed species as well as on the thermal stability of the species and the kinetics of their evolution.

Surface chemistry experiments are generally performed on single crystal surfaces, usually of low Miller indices, in order to minimise surface heterogeneity and allow the effect of a limited number of adsorbate binding sites to be determined.

The surface chemistry of platinum has been the subject of extensive research, due to its catalytic activity [24]. It is one of the most versatile heterogeneous catalysts, used for hydrocarbon conversion reactions and for hydrogenation in the chemical and petroleum-

refining industries [25, 26], as well as in the oxidation of ammonia during fertiliser production, and CO and unburned hydrocarbons in the control of car emissions [27, 28]. Pt(111) is one of the most studied crystal surfaces. It is an atomically flat, face-centred cubic surface in which each atom is surrounded by six near neighbours. Its lack of steps and kinks gives it minimum heterogeneity and is therefore ideal as a starting point in surface chemistry studies. Few investigations have been made of the (331) orientated surface [29-31]. The (331) surface consists of three atom wide (111) terraces with one-atom high (111) steps. As such the (331) provides the opportunity to examine the effect of introducing a systematic 'defect' to the (111) plane. It is well established that steps, kinks and defects play an important part in surface reactions [32-37]. The change in the electronic density at step sites results in different adsorption sites, different lateral interactions between adsorbed species and different reaction probabilities. Adsorbed atoms and molecules generally have higher heats of adsorption at defect sites [38].

In this work the thermal decomposition of simple organic amines - methylamine, dimethylamine, trimethylamine and ethylenediamine - on Pt(111) and Pt(331) is studied. Organic amines are known for their poisoning effect in catalysis and are used to control the selectivity in hydrogenation reactions [39].

The adsorption and decomposition of ethylenediamine on Pt(111) have been investigated using thermal desorption spectroscopy, X-ray photoelectron spectroscopy and high resolution electron energy loss spectroscopy [40-42]. Kingsley *et al.* proposed that ethylenediamine undergoes dehydrogenation of the amine groups to form an ethylenedinitrene surface species at or above the adsorption temperature of 285K. This is followed by sequential removal of hydrogens from the methyl groups at higher temperatures to produce a mixture of partially hydrogenated species on the surface, resulting in the desorption of cyanogen and hydrogen at 430K followed by hydrogen cyanide. An alternative model was proposed by Lloyd and Hemminger [41] following HREELS investigations and Lindquist *et al.* [42] from XPS studies. They suggested that a di-imine rather than a dinitrene species is formed between 273K and 373K.

Methylamine has been the subject of a number of investigations on platinum [43-46]. The main desorption products noted have been H₂, HCN and C₂N₂. There is general agreement that methylamine thermal decomposition occurs through a pathway of

dehydrogenation and that the N-C bond is not broken. Discussion now centres on the nature of the intermediate or intermediates formed during the decomposition process.

Few investigations have been carried out on di- and trimethylamine adsorption on single crystal surfaces. Pearlstine and Friend [47] examined trimethylamine adsorption on clean, carbide and oxide covered W(100). The main desorption products from these surfaces were trimethylamine, methane, hydrogen and nitrogen. Nunney *et al.* [48] found that trimethylamine adsorbs molecularly through the nitrogen lone pair on Ni(111) at 110K. Erley *et al.* [49] found that it decomposes completely into atomic species on Pt(111).

Work carried out by Walker and Stair [50, 51] on Mo(100) resulted in the formation of HCN and CO (on oxidised Mo(100) surfaces only) as well as methane, hydrogen and nitrogen. No molecular trimethylamine was detected as a desorption product from molybdenum. They concluded from their research that trimethylamine undergoes complete dissociation into atomic surface species upon adsorption at low coverages at 333K. These products 'partially passivate' the surface allowing molecular adsorption of trimethylamine at higher coverages which decomposes to form HCN and CH₄ desorption products.

The techniques used in this work were Auger electron spectroscopy, low energy electron diffraction, X-ray photoelectron spectroscopy and thermal desorption spectroscopy. The remainder of this chapter is devoted to a brief description of the theory behind each of these techniques. Their application is described in chapter 2.

1.2 LOW ENERGY ELECTRON DIFFRACTION

In the LEED experiment, a beam of energetically well-defined electrons is directed onto the crystal surface, and the angular distribution of elastically back-scattered electrons is monitored to yield information on the periodicity of the surface.

The theory of low energy electron diffraction has been discussed and reviewed in detail [6-8, 52]. Only a brief description of LEED and the information attainable from it will be given here.

An incident beam of electrons of energy between 10 and 200eV produces electron wavelengths of 3.9 to 0.93Å, given by:

$$\lambda = \sqrt{(150.4/E)} \quad (1.2.1)$$

where λ , the wavelength, is in Å and E, the energy, is in eV. The possibility of diffraction arises at these electron energies because the corresponding wavelengths are similar to the interatomic distances in the crystal lattice. The electrons have a high elastic back-scattering cross-section resulting in a high probability of being back-scattered before penetrating any great distance into the bulk.

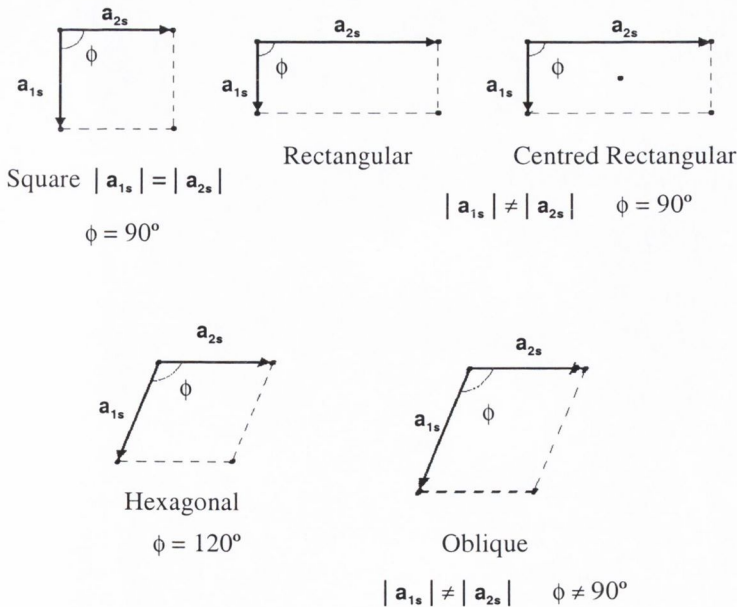


Fig. 1.1 Unit meshes of the five possible surface nets.

The periodic two-dimensional arrangements of atoms at the surface can be grouped into five types of surface nets, which describe all possible diperiodic surface structures. The unit areas or unit meshes of these five possible nets are shown in figure 1.1.

The periodicity of the surface is described by the two vectors a_1 and a_2 . In reciprocal space, the corresponding vectors are a_1^* and a_2^* , defined by:

$$a_i^* \cdot a_j = 2\pi\delta_{ij} \quad (1.2.2)$$

where δ_{ij} is the Kronecker delta ($\delta_{ij} = 1$ for $i = j$; $\delta_{ij} = 0$ for $i \neq j$). The 2π in the equation replaces the value of unity conventionally used in X-ray diffraction, allowing the wave vectors \mathbf{k} to be drawn on the reciprocal crystal lattice diagram. The energy E of the incident electron is given by:

$$E = (\hbar^2/2m) \cdot k^2 \quad (1.2.3)$$

where $\hbar = h/2\pi$ (h is Planck's constant) and m is the mass of the electron. The wave vector is related to the wavelength of the electron by:

$$\mathbf{k} = 2\pi/\lambda \quad (1.2.4)$$

Diffraction occurs when the conservation of energy and momentum selection rules are satisfied. These rules are given by:

$$|\mathbf{k}'| = |\mathbf{k}_0| \quad (1.2.5)$$

$$\mathbf{k}'_{||} = \mathbf{k}_{0||} + \mathbf{g}_{hk} \quad (1.2.6)$$

where \mathbf{k}' and \mathbf{k}_0 are the wave vectors of the diffracted and primary electrons respectively. Since there is a loss of periodicity in one dimension, only the component of the momentum parallel to the surface is conserved, hence the $||$ subscript. \mathbf{g}_{hk} is a general reciprocal lattice vector, which lies in the plane of the surface, and is given by

$$\mathbf{g}_{hk} = h \cdot a_1^* + k \cdot a_2^* \quad (1.2.7)$$

where h and k are integers.

It is possible to derive the symmetry and dimensions of the clean surface unit mesh and also the symmetry and dimensions of ordered adlayers relative to the clean surface from a

knowledge of the direction of the diffracted beams and the primary beam energy. The relationship between the surface unit mesh and that of a monolayer of some adsorbed species can be described by using a transformation matrix \mathbf{M} :

$$\mathbf{M} = \begin{bmatrix} m_{11} & m_{12} \\ m_{21} & m_{22} \end{bmatrix} \quad (1.2.8)$$

such that:

$$\mathbf{a}_{1s} = m_{11}\mathbf{a}_{1b} + m_{12}\mathbf{a}_{2b} \quad (1.2.9)$$

$$\mathbf{a}_{2s} = m_{21}\mathbf{a}_{1b} + m_{22}\mathbf{a}_{2b} \quad (1.2.10)$$

or, in matrix notation:

$$\mathbf{a}_s = \mathbf{M}\mathbf{a}_b \quad (1.2.11)$$

where \mathbf{a}_s represents the translation vectors of the adsorbed layer unit mesh, and \mathbf{a}_b represents those of the substrate unit mesh. The areas of the two unit meshes are given by:

$$A = | \mathbf{a}_{1s} \times \mathbf{a}_{2s} | \quad (1.2.12)$$

$$B = | \mathbf{a}_{1b} \times \mathbf{a}_{2b} | \quad (1.2.13)$$

It can be shown that:

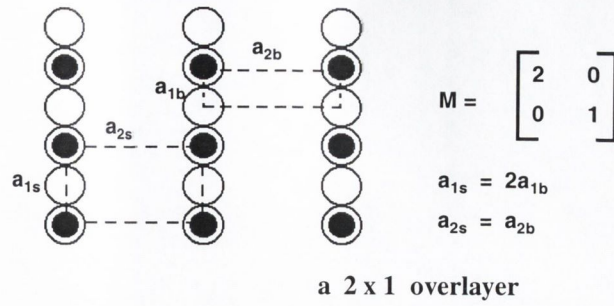
$$A = B\det\mathbf{M} \quad (1.2.14)$$

The type of superposition of adlayer upon substrate can be defined by reference to the values of $\det\mathbf{M}$:

- (a) if $\det\mathbf{M}$ is an integer, the structure is referred to as a simple lattice;
- (b) if $\det\mathbf{M}$ is a rational fraction, the structure is a coincidence lattice;
- (c) if $\det\mathbf{M}$ is an irrational fraction, the structure is incoherent.

(a) and (b) are illustrated in figure 1.2.

(a) SIMPLE $\det M \mid$ integer



(b) COINCIDENCE $\det M$ a rational fraction

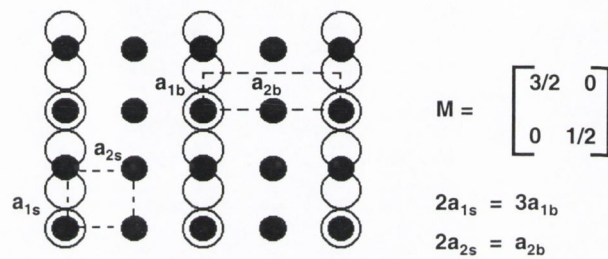


Fig. 1.2 Relationship between surface and bulk meshes. The simple and coincidence meshes are illustrated by the cases of deposit atoms (filled circles) on the bulk exposed (110) plane of an f.c.c. material (open circles).

A simple notation has been proposed by Wood [53] where the relationship between the unit meshes is described by the ratio of the lengths of the translation vectors and by a rotation R expressed in degrees. This notation is illustrated in figure 1.3. Unfortunately, Wood's notation is inadequate in describing certain surface structures, for example incoherent structures. However, its simplicity and suitability for very many structures means that it is widely and frequently used.

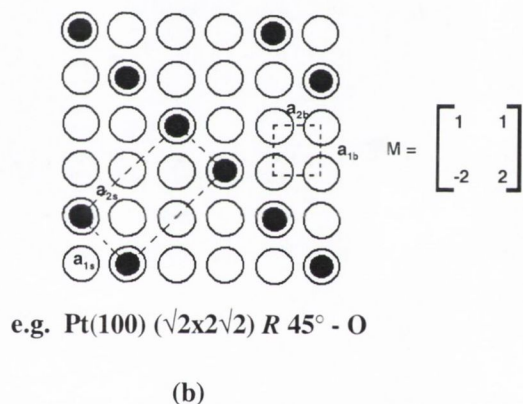
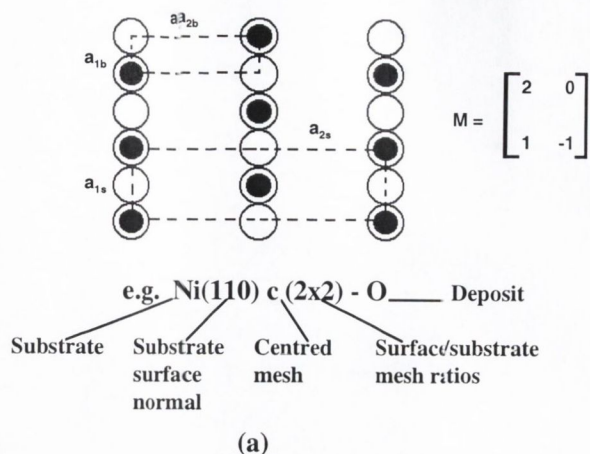


Fig. 1.3 Two notional examples of Wood's notation for structures compared with the matrix notation. In example (a) for a Ni(110) face exposed to oxygen, the notation can be shortened to Ni(110)c2-O because the deposit mesh is rectangular.

In this work, LEED has been used for the determination of surface and overlayer symmetries and dimensions as described above.

1.3 AUGER ELECTRON SPECTROSCOPY

Auger electron spectroscopy involves analysis of the energy of the secondary electrons emitted by the Auger process [1] from a surface.

Irradiation of the surface with a 2-3keV electron beam or X-ray photons in a similar energy range results in the ionization of an atomic core level (E_1). This then relaxes by an electronic transition such as E_2 to E_1 . The energy released by this deexcitation process is transferred by a radiationless mechanism to a third electron in E_3 which is emitted from the atom (see figure 1.4). This emitted electron is the Auger electron and has a characteristic kinetic energy E_k given by:

$$E_k = E_1 - E_2' - E_3' \quad (1.3.1)$$

where E_2' ($\sim E_2$) and E_3' ($\sim E_3$) take account of the shifts in energy of these levels due to ionization of the atom. Therefore, the kinetic energy imparted to the electron is independent of the primary radiation. The ionization cross-section of the core level, however, is dependent on the energy of the primary radiation (E_p), rising from 0 for $E_p < E_1$ to a maximum for $E_p/E_1 \sim 3$, followed by a slow decrease at higher values, but with little variation in the range $2 < E_p/E_1 < 6$ [54].

Although the primary electron can penetrate deep into the bulk of the specimen and produce secondary electrons within the bulk (due to an inelastic mean free path of $\sim 200\text{\AA}$, for a typical beam energy of 2 - 5keV), the short escape depth (4 - 10 \AA) for secondary electrons means that only those electrons at or near the surface escape without scattering and are detected. Furthermore, by decreasing the angle of incidence of the primary electron beam to near grazing incidence, a greater number of surface atoms are sampled, thus increasing the surface sensitivity. Experimentally, the optimum angle lies between 10 and 15° from grazing incidence.

Electronic differentiation of the signal from the retarding field analyser during AES analysis yields the secondary electron distribution ($N(E)$) curve. Auger electrons are observed as weak perturbations on this total secondary electron distribution; however,

further differentiation of the $N(E)$ curve to give $dN(E)/dE$ results in greater sensitivity and resolution, such that the lower limit of the detection is in the range of 1 - 5% of a monolayer.

It is important to note that de-excitation of the ionized atom can also result in X-ray emission, a competitive relaxation process to Auger emission (again, see figure 1.4). Following the ionization of a K-shell, for atomic numbers (Z) < 19 more than 90% of the relaxation is by Auger emission; at $Z = 32$ (Ge) there is an equal probability of relaxation via these two competing processes; and for $Z > 33$ X-ray emission becomes the dominant process [55]. Thus, the Auger yield is maximised for the first and second row elements, making AES most useful for the study of these elements adsorbed on surfaces.

Auger electron spectroscopy is used primarily as a means of monitoring the chemical composition at the surface. However, it may also be used to measure relative coverages, diffusion coefficients [56], rates of adsorption [57] and desorption [58], and depth profiles [59], as well as a monitor in NEXAFS experiments [60].

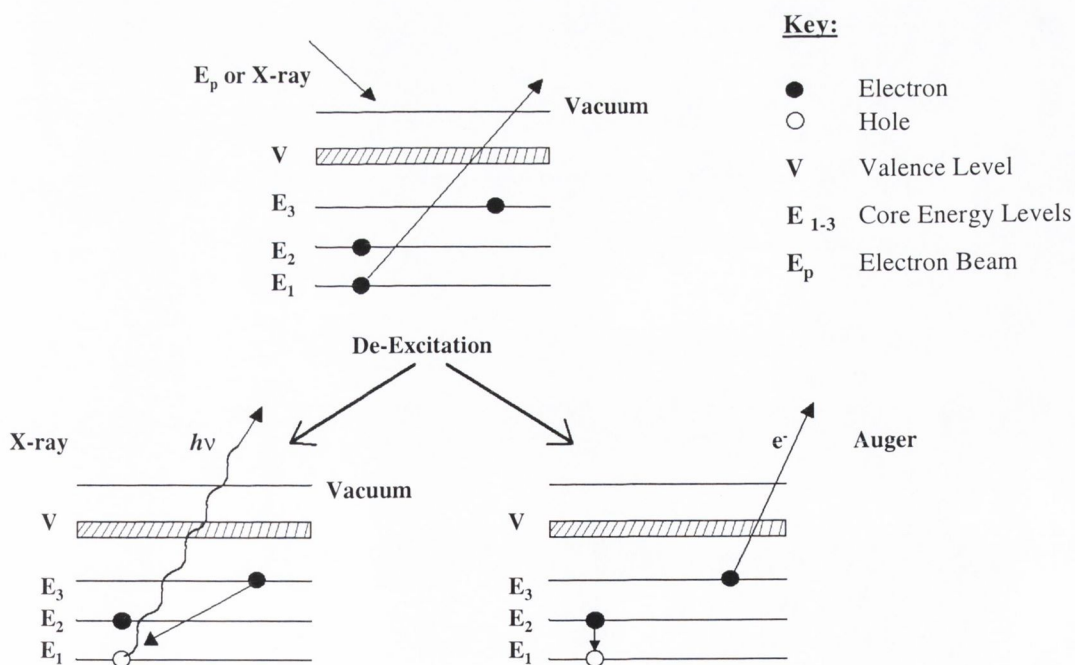


Fig. 1.4 Schematic diagram of Auger and X-ray processes.

1.4 THERMAL DESORPTION SPECTROSCOPY

This technique involves heating the sample at a controlled heating rate and monitoring the partial pressure of a species desorbing from the surface as a function of temperature.

Analysis of desorption spectra yields information on the nature and number of adsorbed species, the number of various desorbing phases for each species and their relative populations; the activation energies of desorption (E_d) of the individual phases and the order of the desorption process.

Thermal desorption has been the subject of a number of articles [21-23] and only a brief discussion of the technique will be presented here.

When the pumping speed to volume ratio is large, the partial pressure at any time is proportional to the rate of desorption. The rate of desorption from unit surface area is given by:

$$-d\theta/dt = v_n \cdot \theta^n \cdot \exp(-E_d/RT) \quad (1.4.1)$$

where θ is the surface coverage, n is the order of the desorption reaction, v_n is the rate constant, R the gas constant and T the temperature. With linear heating rates, the integral of the partial pressure change over the temperature range is proportional to the coverage. Redhead showed [21] that, in the absence of any coverage dependence on E_d , the peak temperature (T_p) for a first order desorption process is independent of coverage:

$$E_d/RT_p^2 = (v_1/\beta) \exp(-E_d/RT_p) \quad (1.4.2)$$

where β is the heating rate and v_1 is the pre-exponential (frequency) factor. Thus E_d can be determined directly from a measurement of T_p , provided a value of v_1 is assumed, using the Redhead formula:

$$E_d/RT_p = \ln(v_1 T_p / \beta) - 3.64 \quad (1.4.3)$$

The relation between E_d and T_p is very nearly linear and for $10^{13} > v_1/\beta > 10^8$, the error induced is small (approx. 2%).

$$\ln(T_p^2/\beta) = E_d/RT_p + \ln(E_d/R) \quad (1.4.4)$$

A plot of $\ln(T_p^2/\beta)$ versus $1/T_p$ yields a straight line with a slope of E_d/R . No value of v_1 need be assumed using this equation, but can be calculated subsequently by substituting E_d in the rate equation (1.4.1).

A more general expression, valid for all desorption orders, n , greater than zero has been derived by Falconer and Madix [23]:

$$\ln(\beta/T_p^2) = \ln(R \cdot v_n \cdot \theta^{n-1}/E_d) - E_d/RT_p \quad (1.4.5)$$

Plotting $\ln(\beta/T_p^2)$ versus $1/T_p$ for a number of heating rates yields a straight line of slope $-E_d/R$.

In general, T_p increases as the heating rate is increased, but since the dependence of T_p on β is small, changes in β of several orders of magnitude are necessary to obtain reasonable accuracy in the determination of E_d from heating rate variation methods.

The desorption activation energy can be determined for any n without recourse to heating rate variation methods, by direct analysis of the desorption profile. From (1.4.1) it can be shown that:

$$\ln(-d\theta/dt / \theta^n) = -E_d/RT \quad (1.4.6)$$

By using the partial pressure change as a measure of the rate and the area under the remaining higher temperature portion of the curve as a measure of the coverage, a plot of $\ln(-d\theta/dt / \theta^n)$ versus $1/T$ should yield a straight line of slope $-E_d/R$ for the appropriate order.

When analysing thermal desorption spectra, consideration must be given to the possibility of lateral interactions between adsorbed species, changes of bond strength with coverage and the interconversion of states in the adlayer. These can complicate spectral interpretation. In the case of lateral interactions, the activation energy and peak temperature become dependent on coverage. Repulsive interactions can result in a first order desorption process displaying a second order peak shape and T_p versus θ behaviour [61]; and a second order desorption process showing a much greater shift of T_p with θ . Also, lateral interactions can result in the appearance of multiple desorption peaks from a single desorbing state, due to sharp decreases in E_d at, for example, $\theta = 0.5$ [62].

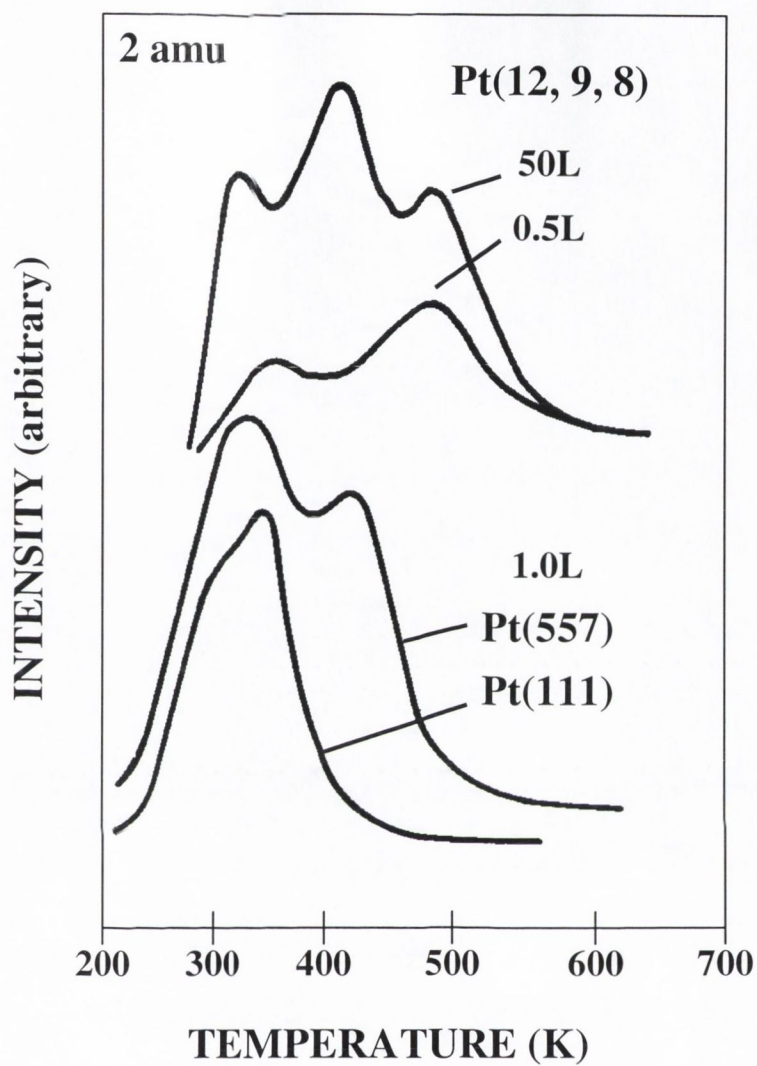


Fig. 1.5 Thermal desorption spectra of H₂ following exposures of H₂ to various platinum surfaces.

1.5 X-RAY PHOTOELECTRON SPECTROSCOPY

X-ray photoelectron spectroscopy (XPS) provides information about the elemental composition and chemical environment of a surface. The process involves the excitation of electrons in an atom or molecule into the vacuum by means of X-rays.

A photon with sufficient energy $h\nu$ (where h is Planck's constant and ν is the frequency of the electromagnetic radiation) will ionize an electronic shell, imparting to an electron enough energy for it to escape into the vacuum. The kinetic energy of this photoelectron is given by:

$$E_k \approx h\nu - E_b \quad (1.5.1)$$

where E_b is the calculated binding energy of the electron. The kinetic energy may be modified by several atomic parameters associated with the electron emission process, such as relaxation of orbitals and core level screening. Therefore, equation (1.5.1) represents a highly simplified relationship between E_k and E_b .

Incident photons with energies in the ultra-violet and X-ray regions of the electromagnetic spectrum provide sufficient energies to produce photoelectrons. In ultra-violet photoelectron spectroscopy (UPS) the energy of the incident radiation (21.2 eV using a helium discharge lamp) is insufficient to eject deep core electrons. UPS is therefore generally used to study electrons in the valence band of the solid. X-rays on the other hand have energies capable of ionizing core electron levels. Since core level energies are element specific XPS provides a powerful tool for identifying surface species.

In XPS the sources of radiation are usually aluminium or magnesium anodes which give K_α lines at 1486.6 eV and 1253.6 eV respectively. Combining these two sources in a switchable twin-anode can enable the separation of those photoelectrons whose kinetic energies are directly dependent on the incident photon energy from Auger electrons, which are also produced during core level ionization, and whose energies are fixed, regardless of the energy of the incident beam (see section 1.3).

In addition to Auger peaks, many other features appear in an XPS spectrum along with the core electron lines, adding a degree of complexity to the spectrum. The most obvious

feature is the step like background, the steps occurring at the low kinetic energy (high binding energy) side of the photoelectron lines. These steps are generated by cascades of inelastic collisions undergone by those photoelectrons generated at depths below the surface much greater than the mean-free-path for inelastic scattering.

As stated earlier, equation (1.5.1) represents a simplistic picture in which the electrons remaining after ionization are assumed to be in the same initial state as before the ionization event. However, as an electron is ejected from a core level, the other electrons relax in energy to lower energy states to screen this hole and so make more energy available to the outgoing photoelectron. This is called a relaxation shift. Furthermore, an outgoing photoelectron may interact with a valence electron, either promoting it to a higher energy level (a process referred to as a shake-up), or even promoting it above the vacuum level (known as a shake-off). In doing so the outgoing photoelectron loses kinetic energy. This process results in satellite peaks at the high binding energy side of the photoelectron peak. Another potential source of spectral features are plasmons, which are collective density fluctuations in the electron cloud in a solid.

Finally, the X-ray source itself contributes features to the XPS spectrum. Both Al- K_{α} and Mg- K_{α} have $K_{\alpha 3,4}$ satellites some 10 eV below the main $K_{\alpha 1,2}$ lines, with around 10% of their intensity.

Overall, these features essentially reflect the difference in energy between the initial (unexcited) state and the final state.

In addition to identifying surface species XPS allows information about the chemical environment of an element to be deduced. This is because the binding energy of a core electron is influenced by electrostatic interaction with the valence electrons. The contribution of the valence electrons to the energy of the core levels depends on the type of bonding in which the valence electrons are involved. In simple terms, the greater the electronegativity of the surrounding atoms that are involved in chemical bonding, the more the electronic charge is redistributed away from the atom and the higher the observed binding energies of the core electrons. These 'chemical shifts' may be as large as 10 eV and provide information on the valence states of the surface elements and consequently their bonding.

In XPS the energy resolution is limited by the line width of the photon source. Therefore, if an element exists in two different chemical environments on the surface, the difference between their respective chemical shift values must exceed the line width of the source to be fully resolvable in the spectrum. The line width of the Al-K $_{\alpha}$ and Mg-K $_{\alpha}$ sources are about 0.85 eV and 0.7 eV respectively.

Sometimes, the peaks in X-ray spectra are labelled by conventional X-ray notation where the principal quantum numbers ($n = 1, 2, 3, \dots$ etc.) of the orbitals are assigned the letters K, L, M, N, O, ...etc., with the orbital and total angular momentum quantum numbers l and j of the hole left after photoemission assigned respective suffixes. However, it is not uncommon for atomic notation - $1s, 2p_{1/2}, 2p_{3/2}, \dots$ etc. - to be used. It is this notation that is used in this work.

CHAPTER TWO

EXPERIMENTAL TECHNIQUES

CHAPTER 2 EXPERIMENTAL TECHNIQUES

2.1 THE EXPERIMENTAL SYSTEMS

2.1.1 *The LEED/Auger System*

This is a bakeable, 12 inch diameter, stainless steel chamber constructed by Vacuum Generators Ltd.. A number of ports were later added to the chamber by Vacuum Science Workshop Ltd.. These ports were positioned so as to give line of sight to the centre of curvature of the LEED optics.

The ports and flanges on the chamber are sealed using high purity copper gaskets; the main chamber is sealed using gold wire as a gasket.

A section through the experimental level of the chamber is shown in figure 2.1.

Key:

AG	Argon Ion Gun
EG1	Auger Electron Gun
EG2	LEED/Auger Gun
GD	Gas Doser
LV	Leak Valve
QMS	Quadrupole Mass Spectrometer
RFA	Retarding Field Analyser
S	Sample
V	Viewport

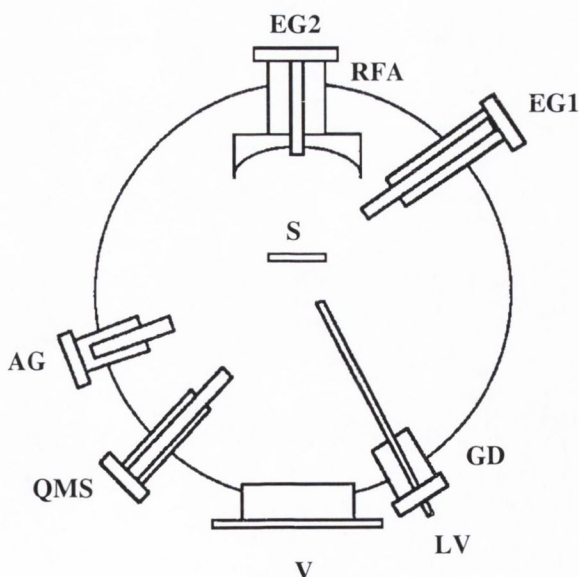


Fig. 2.1 Schematic diagram through the experimental level of the LEED-Auger system.

(not to scale)

The chamber was fitted with a quadrupole mass spectrometer (VG Supavac) for residual gas analysis and thermal desorption spectroscopy; a display type three grid retarding field analyser (RFA) (Vacuum Generators Ltd.) which could be used for LEED or AES experiments; a normal incidence electron gun (LEG2) for LEED and a glancing incidence electron gun (Vacuum Science Workshop Ltd.) for AES; and two ionization gauges (Bayard-Alpert type), one for pressure measurement in the 10^{-3} - 10^{-10} torr pressure range, located below the experimental level of the chamber, the other for argon ion bombardment (see section 2.3.3), located in the line of sight of the sample.

The main chamber attained pressures of below 2×10^{-10} torr. This was achieved by use of a 50 litre per second diode ion pump in conjunction with a titanium sublimation pump. The diode ion pump works by ionizing the gas in the system by means of an electrical discharge which, under the influence of a magnetic field of a few thousand Gauss, follows a flat helical path, thus maximising the path length and resulting in a high efficiency of ion formation. The gaseous ions are then captured or chemisorbed at the electrodes. The titanium sublimation pump is located below the main chamber and is separated from the chamber by a steel plate. Electrical resistance heating of titanium/molybdenum alloy filaments results in the sublimation of titanium. This condenses on the chamber walls and reacts chemically with the active gases to form low vapour pressure solid compounds.

An auxiliary pumping system was also employed to pump the chamber to less than 10^{-5} torr, at which pressure the ion pump could be started. This system consists of a liquid nitrogen trapped oil diffusion pump and a rotary pump with a liquid nitrogen cooled foreline trap. The rotary pump is an oil-sealed mechanical pump which traps and compresses a sample of gas to slightly above atmospheric pressure with each rotation of the vane. The gas is then expelled via an exhaust valve. Once the rotary pump has reached a pressure of about 10^{-2} torr, the oil diffusion pump can be started. A jet of oil vapour from a heated well of liquid is directed downward and radially across a space within the pump. Gas particles are carried downwards with the jet and compressed until they can be removed by the rotary pump. Meanwhile, the oil vapour is cooled back to liquid as it descends, to be reheated again in the well at the base of the pump. This auxiliary system was also used to pump the gas handling lines and it can be isolated from the main chamber by means of an isolation valve.

The system contains two gas handling lines both of which can be pumped to less than 10^{-6} torr by the auxiliary pumping system. One line is constructed mainly of stainless steel. Gas dosing from this line is achieved by filling the chamber to the required pressure. The other line is constructed of glass, for handling gases which react in the steel line. Gas dosing is achieved by means of a doser attached to the leak valve. A block diagram of the entire pumping system is shown in figure 2.2.

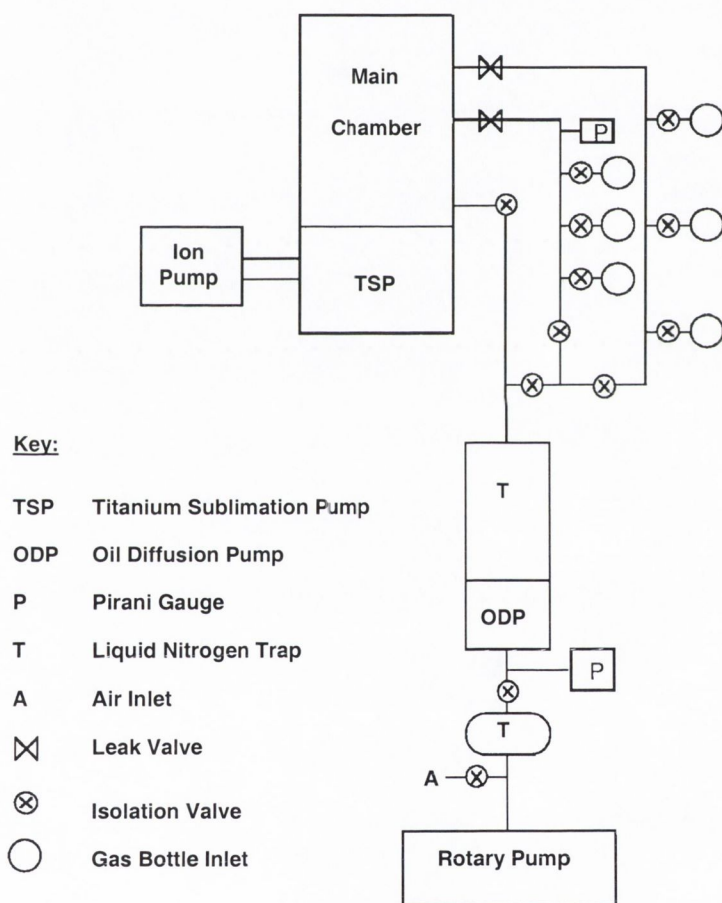


Fig. 2.2 Block diagram of the vacuum and pumping systems.

2.1.2 The ESCA System

The ESCA (Electron Spectroscopy for Chemical Analysis) system is a three-chambered system constructed by VSW Scientific Instruments Ltd.. The three chambers are: a sample preparation chamber (SPC) which was used to clean and dose the sample; a sample analysis chamber (SAC), used to carry out the XPS experiments; and a fast entry chamber (FEC) which was not used in this work.

The SPC and FEC are each separated from the SAC by means of a gate valve. The SPC and SAC are both pumped by their own liquid nitrogen trapped, water cooled 200l/s oil diffusion pumps. Each pump is backed by a two-stage rotary pump (Edwards). Additionally, the SPC is pumped by a standard TSP whilst the SAC is pumped by a water-cooled TSP.

A sketch of the experimental level of the SAC chamber is shown in figure 2.3.

Key:

FEC Fast Entry Chamber

IG Ion Gauge

S Sample

SPC Sample Preparation Chamber

UPS Ultraviolet Photon Source

V Viewport

XPS X-ray Photon Source

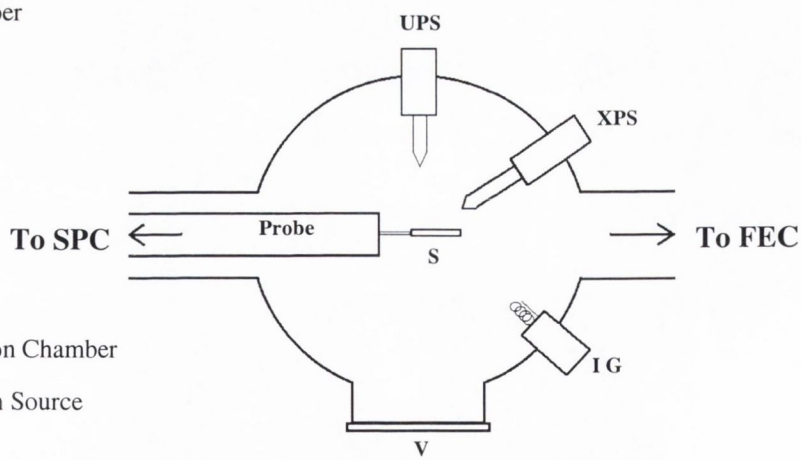
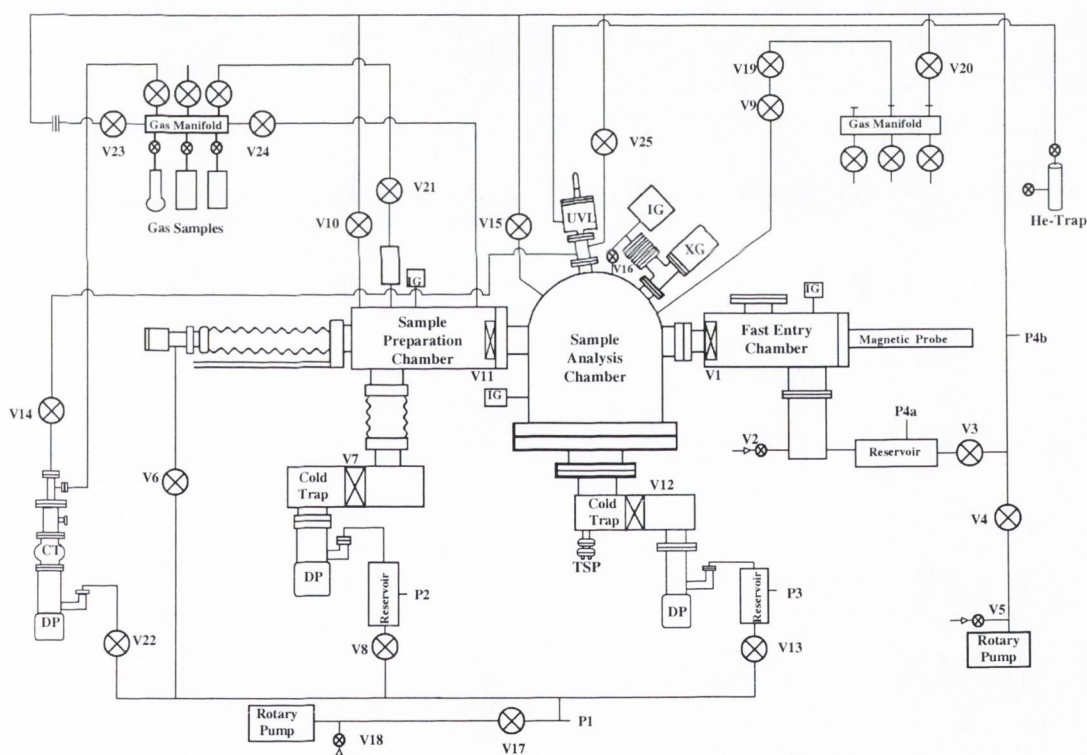


Fig. 2.3 Sketch of the experimental level of the SAC on the ESCA system (analyser not shown).
(not to scale)

Gas dosing (i.e. exposing it to the adsorbate) is achieved by filling the chamber from a gas handling manifold. Admission of the gas is via a leak valve (VG MD6 series). The manifold is pumped by a rotary-backed diffusion pump. A block diagram of the entire pumping system is shown in figure 2.4.

The SAC is fitted with an X-ray photoelectron source (VSW TA10 Twin Anode), an ultra-violet photoelectron source, an ion gauge (Bayard-Alpert type) and a hemispherical electron analyser (VSW HA 100) (not shown).

Crystal cleaning and dosing was carried out in the SPC. The XPS experiments were carried out in the SAC.



Key:

- | | | | |
|----|----------------|-----|---------------------------|
| CT | Cold Trap | TSP | Titanium Sublimation Pump |
| DP | Diffusion Pump | UVL | UV-lamp |
| IG | Ion Gauge | V | Valve |
| P | Pirani Gauge | XG | X-ray Gun |

Fig. 2.4 Block diagram of the ESCA pumping system.

2.2 EXPERIMENTAL TECHNIQUES

2.2.1 Low Energy Electron Diffraction

The apparatus consists of a display-type 3-grid LEED optics and an axial LEG2 electron gun, shown schematically in figure 2.5.

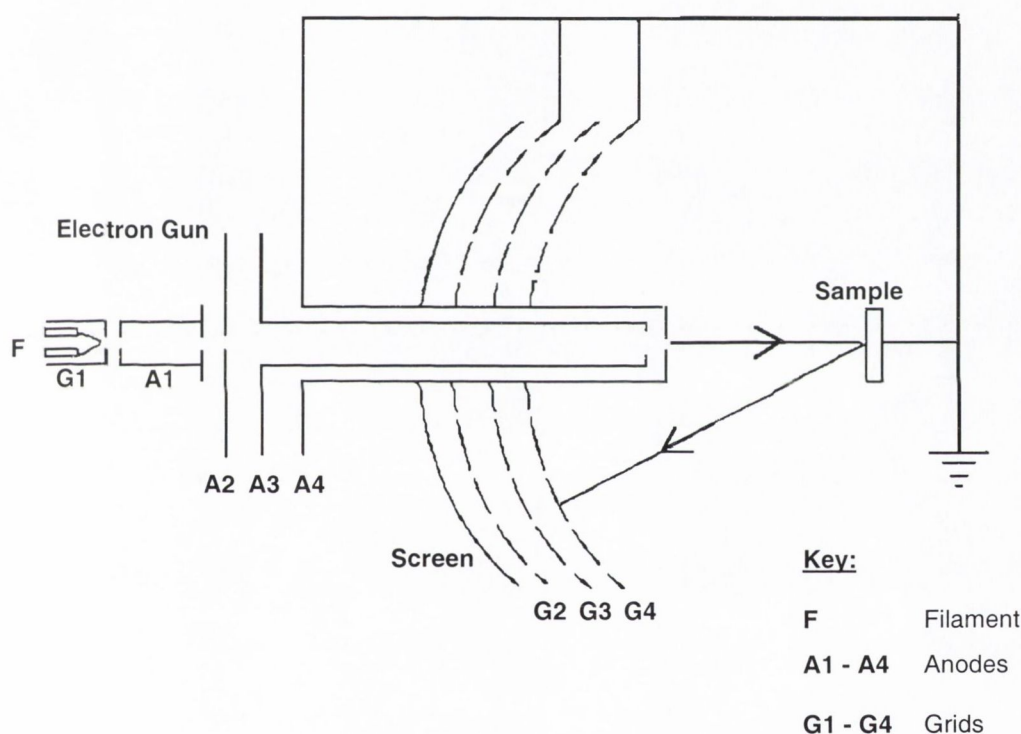


Fig. 2.5 Schematic of the LEED optics.

Electrons from the directly heated filament emerge as a divergent beam into the anode A1 as a result of field penetration from A1 at 1000V through the grid G1. The beam is focused by the electrodes A1, A2 and A3. The beam current is trimmed down to a few microamps from an initial current of approximately 0.5 mA by means of an aperture at the end of A1.

The incident beam strikes the sample, producing elastic, inelastic and secondary electrons. The inelastic and secondary electrons are filtered out by a retard potential on grid G3. The anode A4 and grids G2 and G4 are held at earth; A4 and G4 to ensure that the electrons of the incident beam and the back-scattered electrons travel in a field free zone; and G2 to prevent field penetration from the screen to G3. This set-up is known as a retarding field analyser.

The screen is coated with fine grain phosphor with no organic binders. Electrons elastically diffracted from the sample are accelerated to the screen by a 5kV potential on the screen. The accelerated electrons produce excitation of the phosphor to display the LEED pattern. The pattern can be viewed and photographed through the viewport opposite the LEED optics (see figure 2.1).

2.2.2 Auger Electron Spectroscopy

Auger spectra are recorded by energy analysis of the secondary electrons emitted from the crystal upon irradiation with an electron beam of energy between 3 - 5keV. The source of the electron beam is an electron gun with focusing and deflection electrodes. Adjusting the intensity of the primary electron beam alters the intensity of the secondary electrons.

In the LEED/Auger chamber Auger electron spectroscopy was performed using a VG LEG1 electron gun (EG1 in fig. 2.1) and the VG LEED optics as a retarding field analyser (RFA). A field free zone was maintained around the sample by holding the sample, the outermost grid (G4) of the RFA and the final anode of the electron gun at earth. The collector of the RFA was held at +250V to ensure high collection efficiency by preventing losses due to secondary electron emission. Grid G3 (see fig. 2.5) was used as a high pass filter by placing a retarding potential ($-E$) upon it, so that only electrons with an energy greater than E were collected. Sweeping this retarding potential from $E = 0$ to $E = E_p$ (the energy of the primary electron beam) produced a retarding potential curve. By differentiating this curve, a secondary electron energy distribution curve ($N(E)$ versus E) was obtained. Further differentiation of the $N(E)$ curve to give the $dN(E)/dE$ curve provided greater sensitivity. The spectra were recorded on computer. A detailed discussion of the electronic instruments used for data analysis is given in reference [63].

2.2.3 Thermal Desorption Spectroscopy

In the thermal desorption experiment the partial pressure of a particular species is monitored as a function of crystal temperature. A block diagram of the experimental arrangement is shown in figure 2.6.

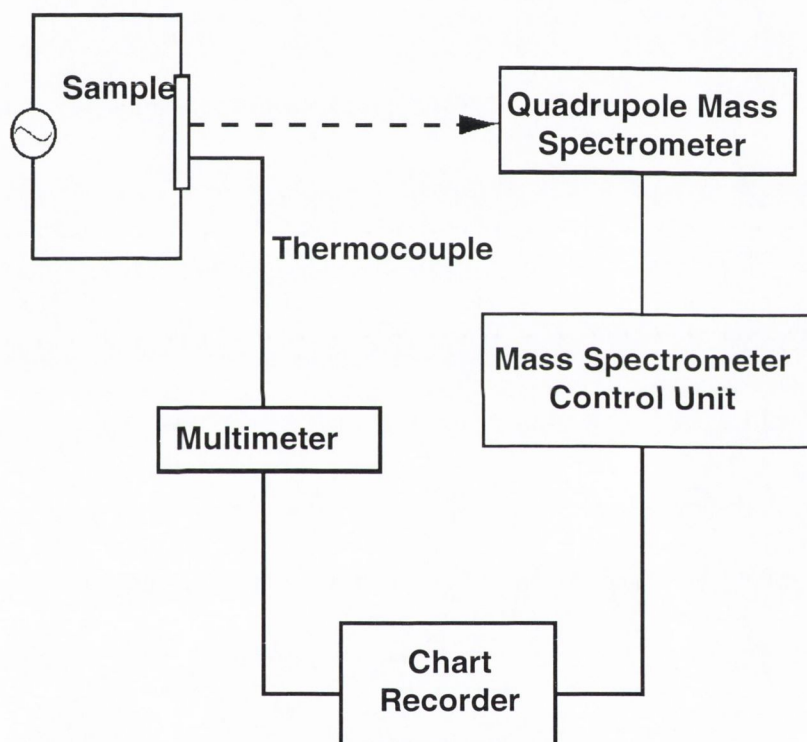


Fig. 2.6 Block diagram of the thermal desorption experiment.

Prior to dosing the crystal the mass spectrometer filament is degassed and the crystal flashed to 1000K. Once the crystal had cooled to the desired temperature it was exposed to the gas under investigation by preferential front face dosing from a capillary tube. The

degree of exposure is measured in Langmuirs, L, where $1L = 10^{-6}$ torr s exposure. The sample was then rotated to the line of sight of the mass spectrometer.

The mass spectrometer itself was set to the required e/m value by tuning the first mass control on the control unit. The partial pressure output was fed directly into the y-axis of an X-Y recorder, whilst the crystal temperature was measured using a chromel/alumel thermocouple which drove the x-axis of the X-Y recorder. For calibration purposes the thermocouple voltage was also displayed on a digital voltmeter.

By passing a current through the crystal support wires at a constant applied a.c. voltage, a linear heating rate of $13Ks^{-1}$ in the 300 - 800K region was obtained.

The data was collected directly onto the chart recorder. The thermocouple voltage could then be converted into a temperature scale by means of a standard conversion table, with the appropriate correction made for room temperature.

2.2.4 X-ray Photoelectron Spectroscopy

X-rays are produced by the acceleration of thermally emitted electrons from a hot filament at ground potential towards an anode. This anode is typically held at a potential between 12kV and 20kV. The anode used was a twin anode configuration of aluminium and magnesium (VSW TA 10). The aluminium anode provides a K_{α} radiation energy of 1486.6 eV with a line width of 0.85 eV. The magnesium generates K_{α} radiation energy of 1253.6 eV with a line width of 0.7 eV.

The X-ray spectrometer and the sample under investigation are connected electrically, ensuring that their Fermi energy levels are at the same energy.

The analyser is a concentric hemispherical sector analyser. This is a dispersion analyser, and is normally operated in a mode in which a constant potential difference, called the pass energy (E_0), is applied across the inner and outer hemispheres so that electrons with energies close to E_0 (within a range ΔE) are focused on the exit slit of the analyser by means of electrostatic deflection between these hemispheres.

In order to scan through a range of photoelectron energies, the electrons are retarded before they enter the analyser. This is achieved by means of a retarding lens system. By ramping the retarding field potential, electrons of different energies can be analysed.

Pre-retardation of the electrons also has the important advantage of improving the resolution. This is because the resolving power, ρ , of the analyser, given by:

$$\rho = E_0/\Delta E \quad (2.2.1)$$

is fixed by the geometry of the system. Consequently, a decrease in E_0 results in a decrease in ΔE , i.e. a decrease in the spread of energies that arrive at the exit slit.

A channeltron (channel electron multiplier) detects the electrons that exit the analyser. It consists of a cone like opening and a continuous tube of high resistivity semi-conducting glass. When a high electric field is applied along the tube, electrons from the analyser striking the channeltron create a shower of secondary electrons. These in turn strike the tube walls, resulting in further secondary electrons. The signal produced by these electrons is

amplified and then counted by a ratemeter. The output is displayed and stored on computer. A schematic of the photoelectron detector/analyser set-up is shown in figure 2.7.

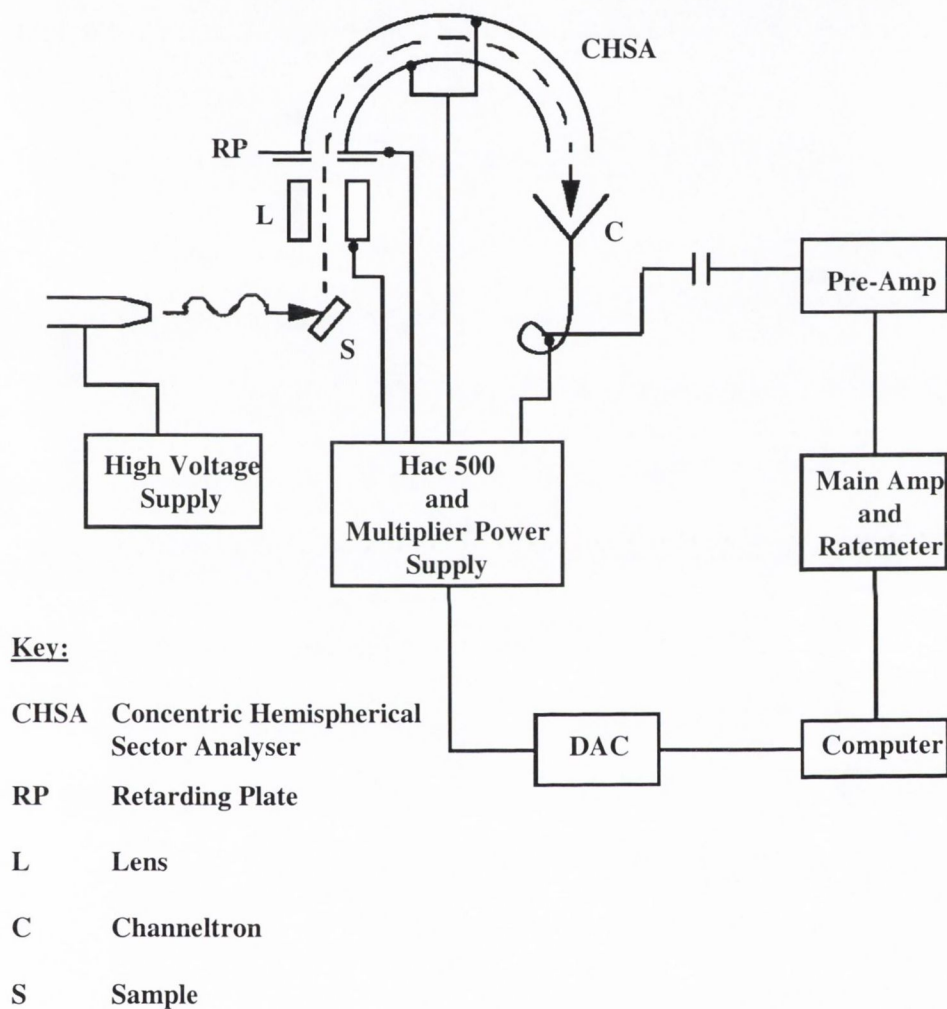


Fig. 2.7 Schematic of the X-ray source and photoelectron detector/analyser set-up.

2.3 CRYSTAL PREPARATION

2.3.1 *The Platinum Crystals*

The Pt(331) sample was cut from a 99.99% pure single crystal rod at the Material Science Centre of the University of Birmingham. This rod was mounted on an X-ray goniometer, oriented to within 0.25° of the (331) direction and a disc, 9mm in diameter and 1mm thick, was cut in a spark cutting machine. The crystal was then polished with 0.25μ diamond paste. The Pt(331) surface consists of three atom wide (111) oriented terraces divided by one atom high (111) oriented steps (see figure 2.8).

The Pt(111) sample was supplied by MaTech (Jülich). It was cut on both sides to the above specifications and polished on one side to $0.03\mu\text{m}$.

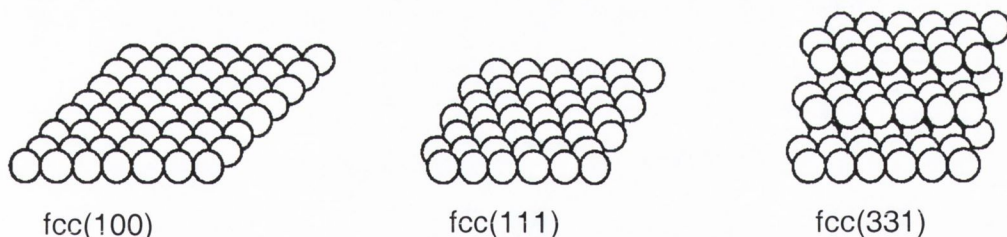


Fig. 2.8 Representations of the (100), (111) and (331) surfaces of platinum. The (100) diagram represents a bulk truncated surface. In reality, reconstruction occurs.

2.3.2 *Crystal Mounting*

Each platinum crystal was spot-welded between two tantalum wires of diameter 0.25 mm, positioned opposite each other on the edge of the crystal. The wires were then clamped between the two plates of a copper holder.

To the edge of each crystal was spot-welded a chromel/alumel thermocouple of diameter 0.05 mm. This assembly was treated in an ultrasonic acetone bath to remove any residues of grease that might be a source of contamination.

In the case of the LEED/Auger system the arms of the copper holder were screwed to a ceramic block to provide the connections for the heating wires and a channel for the electrical feed-throughs to the thermocouple wires (see figure 2.9).

Attached to the top of this ceramic block was a steel driving rod which in turn was attached to the sample manipulator, allowing the crystal to be manipulated through the x, y, z plane. The manipulator used was a standard Vacuum Generators sample manipulator (UMDI).

Heating the crystal was achieved by passing an a.c. current through the copper holders and tantalum wires.

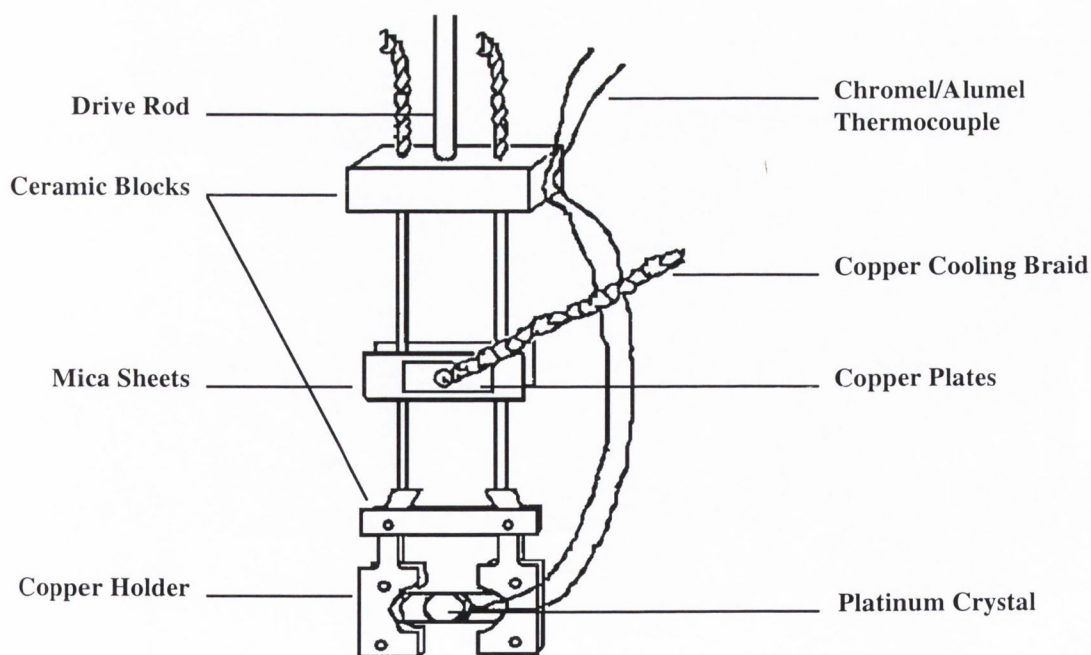


Fig. 2.9 Diagram of crystal mounting for the LEED-Auger system.

In the ESCA system the copper holder was attached to a copper 'L' piece. This in turn was screwed into the horizontally positioned stainless steel probe (see figure 2.10). Positioning the sample relative to the X-ray source was achieved by means of an x, y, z manipulator.

A liquid nitrogen well running through the core of the probe enabled cooling of the crystal. The end of the stainless steel probe is thick to allow the sample to be screwed into place. This, however, results in low thermal conductivity. To overcome this a copper sleeve was fitted tightly around the probe and the copper 'L' piece attached to the probe through the sleeve [32]. With this arrangement the crystal could be cooled to 83K.

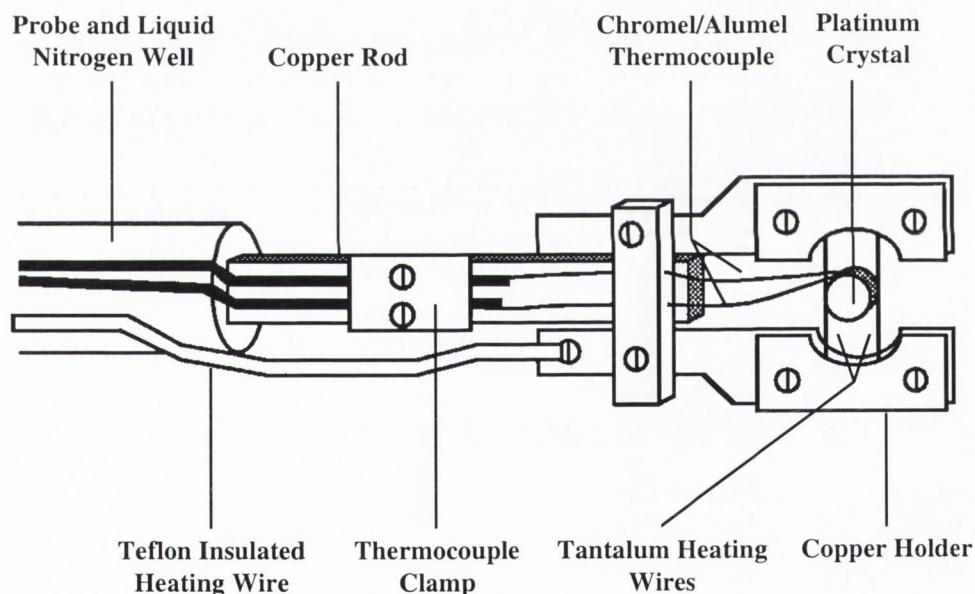


Fig. 2.10 Diagram of crystal mounting for the ESCA system.

2.3.3 Crystal Cleaning and Characterization in Vacuo

Mere exposure to the atmosphere alone is sufficient to produce considerable surface contamination of a crystal sample. Once such a sample has been mounted in the UHV chamber this surface contamination must be removed.

Volatile surface contaminants such as CO, CO₂ and SO₂ were desorbed from the surface simply by heating. The main non-volatile contaminants of the platinum samples detected by AES were carbon, calcium and sulphur. Removal of these substances was achieved by heating the crystal at 1000K in 5×10^{-7} torr of oxygen, producing volatile oxides. Following oxygen treatment, bombardment of the crystal surface with argon ions was necessary to remove the oxygen incorporated into the specimen as well as any stubborn contaminants left behind. This procedure was repeated until a clean surface was established, as ascertained by AES and by comparison of the CO desorption spectrum to that from a previously established clean surface.

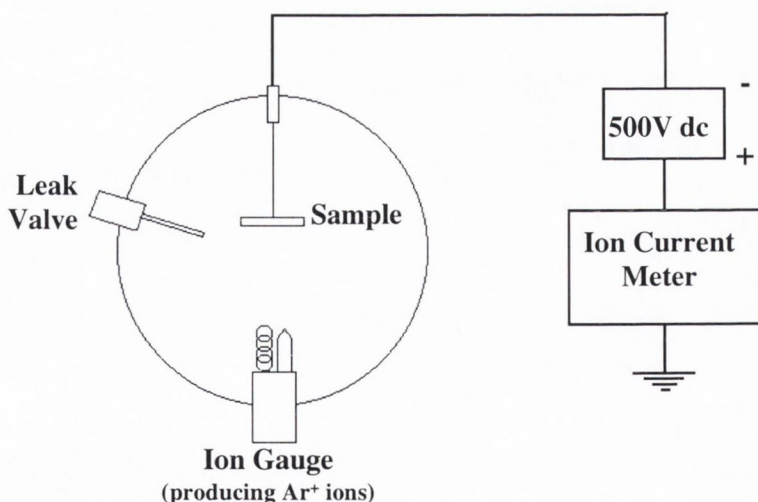


Fig. 2.11 Set-up for argon bombardment.

Argon ion bombardment was performed using an ion gauge as the ionizing agent. The crystal surface was set facing the ion gauge and the ion gauge emission controller was switched to 10mA. The pumps were then switched off and the chamber back-filled with argon to a pressure of $\sim 5 \times 10^{-4}$ torr. In the case of the LEED/Auger system, a bias of about -500V was placed on the crystal sample, resulting in an argon ion current of $6 \mu\text{A}$ recorded at the sample (see figure 2.11). Argon bombardment leaves the surface in a heavily damaged condition and it is therefore necessary to anneal the sample to restore the order.

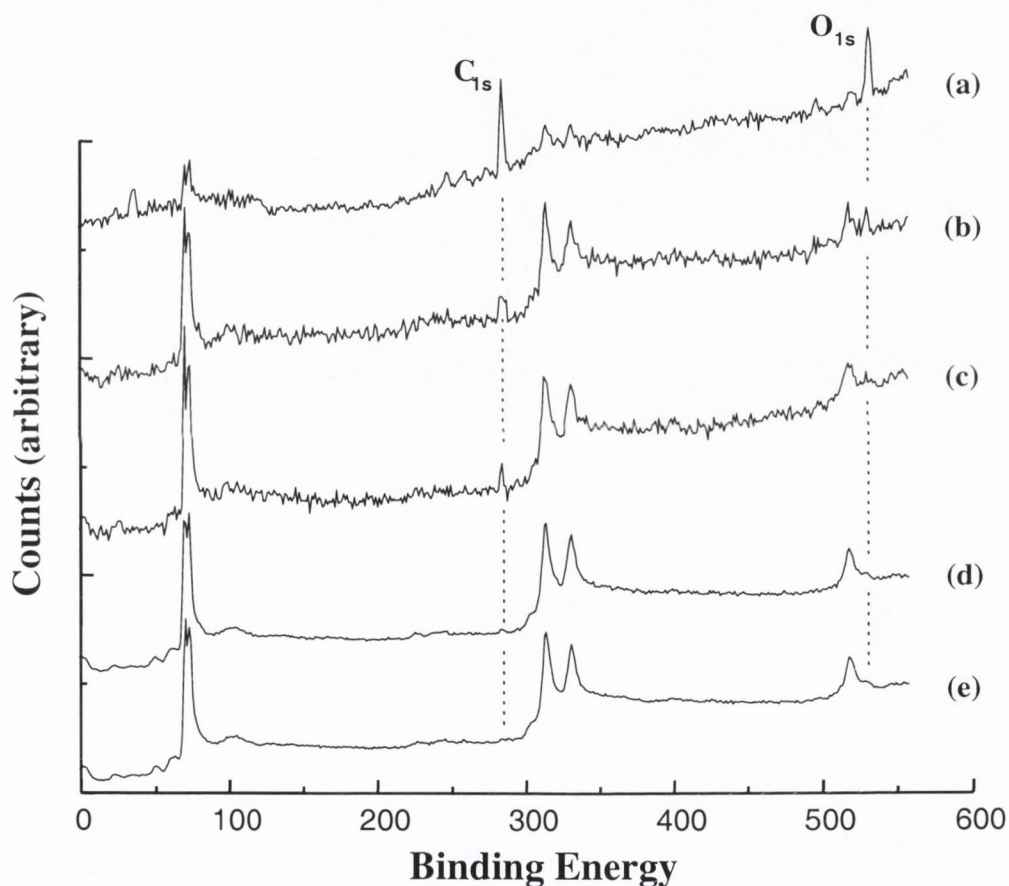


Fig. 2.12 X-ray photoelectron spectra of the Pt(331) crystal; spectrum (a): initial surface condition upon placement in the ESCA system; spectra (b) – (d): surface condition following progressive cleaning cycles; spectrum (e): clean Pt(331) crystal.

Following the cleaning procedure, the Pt(111) crystal displayed a sharp (1x1) LEED pattern, as expected (see figure 2.14). The LEED pattern of Pt(331) should show a pseudo-hexagonal pattern with a series of extra spots along the $[10\bar{3}]$ direction. However, a perfect

LEED pattern was not attained in this work, but rather some streaking of the spots was observed (see figure 2.15). This effect was also observed for Pt(331) by Cong *et al.* [29], who suggested that this was due to multiple step heights on some parts of the (331) surface. Y. Seimiya *et al.* [30, 31] reported a sharp (1x1) pattern from Pt(331), although they did not mention observing double spots. Davies and Lambert [64] observed the expected LEED pattern for Pd(331) but with diffuse spots indicating poor long range order.

Immediately prior to adsorption of the specimen gases the crystal was flashed to 600K, a temperature sufficient to drive off any CO and H₂ that may have adsorbed from the background. As soon as the crystal cooled to the required temperature it was exposed to the adsorbate under study.

All of the adsorbates studied in this work left carbon and nitrogen residues on the crystal surfaces. Consequently, it was necessary to argon bombard the surfaces between each exposure.

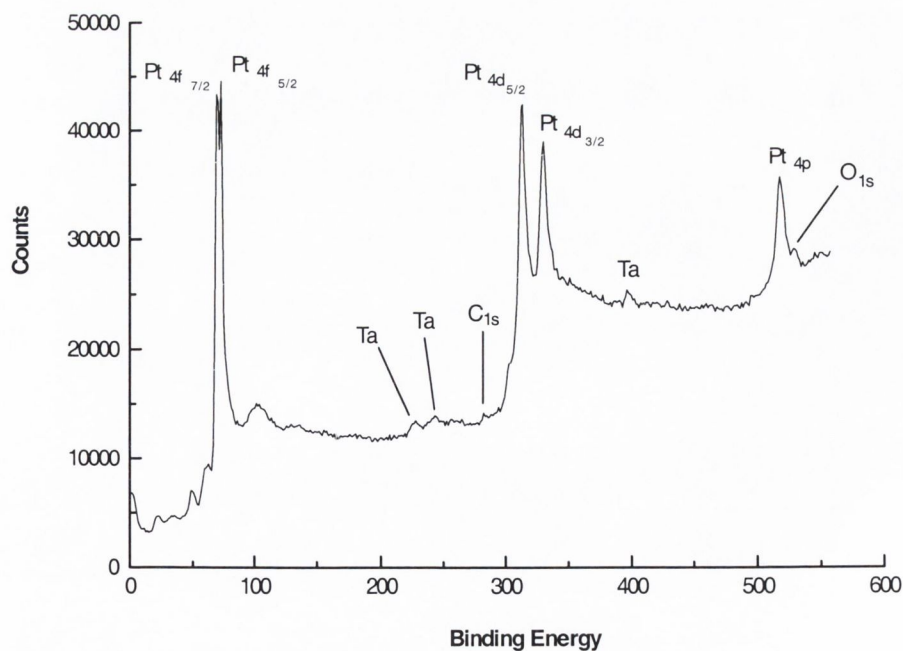


Fig. 2.13 XPS of clean Pt(331) surface (Mg K_α source).

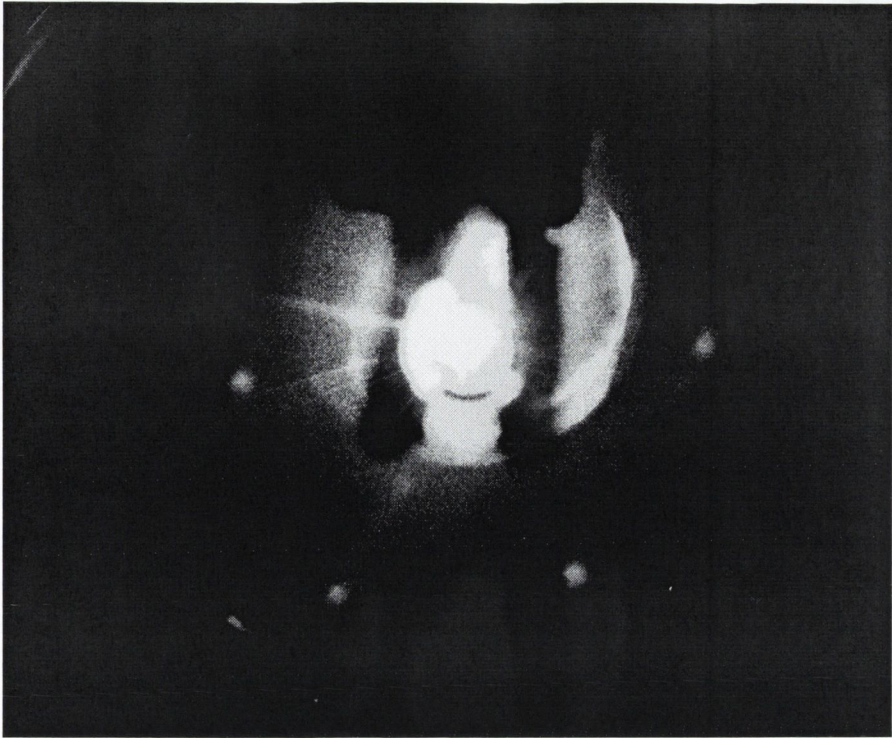


Fig. 2.14 Photograph of LEED of clean Pt(111) crystal. Primary beam energy = 75eV.

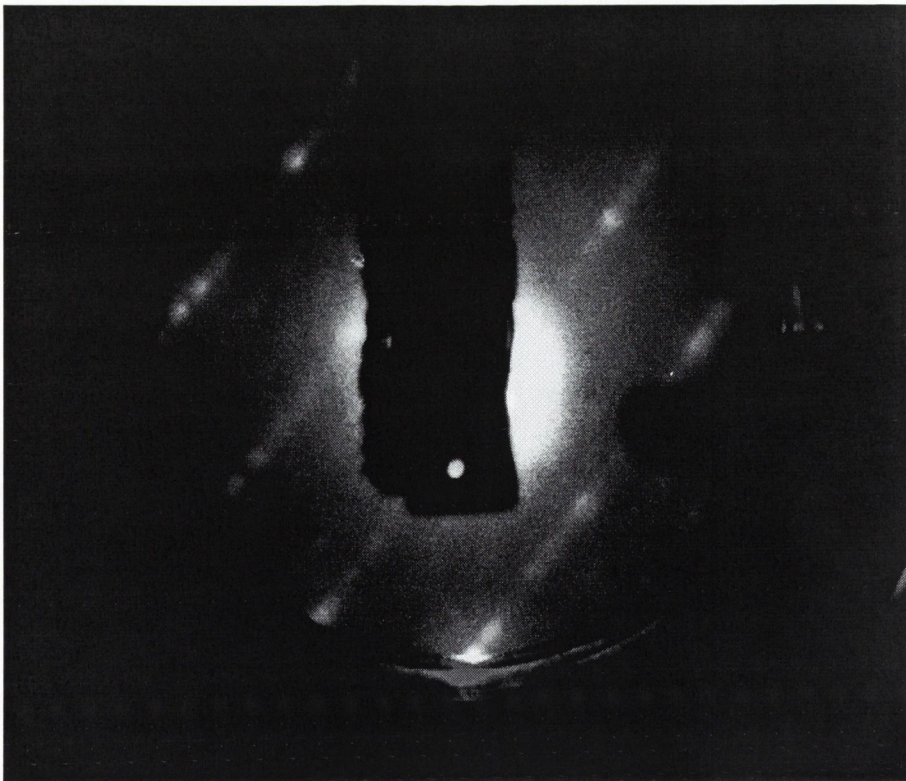


Fig. 2.15 Photograph of LEED of clean Pt(331) crystal. Primary beam energy = 90eV.

2.4 THE ADSORBATES

Methylamine and dimethylamine were prepared in this laboratory. They were prepared by addition of a solution of the corresponding HCl salts of these compounds to solid NaOH. Collection and purification of the resultant gases was achieved by fractionation on low and high vacuum gas-handling lines. The $\text{CH}_3\text{NH}_2\cdot\text{HCl}$ and $(\text{CH}_3)_2\text{NH}\cdot\text{HCl}$ were supplied by Aldrich Chemical Co. and were of reagent grade.

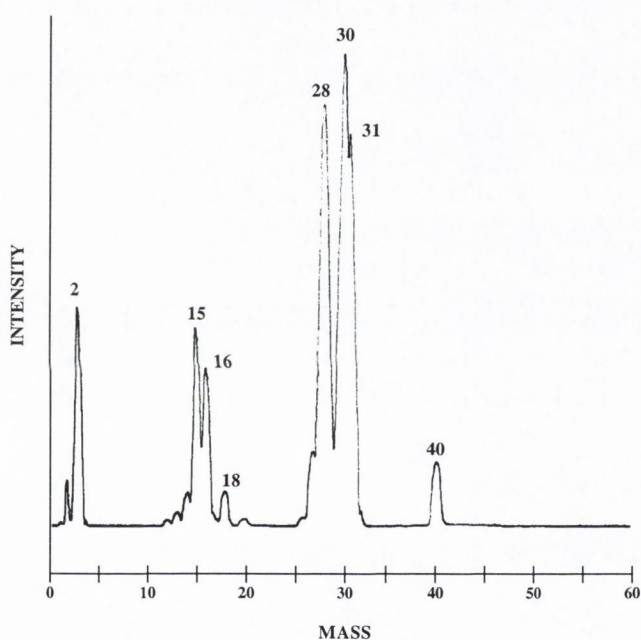


Fig. 2.16 Mass spectrum obtained for methylamine.

The mass spectrum of each compound was recorded (see figures 2.16 - 2.19) and compared to those published in the 'Eight Peak Index of Mass Spectra' (MSDC) and 'The Wiley/NBS Registry of Mass Spectral Data'. The cracking pattern of a chemical can vary depending on the mass spectrometer and differences in experimental conditions. Consequently, the 'Eight Peak Index of Mass Spectra' contains up to a maximum of three spectra for any one compound, selected to reflect differing experimental conditions. In the case of the Wiley/NBS registry, a single spectrum is presented in the form of a bar graph. In

figures 2.16 - 2.17 the peak at mass 40 is due to the presence of small amounts of argon in the gas-handling line.

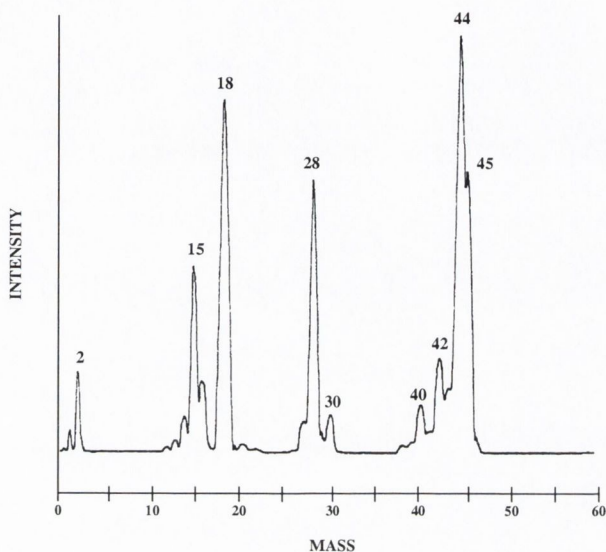


Fig. 2.17 Mass spectrum obtained for dimethylamine.

Trimethylamine was supplied by Fluka Ltd. with a purity > 99%. It was liquified and transferred to a glass gas bottle, after which it was subjected to a number of freeze-pump-thaw cycles.

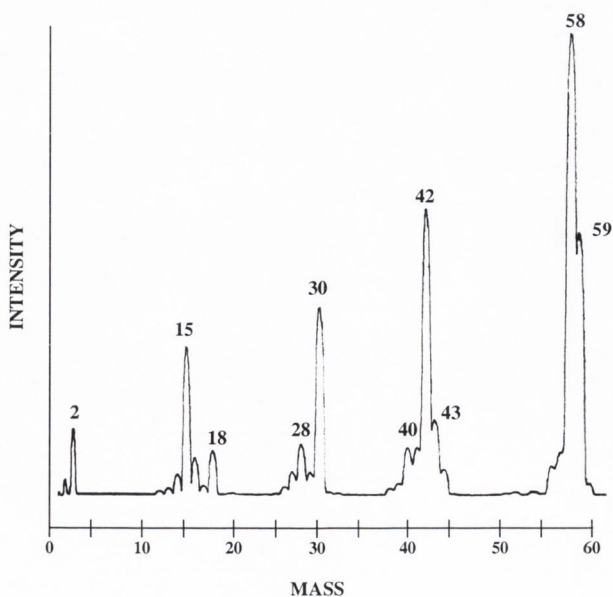


Fig. 2.18 Mass spectrum obtained for trimethylamine.

Ethylenediamine was supplied by BDH Ltd. with a purity $>98.5\%$. At least three freeze-pump-thaw cycles were applied to the ethylenediamine sample to ensure complete degassing.

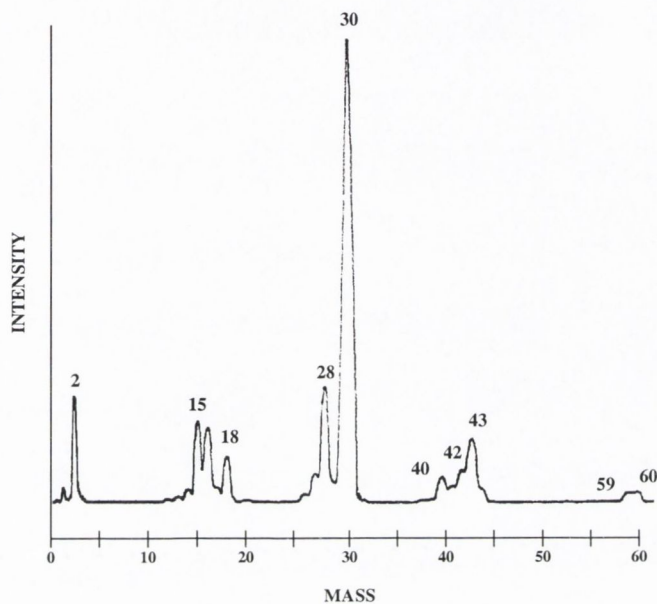


Fig. 2.19 Mass spectrum obtained for ethylenediamine.

Deuterium and argon were supplied by Messer Griesheim GmbH with purities greater than 99.7% and 99.997% respectively. They were used without further purification.

CHAPTER THREE

METHYLAMINE ON Pt(111) AND Pt(331)

CHAPTER 3 METHYLAMINE ON Pt(111) AND Pt(311)

3.1 RESULTS

3.1.1 Methylamine on Pt(111)

The main thermal desorption products observed upon exposure of the Pt(111) surface to methylamine at 300K were HCN, C₂N₂, N₂ and H₂. Sets of thermal desorption spectra for these products are shown in figures 3.1 - 3.5. A number of minor products were also detected. These are presented in figure 3.6.

Thermal desorption spectra for HCN reveal three peaks, two at ~396K and ~447K, and a main peak at ~492K. In addition, there is a high temperature shoulder between ~527K and 590K.

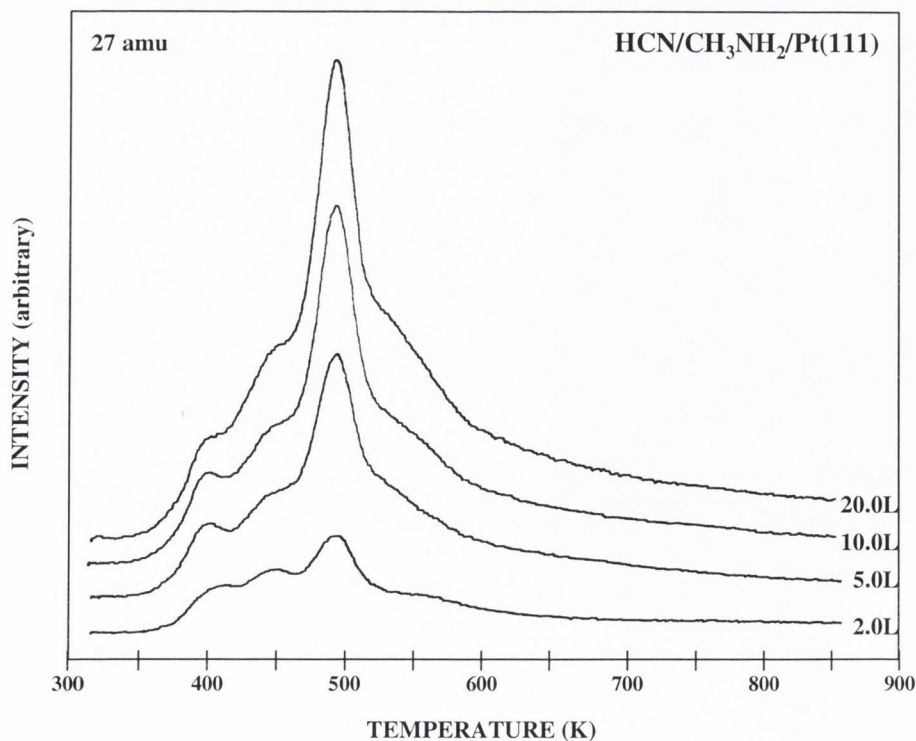


Fig. 3.1 Thermal desorption spectra of HCN following exposures of methylamine to Pt(111).

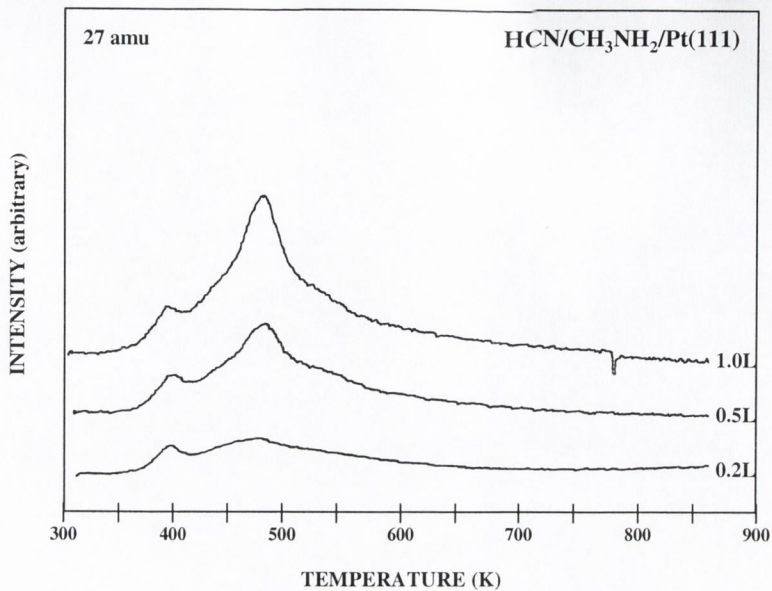


Fig. 3.2 Thermal desorption spectra of HCN following low exposures of methylamine to Pt(111).

A broad feature between 600K and 800K is produced at 52 amu, corresponding to C₂N₂ desorption. Within this feature there is a suggestion of a β_1 peak at ~672K and a β_2 peak at ~720K.

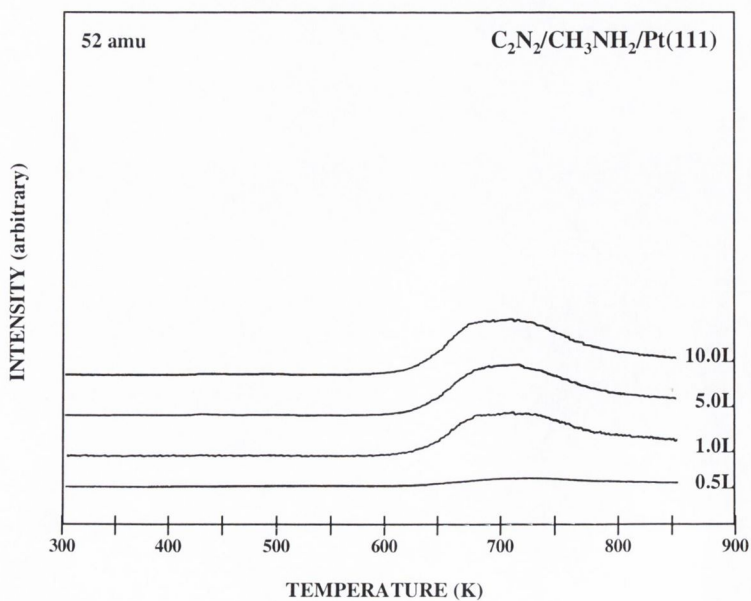


Fig. 3.3 Thermal desorption spectra of C₂N₂ following exposures of methylamine to Pt(111).

The H₂ desorption spectra exhibit a main peak at ~394K, along with a shoulder between ~442 - 503K and a second shoulder at ~508 - 543K.

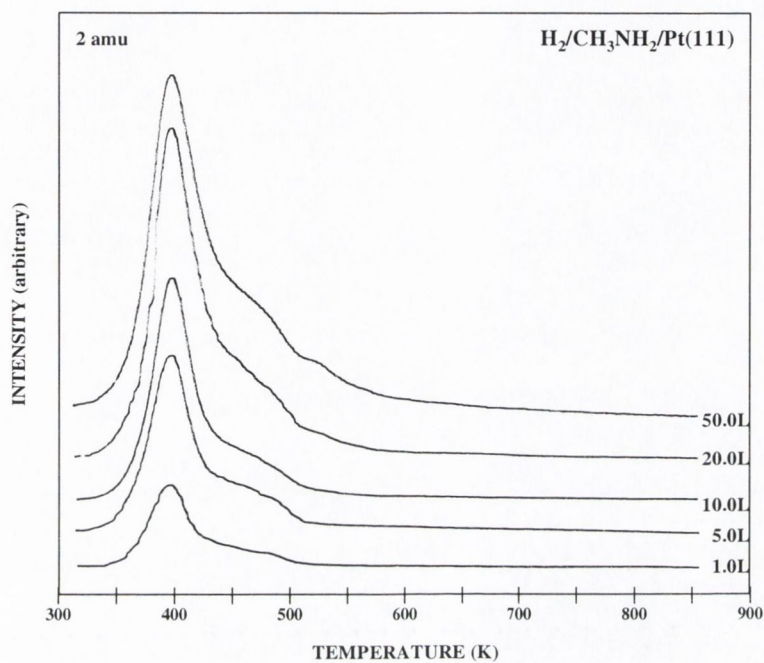


Fig. 3.4 Thermal desorption spectra of H₂ following exposures of methylamine to Pt(111).

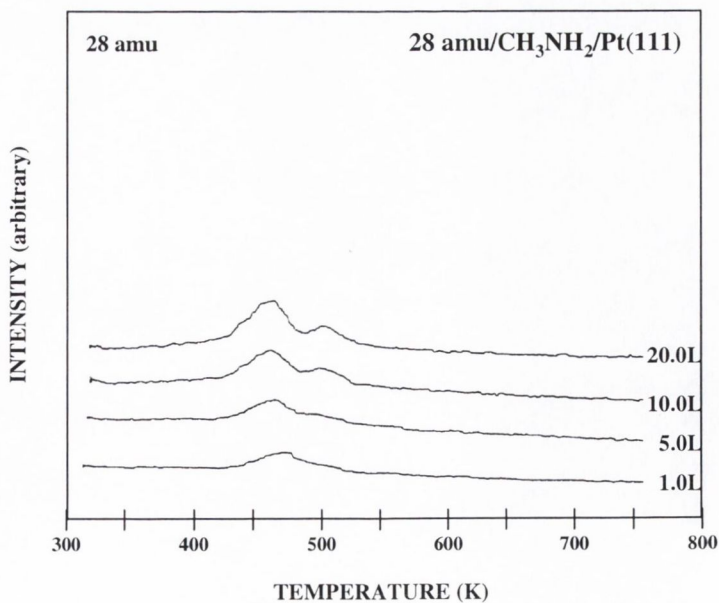


Fig. 3.5 Thermal desorption spectra at 28 amu following exposures of methylamine to Pt(111).

Peaks for 16 amu (~417K), 17 amu (~460K) and 30 amu (~382K) were also observed.

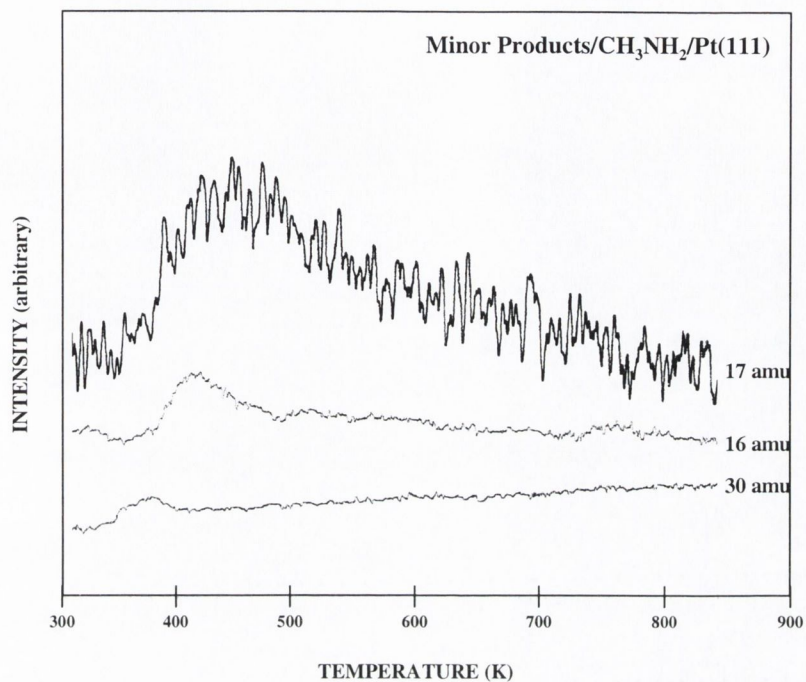


Fig. 3.6 Thermal desorption spectra of minor products following 10L exposure of methylamine to Pt(111).

The XPS data for Pt(111) exposed to MA at 140K were recorded for a set of annealing temperatures corresponding to the desorption processes of the various decomposition products (see figure 3.7). The electron analyser was set at a pass energy of 90eV. The photon source was the Al-K α anode. Measurements were taken in the C_{1s} and N_{1s} regions. One hundred scans per C_{1s} and N_{1s} window were recorded, with a range for each window of 25eV. All peaks were referenced to the Fermi level. The results are shown in figures 3.8 and 3.9. Interpretation of the data is complicated by the fact that all spectra were taken after the crystal had been allowed to cool back to adsorption temperature. It is possible that some re-adsorption of MA may have occurred during the cooling process.

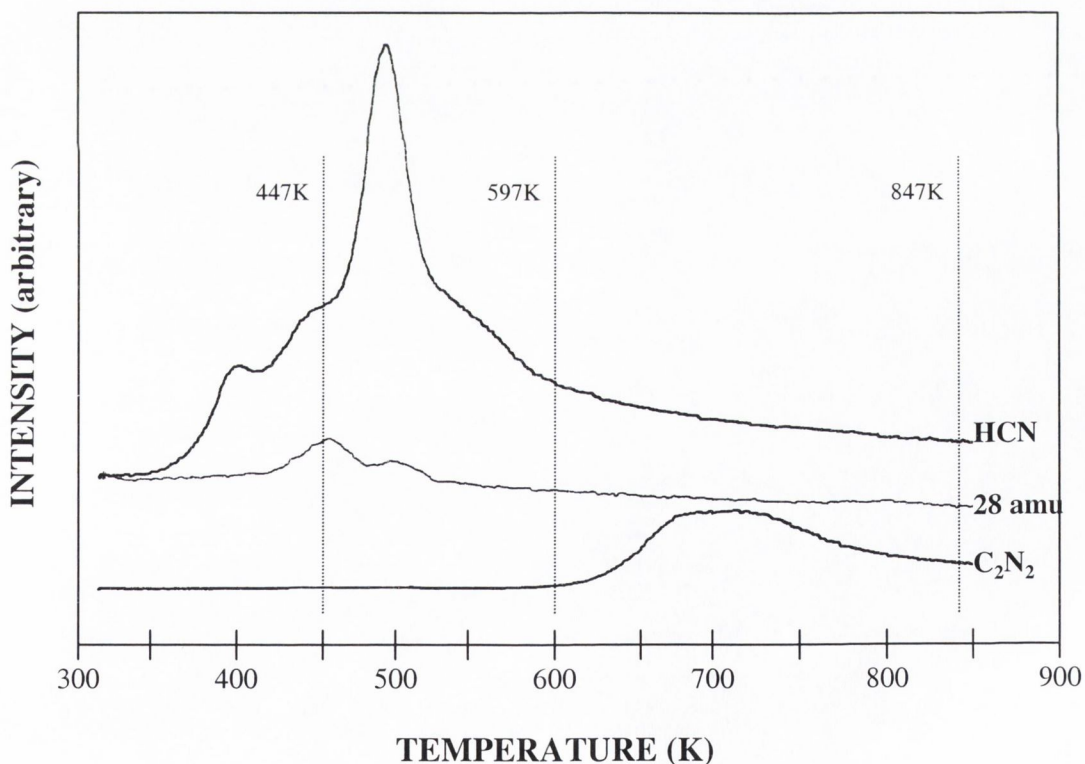
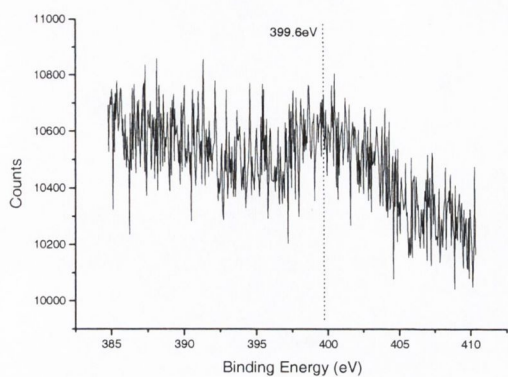
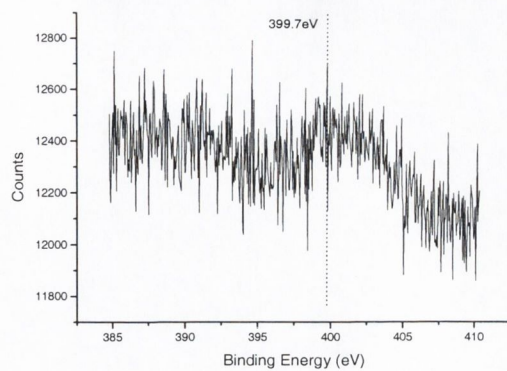


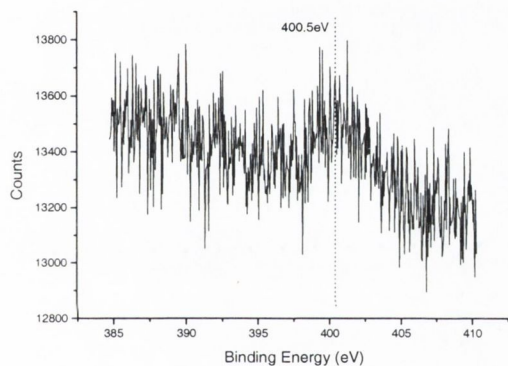
Fig 3..7 Diagram of annealing temperatures employed during the XPS experiments on Pt(111) following MA adsorption.



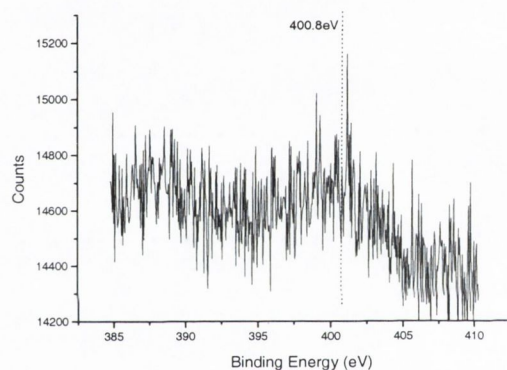
(a)



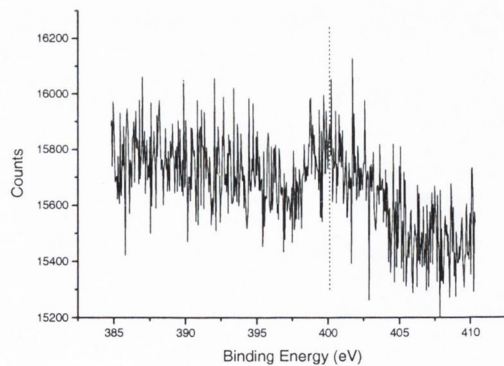
(b)



(c)

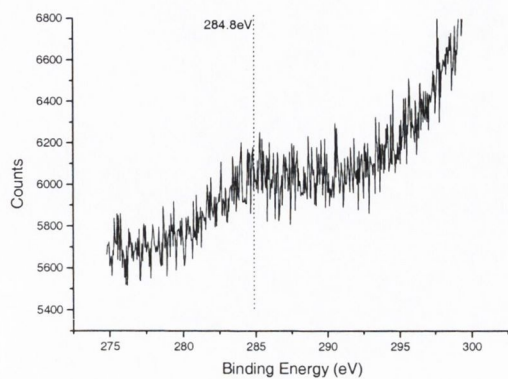


(d)

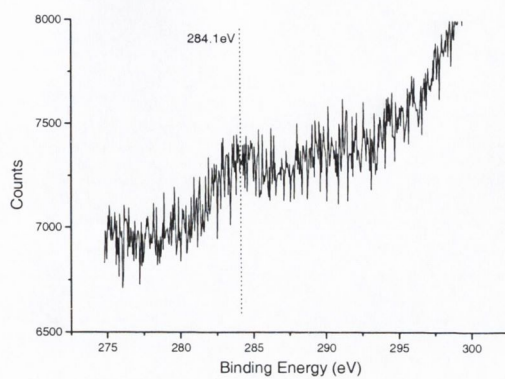


(e)

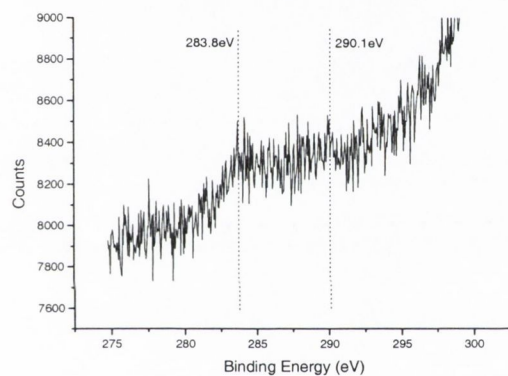
Fig. 3.8 N1s XPS following MA adsorption on Pt(111):
 (a) 132K; (b) 273K; (c) 447K; (d) 597K; (e) >874K.



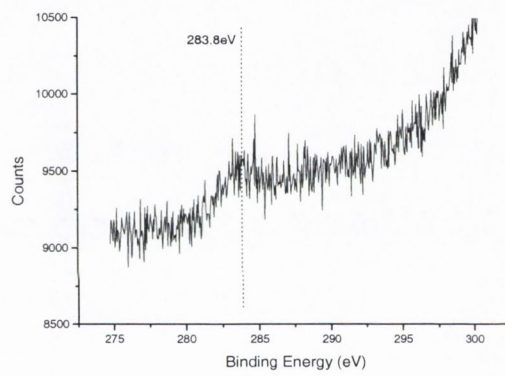
(a)



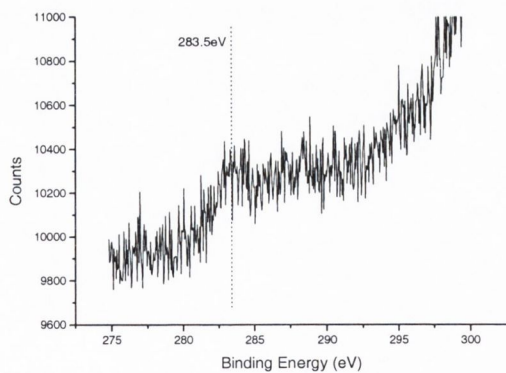
(b)



(c)



(d)



(e)

Fig. 3.9 C1s XPS following MA adsorption on Pt(111):

(a) 132K; (b) 273K; (c) 447K; (d) 597K; (e) 847K.

3.1.2 Methylamine on Pt(331)

The main thermal desorption products observed upon exposure of the Pt(331) surface to methylamine at 300K were HCN, C₂N₂, H₂ and 28 amu. Sets of thermal desorption spectra for these products are shown in figures 3.10 - 3.12.

Two peaks are noted for HCN at ~439K and ~396K. The desorption temperatures are significantly lower than for Pt(111) and clearly indicate the influence of the (331) steps.

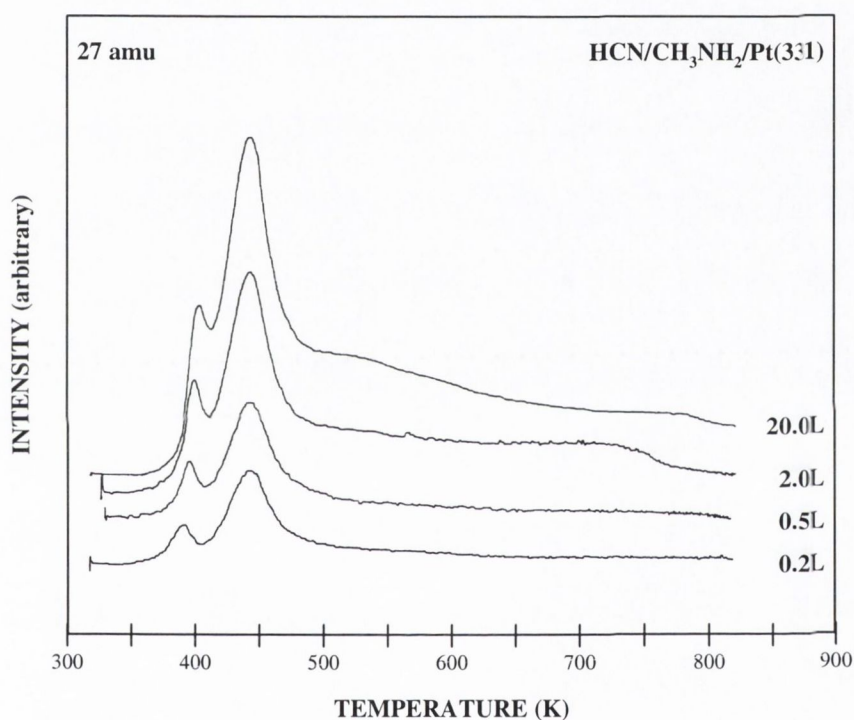


Fig. 3.10 Thermal desorption spectra of HCN following exposures of methylamine to Pt(331).

A single peak is produced for C₂N₂ desorption. This peak shifts to lower temperatures upon increasing exposure of methylamine. This shift is from ~722K for a 0.02L exposure to ~696K for a 1L exposure.

The H₂ desorption spectra exhibit two peaks, a main peak at ~386K and a lesser peak at ~437K.

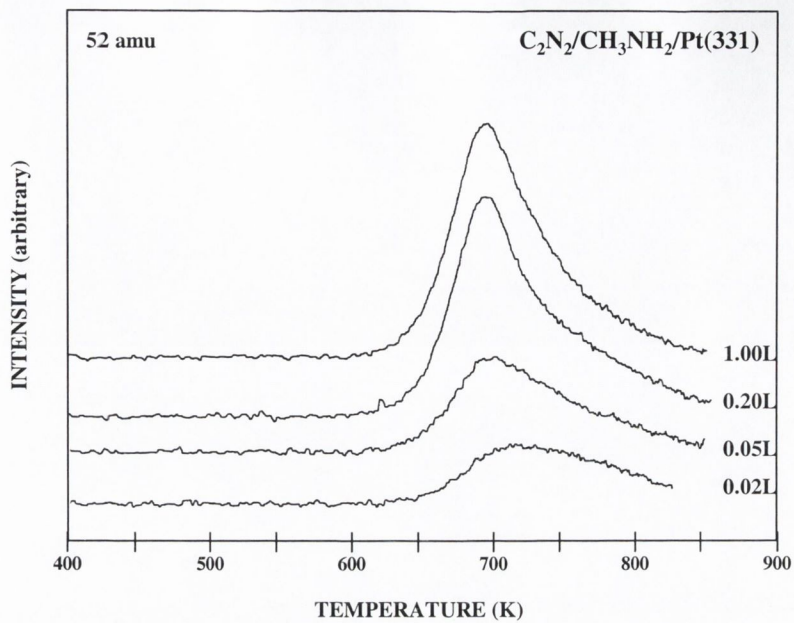


Fig. 3.11 Thermal desorption spectra of C₂N₂ following exposures of methylamine to Pt(331).

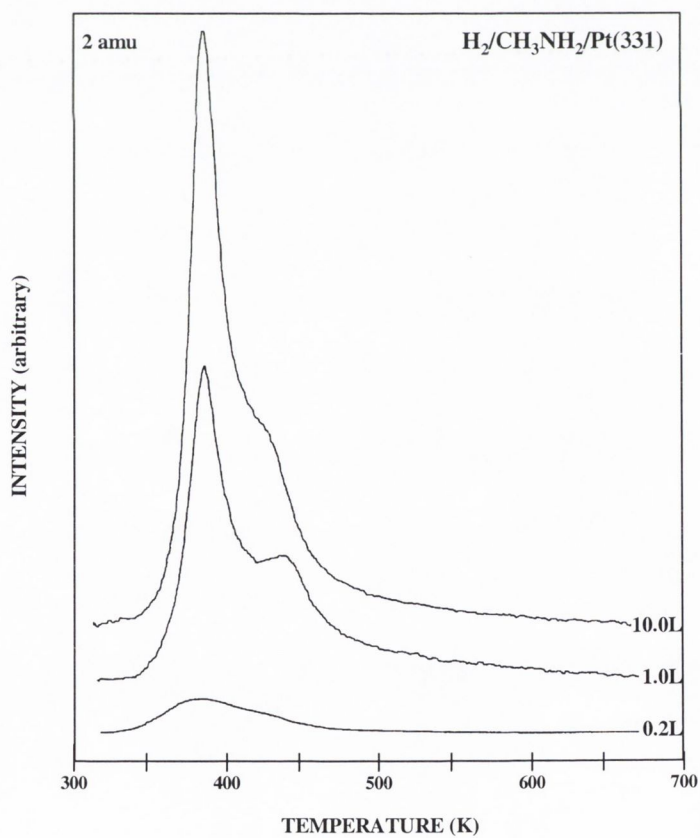


Fig. 3.12 Thermal desorption spectra of H₂ following exposures of methylamine to Pt(331).

Measurements taken at 28 amu produced three desorption signals at ~434K, ~523K and ~855K. Minor products were detected at ~450K for 16 amu, ~445K for 17 amu and ~383K for 30 amu.

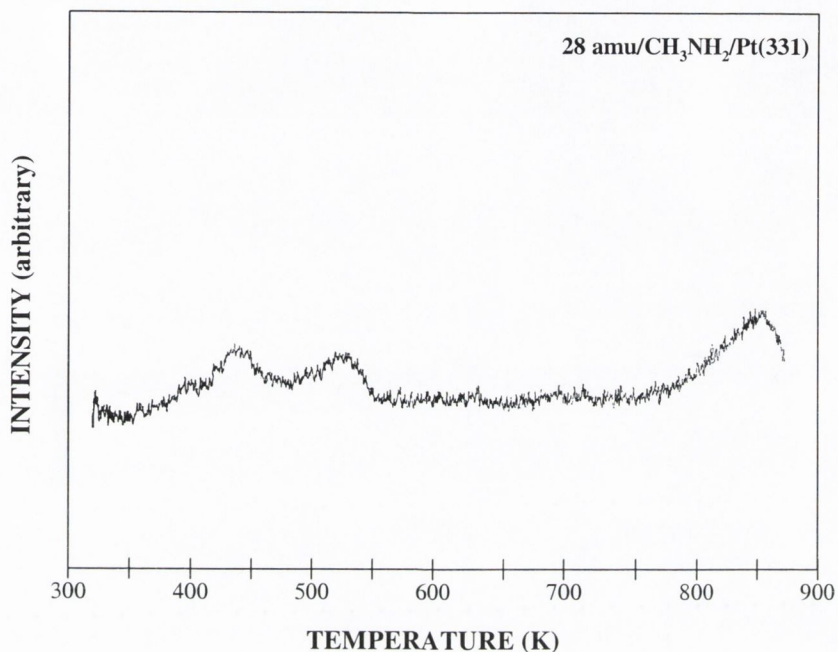


Fig. 3.13 Thermal desorption spectrum of 28 amu following exposure of methylamine to Pt(331).

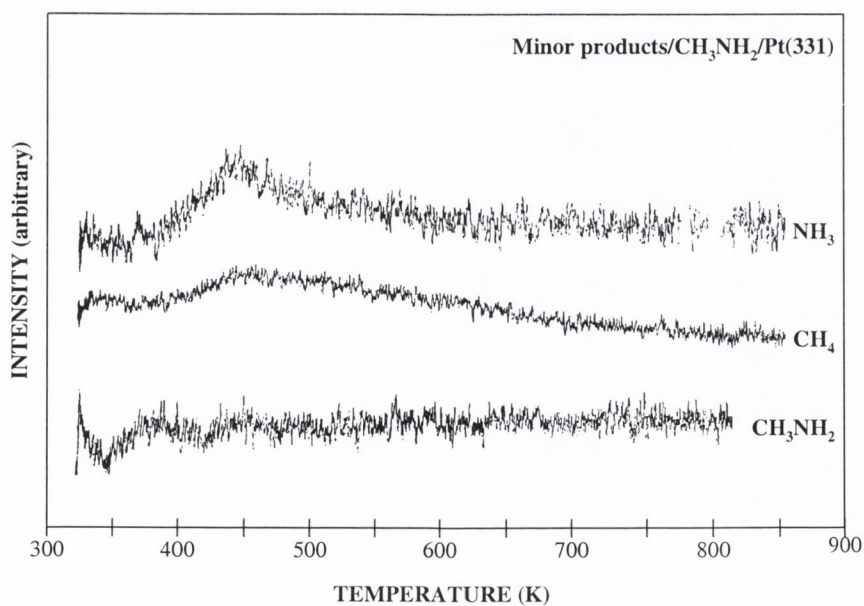


Fig. 3.14 Thermal desorption spectra of minor products following exposures of methylamine to Pt(331).

XPS spectra were collected under the same conditions as outlined in section 3.1.1. However, the Pt(331) crystal attained a lower temperature of 119K. The results are shown in figures 3.15 – 3.17.

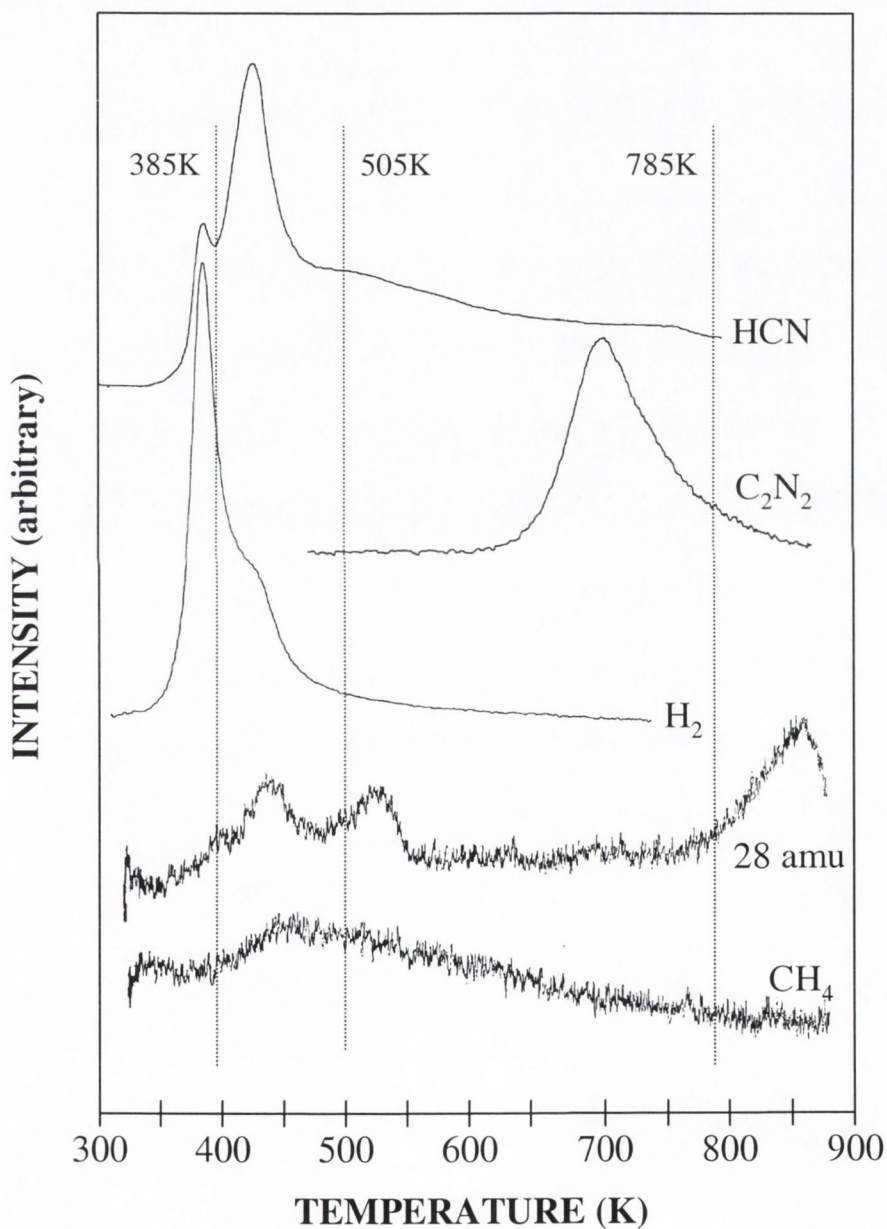
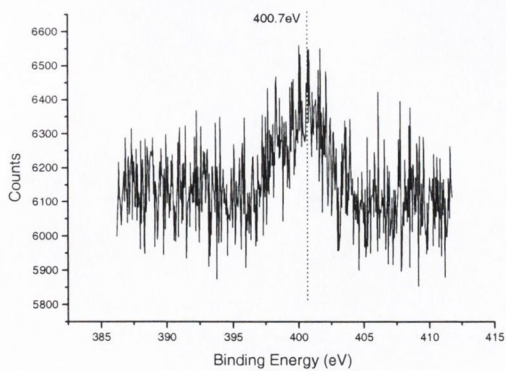
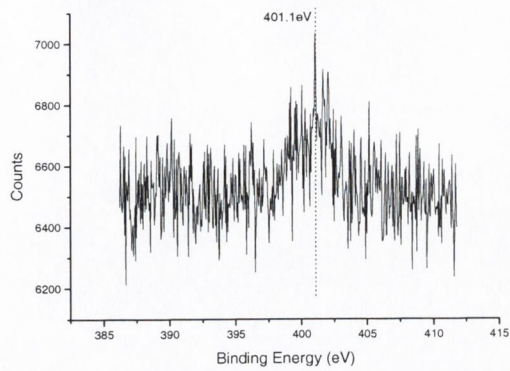


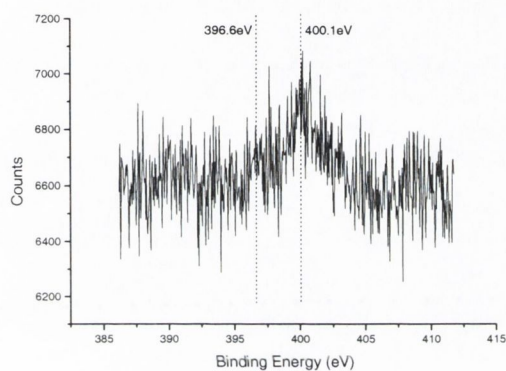
Fig 3.15 Diagram of annealing temperatures employed during the XPS experiments on Pt(331) following MA adsorption.



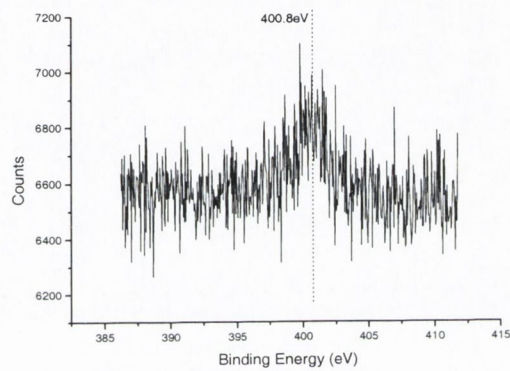
(a)



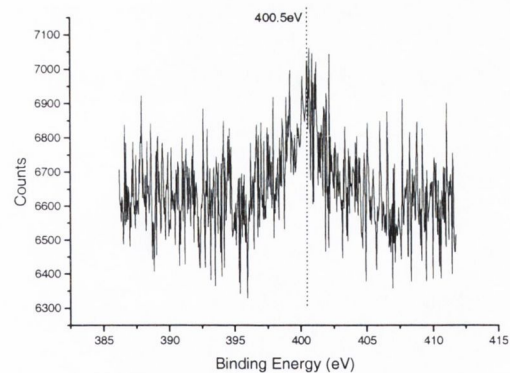
(b)



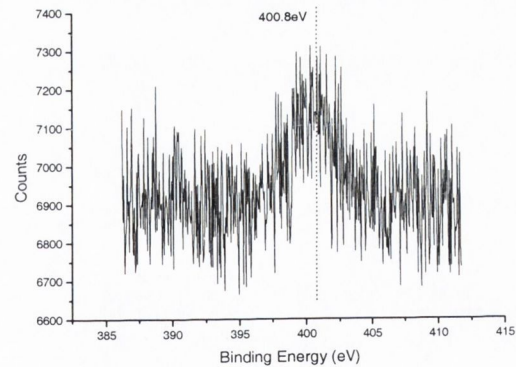
(c)



(d)



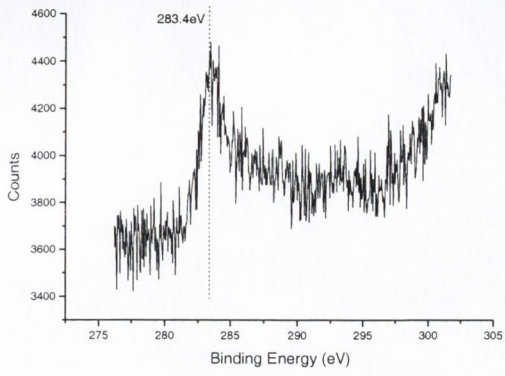
(e)



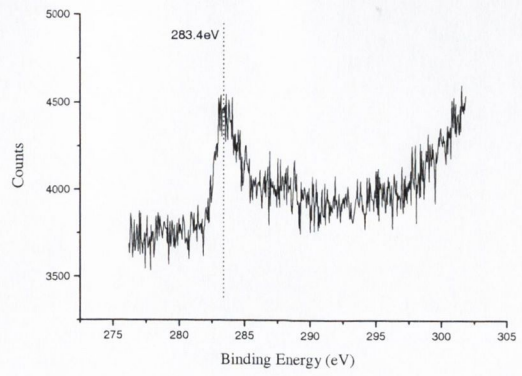
(f)

Fig. 3.16 N1s XPS following MA adsorption on Pt(331):

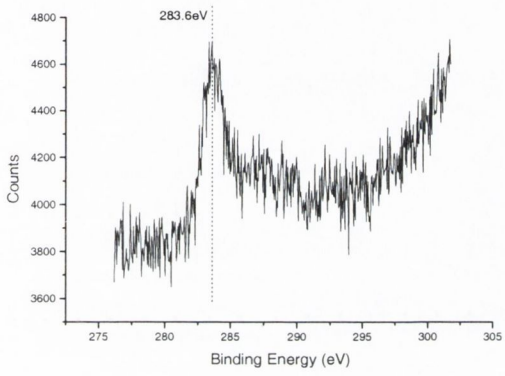
(a) 119K; (b) 273K; (c) 385K; (d) 505K; (e) 711K.



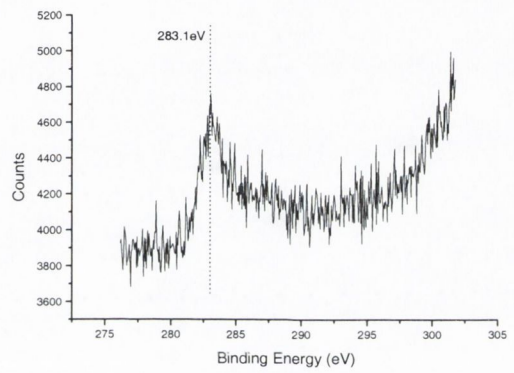
(a)



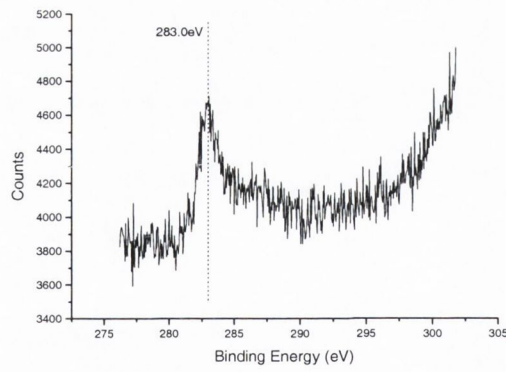
(b)



(c)



(d)



(e)

Fig. 3.17 C1s XPS following MA adsorption on Pt(331):

(a) 123K; (b) 273K; (c) 385K; (d) 505K; (e) 711K.

3.2 DISCUSSION

3.2.1 HCN desorption

The most striking difference between the HCN desorption spectra obtained from Pt(111) and those obtained from Pt(331) is the temperature of the main desorption peak (see Table 3.1). On Pt(111) the main peak is at 492K, whereas on Pt(331) it is at 439K, corresponding in temperature to the second desorption feature on the Pt(111) spectra.

	Pt(111) ¹			Pt(331) ²	Pt(110) ³
	(a)	(b)	(c)		
H ₂	394 (M) 442 - 503 508 - 543	420 (M) 480 520	375 385 410 >460	386 437	464 538 - 611 625 - 738
HCN	396 447 492 (M) 527 - 590	390 (low θ) 480 (M) 520 560 (high θ)	383 443 471 513(M) 565	396 439 (M)	400 434 (M) 515 - 642
C ₂ N ₂	611 - 800 ~672 (β_1) ~720 (β_2)	700 - 1200 710 810 1150	 751	722 - 696 696 722	 730 765 840
16 amu	417	420	320 420	450	425
17 amu	460			445	449
28 amu	458 500	 ~500 ~780	386 420 530 >800	434 523 855	434 512 826
30 amu	382	~380	380	383	

- 1 (a) this work
- (b) Hwang *et al.* [75]
- (c) Bridge and Somers [43]
- 2 this work.
- 3 E. Timothy, work in progress.

(M) = main peak.

Table 3.1 Peak temperatures of desorption products following methylamine adsorption.

There is no evidence of a peak at 492K on Pt(331) (although at higher coverages its presence may be obscured by the presence of a long high temperature tail). Chrysostomou [32] obtained similar results for HCN desorption following HCN adsorption on Pt(111) and Pt(331) – a peak at 460K on Pt(111) and a peak at 430K on Pt(331) (see Table 3.2). Furthermore, by exposing pre-adsorbed CN_{ads} species on Pt(331) to H_2 , he was able to reproduce the 430K peak. Similar experiments carried out by Hagans *et al.* [94] on Pt(112) and Levoguer and Nix [95] on a polycrystalline platinum foil yielded similar results, as did studies by Bridge and Lambert [96] of C_2N_2 co-adsorbed with H_2 on Pt(110). Pt(112) is a stepped crystal surface with three atom wide (111) terraces separated by a single atom step similar to Pt(331), but with a (100) step. The platinum foil used by Levoguer and Nix was found to contain a large concentration of step-like defects and comparatively few (111) terrace domains [97]. Clean Pt(110) exhibits “missing row” reconstruction, in which alternate rows of platinum atoms along the [110] direction are removed completely from the surface giving a stepped surface consisting of (111) oriented terraces. From these experiments it is reasonable to assume that the HCN peak at 439K on Pt(331) is the result of $H_{ads} + CN_{ads}$ recombination.

As stated earlier, the HCN peak at 439K on Pt(331) corresponds in temperature to the second feature on the HCN spectrum obtained in this work and that of Bridge and Somers [43] following MA adsorption on Pt(111). It is possible, therefore, that $H_{ads} + CN_{ads}$ recombination is the source of this peak on Pt(111). A question arises, however, as to whether this peak is a product of the (111) surface or a product of defects on the surface. In the spectrum of Bridge and Somers the 443K peak, along with a peak at 510K, predominates. However, the corresponding features in this work do not predominate and are in fact merely low and high temperature shoulders to a dominant 492K peak. Hwang *et al.* [75] detected no peak or shoulder around 445K following MA adsorption on Pt(111) at room temperature and, as in this work, only a high temperature shoulder to a predominant 480K peak. As part of the same study Hwang *et al.* carried out $CN_{ads} + H_2$ coadsorption experiments on Pt(111). They detected no significant HCN production. Chrysostomou repeated this experiment during his study of HCN adsorption on Pt(111) and again no HCN desorption was detected, in contrast to the results obtained for Pt(331), as mentioned earlier. Furthermore, the peak at 510K in the work of Bridge and Somers corresponded to a peak at the same temperature in the HCN spectrum following HCN adsorption on the same crystal

[98]. Subsequent polishing of this particular crystal by Chrysostomou [32] resulted in the complete disappearance of this peak in the resulting HCN/HCN/Pt(111) spectrum. Chrysostomou concluded that this peak was generated at defect sites. The same conclusion was drawn by Hagans *et al.* [94]. The overall conclusion that can be drawn from these results is that the presence of the 447K feature and the high temperature shoulder to the 492K peak in this work are probably the result of surface defects on the Pt(111) crystal.

	MA/Pt(111) ¹	HCN/Pt(111) ²	MA/Pt(331) ¹	HCN/Pt(331) ²	MA/Pt(110) ³	HCN/Pt(110) ⁴
H ₂	394 (M) 442-503 508-543	395 460	386 437	380 430	464 538-611	~410
HCN	396 447 492 (M) 527-590	shoulder 460 (M)	396 439	~370 430	400 434 515-642	~420
C ₂ N ₂	611-800 ~672 (β_1) ~720 (β_2)	> 600	722-696 696 722		730 765 840	~760 ~845
16 amu	417		450			
17 amu	460		445			
28 amu	458 500		434 523 855			
30 amu	382		383			

1 = this work.

2 = D. Chrysostomou, Ph.D thesis (1997).

3 = E. Timothy, work in progress.

4 = Bridge and Lambert [96].

(M) = main peak.

Table 3.2 Comparison of HCN and MA desorption products and peak temperatures (K).

Since no H_{ads}. + CN_{ads}. recombination has been detected on Pt(111) [32, 75] these peaks have both been assigned to decomposition processes in which the H-C-N bonds of the desorbing molecule remain intact. The high temperatures of desorption have been attributed to the formation of a stable intermediate species or complex. The results presented in this work offer no direct evidence as to the nature of any intermediate state formed during the adsorption/desorption process. However, various models have been proposed by others:

Following the adsorption of MA on Pt(111) at 85K Erley and Hemminger [45] found, using IRAS and HREELS, that upon heating the MA covered surface to temperatures in the range 350K to 390K new IR bands were observed in the spectrum. Bridge and Somers [43] found that heating the surface to 380K produced a change from a diffuse (1x1) LEED pattern to a (2x2) pattern. Simply by adsorbing HCN onto Pt(111) at 300K without any subsequent heating, Jentz *et al.* [100] obtained an IR spectrum identical to that obtained by Erley and Hemminger above, as did Chrysostomou *et al.* [106], who also obtained a (2x2) LEED pattern. This led Chrysostomou to conclude that the same or very similar species acts as the intermediate in both HCN and MA adsorption. In the case of MA, the crystal clearly needs to be heated to 380K in order to initiate dehydrogenation before this intermediate can be formed.

Jentz *et al.* [100, 46] suggested the formation of aminomethylidyne (see figure 3.18) as the intermediate species in the decomposition pathway of HCN, MA and azomethane. In this proposed pathway decomposition to $H_{ads.} + CN_{ads.}$ occurs, upon heating HCN (molecularly adsorbed at 85K) above 100K. Further heating to >250K results in rehydrogenation of some of the $CN_{ads.}$ species to form HNC initially, followed by H_2NC (aminomethylidyne). At 300K this species coexists with $CN_{ads.}$. RAIRS and XPS studies [93] indicates that H_2NC forms two-dimensional hydrogen-bonded aggregates on the Pt(111) surface.

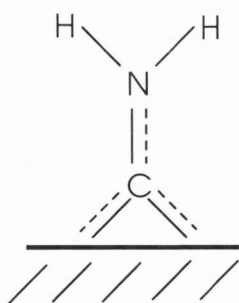


Fig. 3.18 Aminomethylidyne intermediate surface species proposed by Jentz *et al.* [100].

This H_2NC species fits the FT-IRAS spectral data very well [100]. However, a difficulty arises in reconciling this structure with TDS experiments [32, 94] in which no

HCN desorption was detected following $H_{ads.} + CN_{ads.}$ co-adsorption. If the aminomethylidyne model is correct an H-C bond must be formed. It may be that the aminomethylidyne intermediate formed below 300K allows intra-molecular transfer of hydrogen from the nitrogen to the carbon atom, whilst the orientation of the $CN_{ads.}$ species with the flat (111) surface either prevents $H_{ads.} + CN_{ads.}$ recombination or produces a hydrogenated intermediate which dehydrogenates in preference to HCN desorption. This explanation is not entirely satisfactory since Jentz *et al.* [100] detected the deuterated equivalent of aminomethylidyne following $D_2 + CN_{ads.}$ co-adsorption experiments similar to the $H_2 + CN_{ads.}$ experiments of Hagans *et al.* [94] and Chrysostomou [32].

Erley and Hemminger proposed a *cis* – HCNH species as the intermediate formed during MA decomposition (see figure 3.19). Chrysostomou suggested that the same IR data could also be explained in terms of a HCN/HNC mixture, and proposed the formation of a hydrogen-bonded complex involving $HCN_{ads.}$, $HNC_{ads.}$, and upon heating, dehydrogenated $CN_{ads.}$ moieties, in which hydrogen-bonding provides stability for ‘HCN’ on the surface. XPS experiments by Lindquist *et al.* [42] on HCN/Pt(111) produced two clearly resolved N_{1s} signals of equal intensity, with a separation of 1.6 – 1.7 eV, in the temperature range in which a (2x2) LEED structure was observed [32]. Lindquist *et al.* proposed a partially dissociated mixture of $HCN_{ads.} + H_{ads.} + CN_{ads.}$. The IR data obtained by Chrysostomou *et al.* [106] did not support the presence of $CN_{ads.}$. However, the presence of a 50/50 mixture of two separate nitrogen-containing species could be explained by the HCN/HNC model if isomerization of alternate molecules occurs. Whatever the intermediate formed, the evidence suggests that it forms a hydrogen-bonded complex.

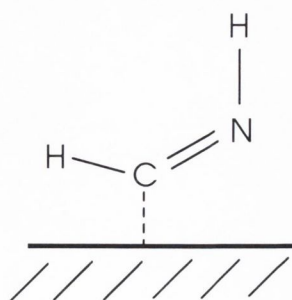


Fig. 3.19 Formimidoyl intermediate surface species proposed by Erley and Hemminger [45].

In the case of Pt(331), the introduction of a step to the (111) plane drastically alters the activity of the surface. HCN desorbs at a significantly lower temperature on Pt(331) than on Pt(111). Hagans *et al.* obtained a similar reduction in HCN desorption temperature following HCN adsorption on Pt(112). They suggested that HCN desorption from both Pt(111) and Pt(112) was the result of $H_{ads.} + CN_{ads.}$ recombination. To prove this they carried out $H_2 + CN_{ads.}$ coadsorption experiments on Pt(112) and found that they could reproduce the HCN peak for that surface. However, they seem to have made the assumption that the desorption process on Pt(111) is similar. As already mentioned on page 57 the HCN peak was not reproduced following $H_2 + CN_{ads.}$ co-adsorption experiments carried out by both Hwang *et al.* [75] and Chrysostomou [32]. However, Chrysostomou was able to reproduce the HCN/HCN/Pt(331) peak by repeating the co-adsorption experiment on Pt(331). Therefore $H_{ads.} + CN_{ads.}$ does indeed seem to be the pathway for HCN formation on Pt(331) following HCN adsorption, but is clearly not the pathway for the production of HCN from Pt(111). It may be that the tendency to form hydrogen-bonded 'chains' or aggregates may be limited or lost upon the introduction of steps to the (111) surface. As a result, dissociation may be favoured. This possibility of associative HCN formation also exists for MA adsorbed on a stepped surface. Both MA and HCN are believed to form the same intermediate on Pt(111), it may be that their response to the Pt(331) environment is similar.

The low temperature desorption feature in the HCN desorption spectra is present in all HCN spectra from MA and HCN adsorption on Pt(111), (331), (110), and (112), either as a peak or a low temperature shoulder to the main peak. This low temperature peak coincides with the main H_2 desorption peak, and is likely to be a decomposition product in which the original H-C-N bonds remain intact.

3.2.2 C_2N_2 desorption

The C_2N_2 thermal desorption spectra on both Pt(111) and Pt(331) exhibit broad features, in which there are probably the β_1 and β_2 desorption states obtained following adsorption of various CN containing compounds on the (111), (110), and (100) surfaces of palladium and platinum [40, 67, 69-74]. The β desorption state is attributed either to the recombination of CN_{ads} or the decomposition of a polymer-like CN_{ads} surface complex [42, 68, 74, 91, 92]. Netzer [67] proposed a polymer-like overlayer of CN_{ads} , suggesting that this would explain the apparent insensitivity to surface structure of the CN_{ads} species. Kingsley and Hemminger [68] supported the proposition of a surface polymer, suggesting the formation of a 'triazine-like' polymer. However, Kordesch *et al.* [101] found no evidence for such a polymer following HREELS investigations on Pd(111) and Pd(110).

CN_{ads} recombination is regarded as the most likely alternative to complex formation. At low coverages high temperature β_2 predominates. At such coverages, CN_{ads} moieties would be expected to have few near neighbours. It is probable, under these circumstances, that surface diffusion of CN_{ads} occurs prior to association. Such a process would be expected to display second order kinetics, and indeed, the behaviour of the β_2 peak is consistent with a second order thermal desorption process [21]. Furthermore, Hoffman *et al.* [69] observed isotopic exchange in the β_2 peak after both simultaneous and consecutive exposures to C_2N_2 and $^{13}C_2^{15}N_2$, consistent with the suggestion of surface migration. In contrast, only simultaneous exposures to C_2N_2 and $^{13}C_2^{15}N_2$ resulted in isotopic exchange in the low temperature β_1 peak. They proposed the formation of CN_{ads} islands with increasing coverage which prevent isotopic exchange upon subsequent adsorption of $^{13}C_2^{15}N_2$. Bridge and Lambert [96] suggested that 'island' formation is not necessary to explain the lack of isotopic exchange in the low temperature β_1 peak, but rather that associative desorption of CN_{ads} occupying adjacent sites occurs. This is in keeping with the first-order characteristics observed for the β_1 peak. Regardless, at least some degree of surface migration is likely, prior to association to produce the β_2 desorption peak.

On Pt(331) the β_1 peak rapidly dominates the C_2N_2 desorption spectrum upon increasing coverage, whereas on Pt(111) the β_2 peak remains a significant presence even after a 10L exposure of MA. It can also be seen in figure 3.20 that the amount of C_2N_2

produced relative to HCN is greatly increased on Pt(331). This was found to be the case for other stepped surfaces.

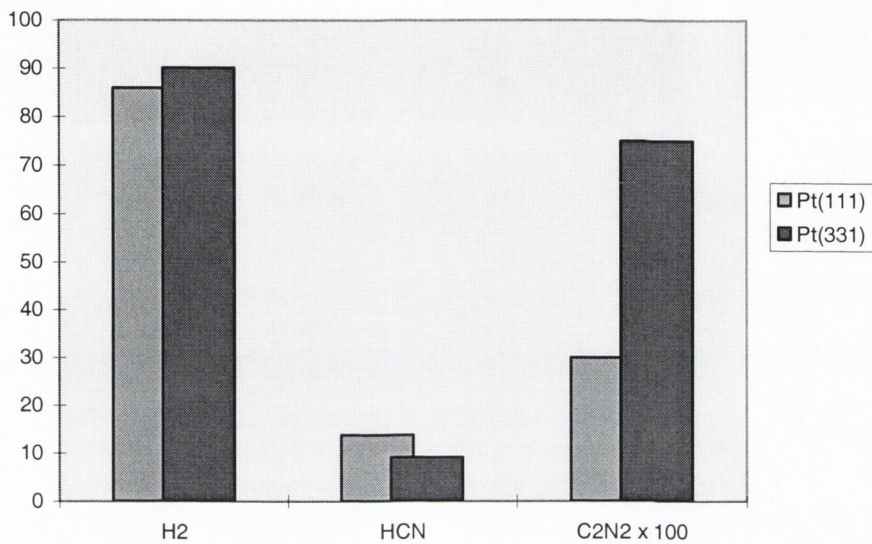


Fig. 3.20 Percentage increase or decrease in products desorbed from Pt(111) and Pt(331). The values presented are uncorrected for mass spectrometer sensitivity, and therefore do not reflect the absolute amounts of each product, but only the relative increase/decrease.

3.2.3 H₂ desorption

The main hydrogen desorption peak on Pt(111) is at 394K and spans a temperature range from 330K – 430K. Work done by Bridge and Somers [43] on CD₃NH₂ adsorption on Pt(111) produced desorption peaks for H₂ (375K), HD (385K) and D₂ (410K). The temperature spans for all three peaks are within that of the main H₂ peak for MA, indicating that dehydrogenation of both carbon and nitrogen atoms contributes to this peak. Based on these experiments, Bridge and Somers proposed a three-step dehydrogenation mechanism to form DCN, as shown:



However, the dehydrogenation process may not be so straightforward since this mechanism suggests that from about 385K to 410K the primary species is a CH₂N_{ads.} moiety, whereas HREELS and IRAS studies [45, 100] of the intermediate formed at this temperature indicate that the nitrogen atom is bonded to at least one hydrogen atom, as discussed in section 3.2.1.

The high temperature tails to the H₂ spectra on Pt(111) coincide with the main HCN desorption feature and its high temperature shoulder. As the intermediate HCN complex breaks up, some dissociation occurs resulting in H₂ formation.

The peak at 437K in the H₂ spectra from Pt(331) is the result of recombination of H_{ads.} species in competition to H_{ads.} + CN_{ads.} recombination.

3.2.4 28 amu desorption

The 28 amu desorption spectra for MA on both Pt(111) and Pt(331) exhibit two peaks. Two peaks are a characteristic of CO desorption from stepped Pt(111) surfaces [79, 89]. Since in both cases the desorption temperatures of the peaks correspond to desorption temperatures for CO on Pt(331) [32] they are assigned to CO adsorbed from the background. The low temperature peak is associated with desorption from (111) terraces, whilst the high temperature peak is associated with desorption from step edges. The Pt(111) crystal used in this work has been shown in section 3.3.1 to contain defect sites which produce HCN desorption features similar to those found on Pt(331). These same defect sites are clearly responsible for the appearance of the high temperature CO peak.

3.2.5 Minor Products

Minor products at 16 amu corresponding to methane, 17 amu corresponding to ammonia and 30 amu corresponding to molecular methylamine were detected following MA adsorption on both Pt(111) and Pt(331). They were also detected in the work of Somers and Bridge [98] on Pt(111) and that of Timothy [102] on Pt(110). However, the amount of these products generated in the desorption process is insignificant compared to the amount of main products formed, even when compared to the CO produced from background adsorption. These products can therefore be considered the result of defect sites.

3.2.6 XPS Experiments

The XPS data for methylamine are preliminary in nature, and further work will be undertaken in this laboratory in the future. The N1s spectra provide the most reliable information, since adsorption of background CO may complicate interpretation of the C1s data. The N1s peak for MA on Pt(111) exhibits the high binding energy associated with amines [104, 105]. On heating to 447K there is a shift to a higher binding energy of 400.5eV. This is prior to desorption from the main HCN peak and represents the formation of the intermediate species. The high binding energy suggests the amine character persists. Pt(331) seems to exhibit similar behaviour.

3.3 CONCLUSIONS

The introduction of a step to the Pt(111) surface does not alter the nature of the products formed following MA adsorption. However, it does alter the reaction mechanism and relative amounts of product formed, reducing the amount of HCN formed relative to H₂ and C₂N₂, and the temperature at which the bulk of the HCN desorbs.

Methylamine decomposition on Pt(111) seems to involve the formation of a hydrogen-bonded intermediate complex which stabilises the 'HCN', resulting in HCN desorption at an elevated temperature. HCN formation is therefore a decomposition rather than recombination process on Pt(111), in which the H-CN bond in the original molecule remains intact. A schematic representation of the thermal reaction mechanism for MA adsorbed on Pt(111) is shown in figure 3.21.

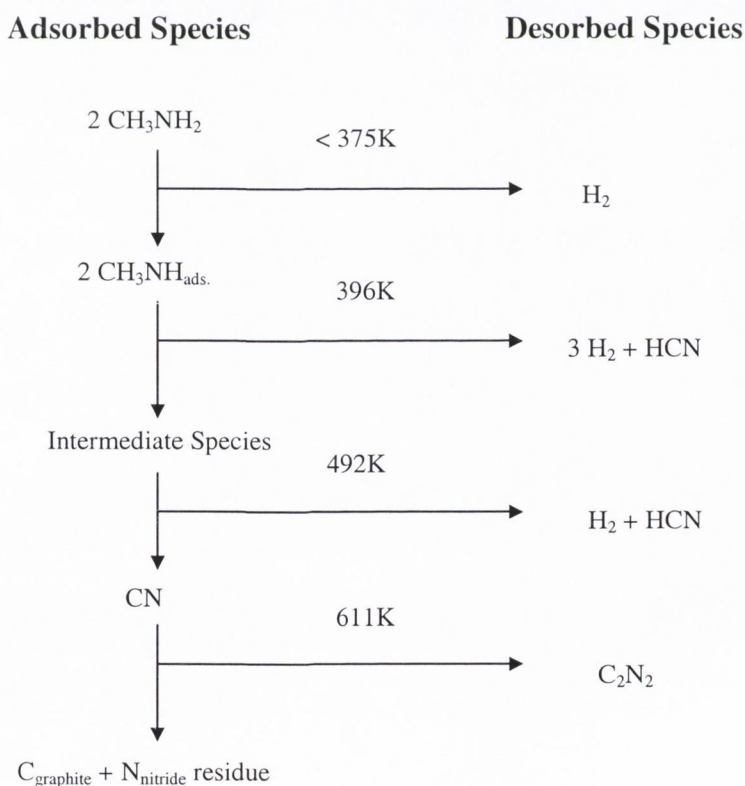


Fig. 3.21 Schematic of reaction pathway of methylamine on Pt(111).

The decomposition of methylamine on Pt(331) occurs at lower temperatures than on Pt(111). It appears that complete dissociation into $H_{ads.}$ and $CN_{ads.}$ species may be favoured. As a result HCN formation may include a process involving recombination of $H_{ads.} + CN_{ads.}$. This recombination process is in direct competition with $H_{ads.} + H_{ads.}$ recombination. Consequently, the amount of HCN produced relative to H_2 and C_2N_2 is smaller than that obtained from the stabilised intermediate on Pt(111). Figure 3.22 outlines the reaction mechanism for MA adsorbed on Pt(331).

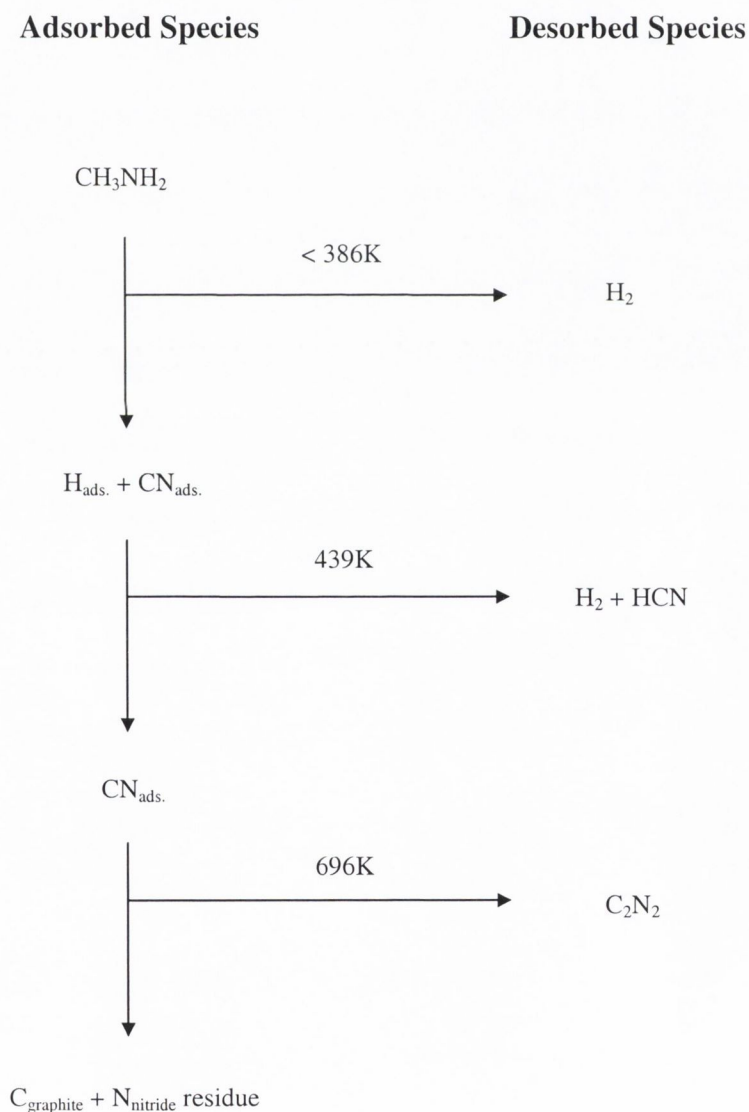


Fig. 3.22 Schematic of reaction pathway of methylamine on Pt(331).

Disparities between the thermal desorption spectra presented in this work and previous studies [43,75] of MA adsorbed on Pt(111) can be explained in terms of surface defects. Peaks present in this work and that of Bridge and Somers [43] but absent in the work of Hwang *et al.* [75] correspond in temperature to peaks obtained from Pt(331) and other stepped surfaces, and can therefore be assigned to step-like defects on the Pt(111) crystal surfaces used in this work and that of Bridge and Somers.

CHAPTER FOUR

DIMETHYLAMINE & TRIMETHYLAMINE ON Pt(111) AND Pt(331)

CHAPTER 4 DIMETHYLAMINE AND TRIMETHYLAMINE ON Pt(111) AND Pt(331)

4.1 RESULTS

4.1.1 Dimethylamine on Pt(111)

HCN, CH₄ and H₂ were the main thermal desorption products recorded following exposure of Pt(111) to dimethylamine (DMA) at 300K. Figures 4.1 - 4.4 show the desorption spectra obtained for each of these products. Peaks were also detected following measurements at 28 amu. No generation of C₂N₂ was observed.

HCN thermal desorption spectra show a peak at ~550K, a shoulder at ~570K, and a long high temperature tail.

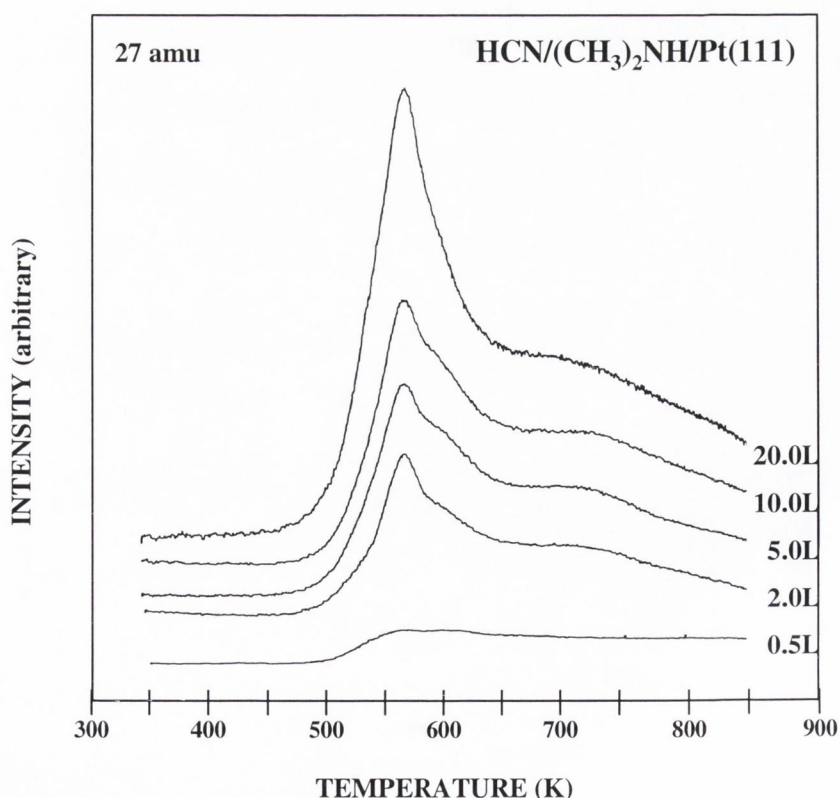


Fig. 4.1 Thermal desorption spectra of HCN following exposures of dimethylamine to Pt(111).

A broad methane peak at 446K was observed which saturated at 5L.

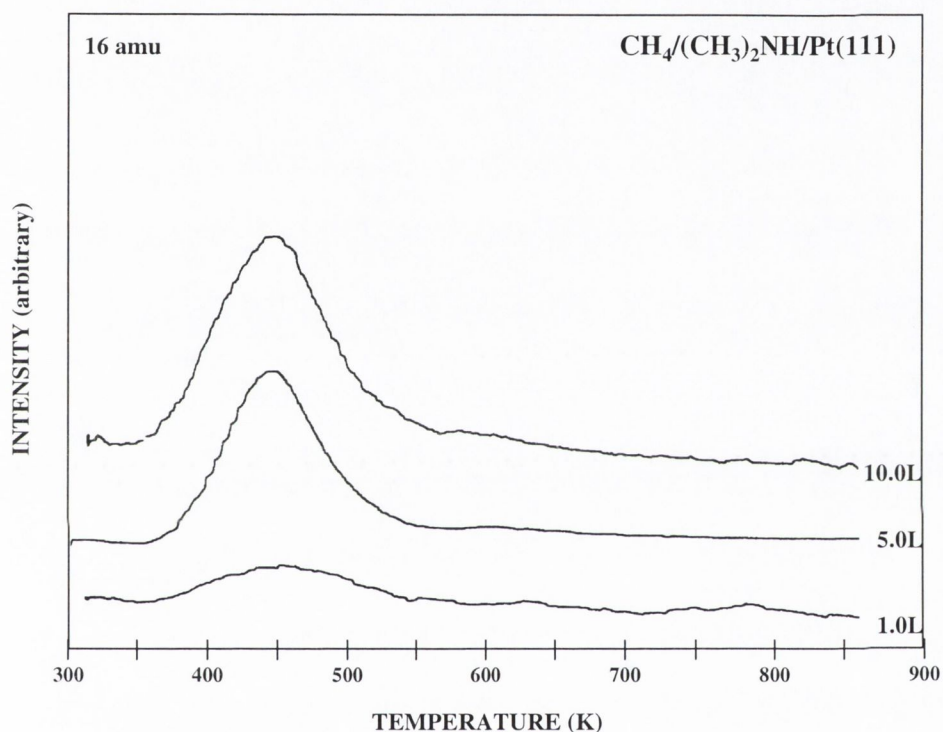


Fig. 4.2 Thermal desorption spectra of CH_4 following exposures of dimethylamine to Pt(111).

Three features are present in the hydrogen desorption spectra of DMA on Pt(111). Peaks at $\sim 466\text{K}$ and $\sim 527\text{K}$ predominate, whilst a small peak at $\sim 371\text{K}$ is apparent at low coverages, becoming a shoulder to the 466K peak at higher coverages.

Measurement at 28 amu results in a peak at $\sim 442\text{K}$ and a small rise in intensity between 550K and 650K .

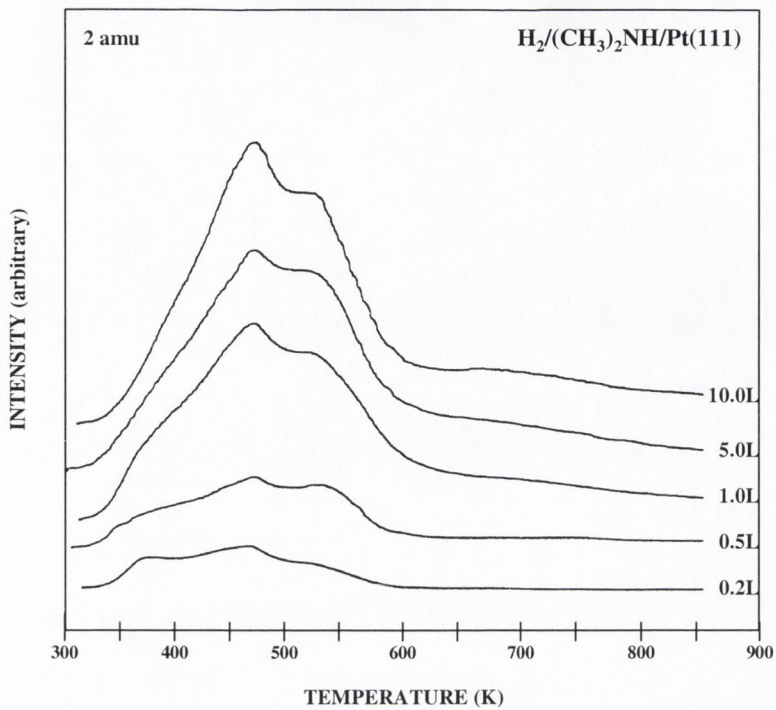


Fig. 4.3 Thermal desorption spectra of H₂ following exposures of dimethylamine to Pt(111).

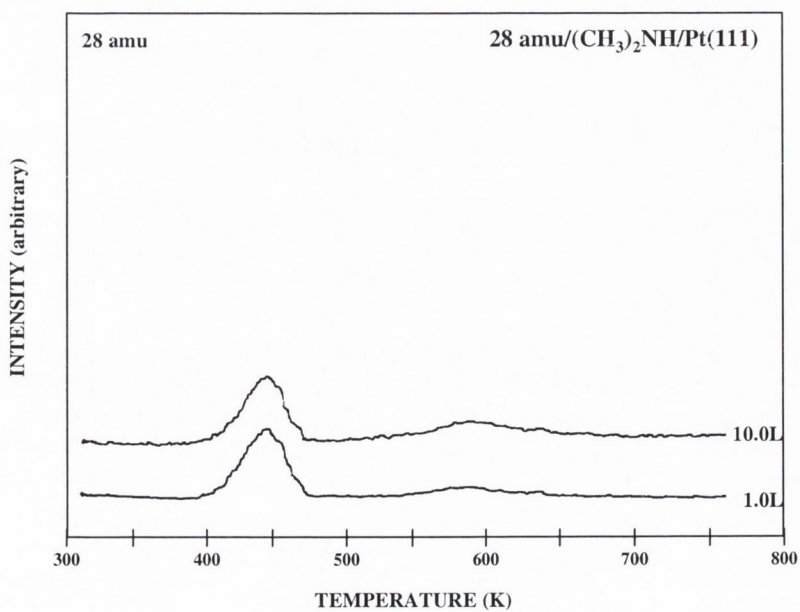


Fig. 4.4 Thermal desorption spectra at 28 amu following exposures of dimethylamine to Pt(111).

XPS spectra for DMA/Pt(111) were collected under the same conditions as outlined in section 3.1.1. The results are shown in figures 4.5 – 4.7.

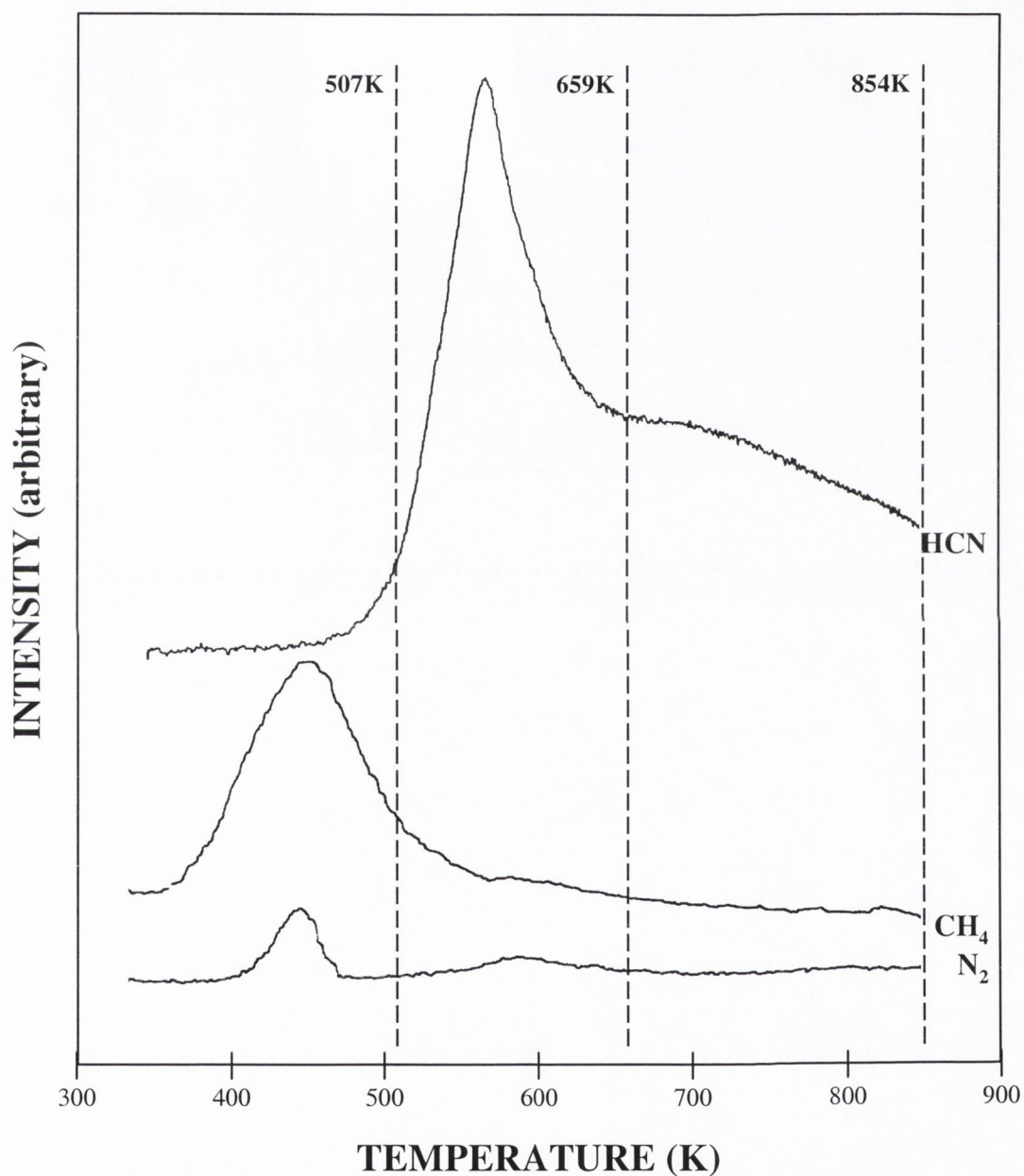


Fig. 4.5 Diagram of annealing temperatures employed during the XPS experiments on Pt(111) following DMA adsorption.

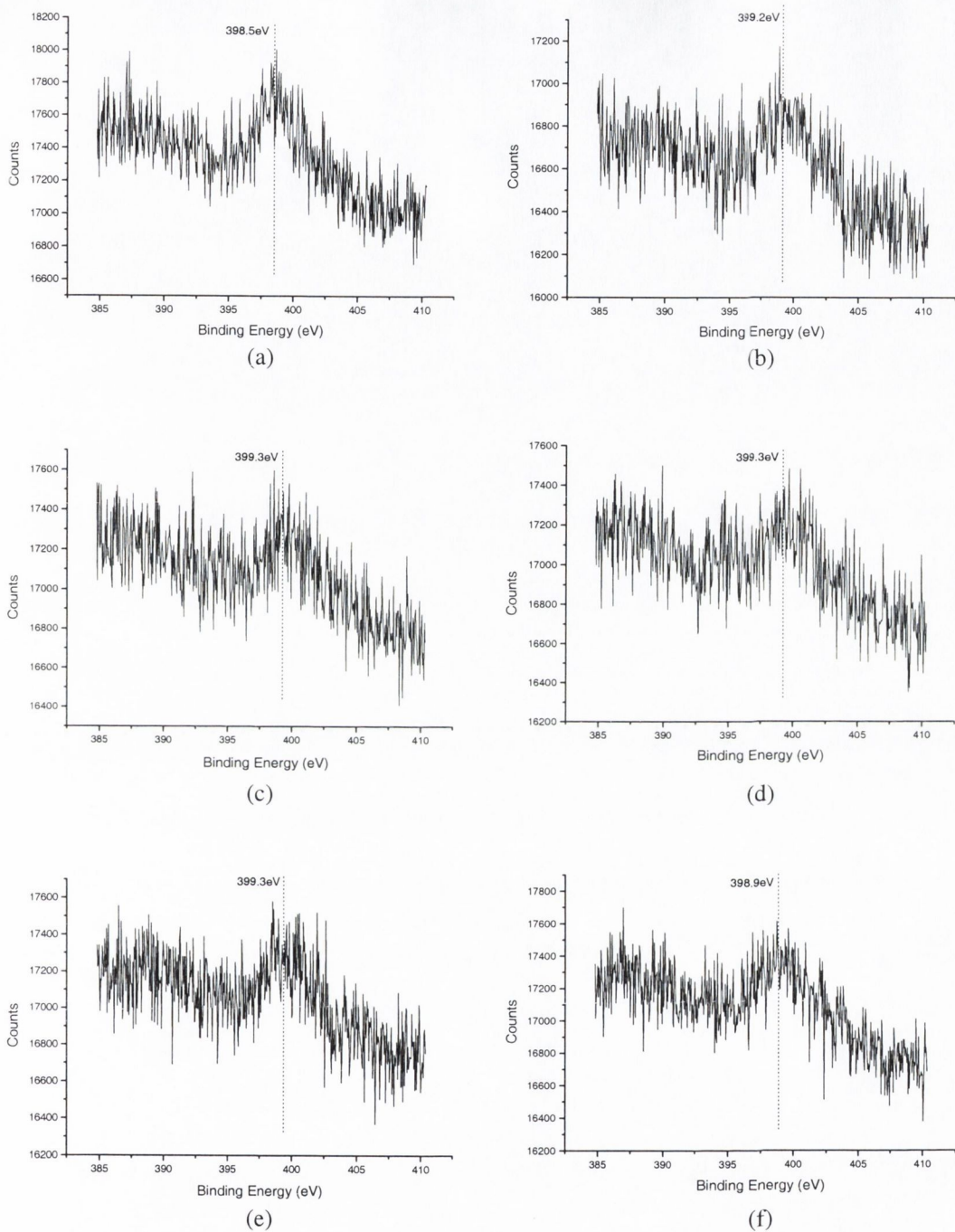


Fig. 4.6 N1s XPS following DMA adsorption on Pt(111):

(a) 136K; (b) 273K; (c) 514K; (d) 659K; (e) 854K; (f) >1000K.

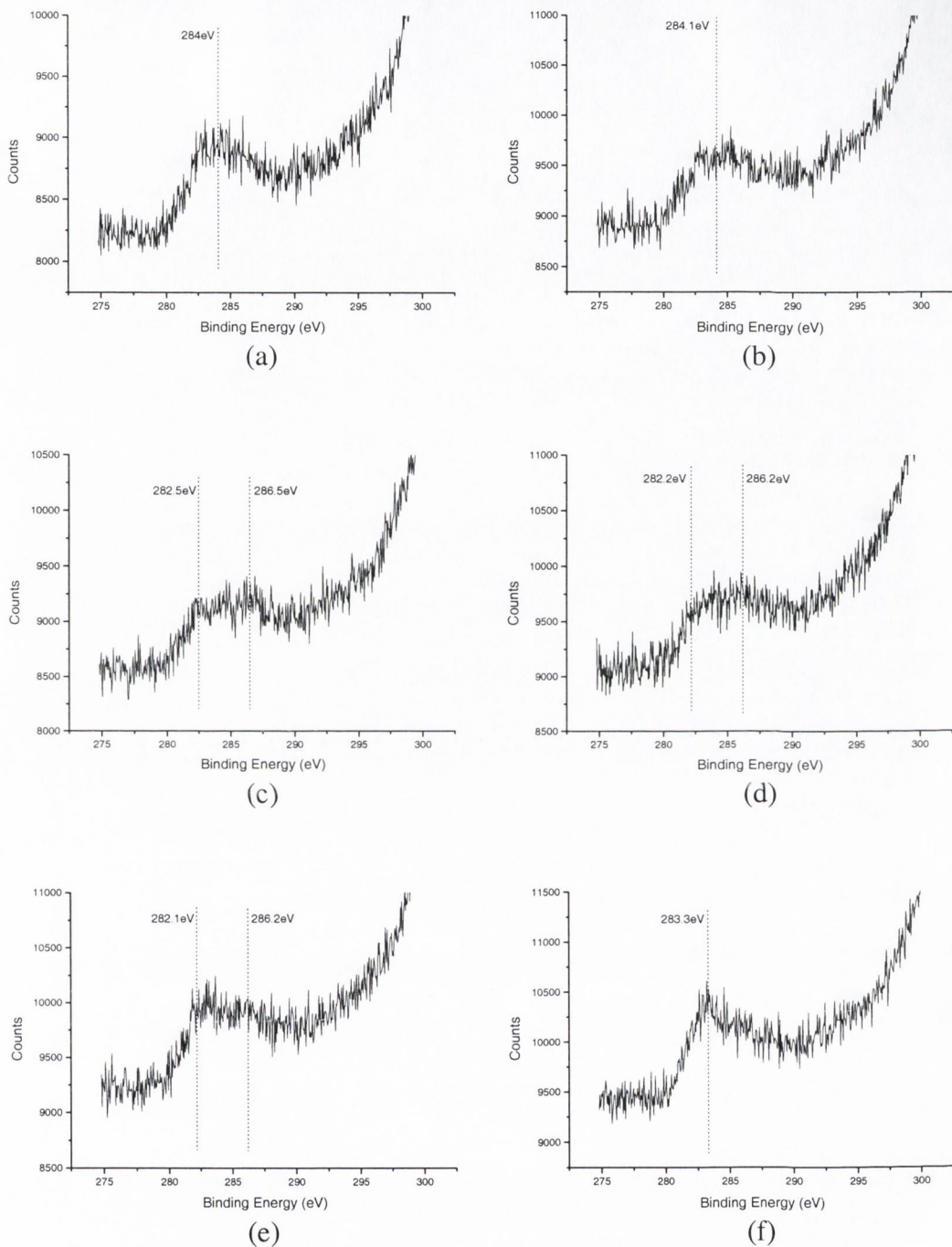


Fig. 4.7 C1s XPS following DMA adsorption on Pt(111):

(a) 143K; (b) 273K; (c) 507K; (d) 659K; (e) 854K, (f) >1000K.

4.1.2 Dimethylamine on Pt(331)

Dimethylamine adsorption on Pt(331) produced HCN, CH₄, and H₂ as the major thermal desorption products. In addition, two small peaks were detected following measurements at 28 amu. These desorption spectra are presented in figures 4.8 – 4.11. As in the case of DMA adsorption on Pt(111), no C₂N₂ desorption was observed.

A main peak at ~488K was obtained for HCN desorption, with a high temperature shoulder at ~572K developing at higher exposures.

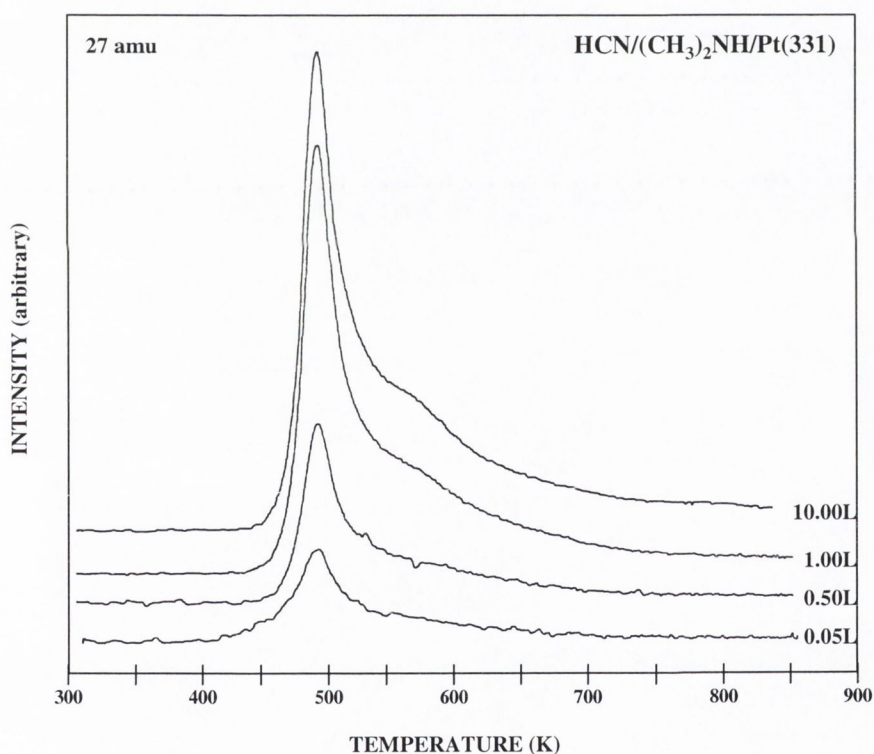


Fig. 4.8 Thermal desorption spectra of HCN following exposures of dimethylamine to Pt(331).

A single peak is observed at ~473K at 16 a.m.u. corresponding to CH₄. This is a broad peak spanning about 300K with desorption commencing at ~360K and ceasing above ~645K. Close examination of the spectra indicates a low temperature shoulder.

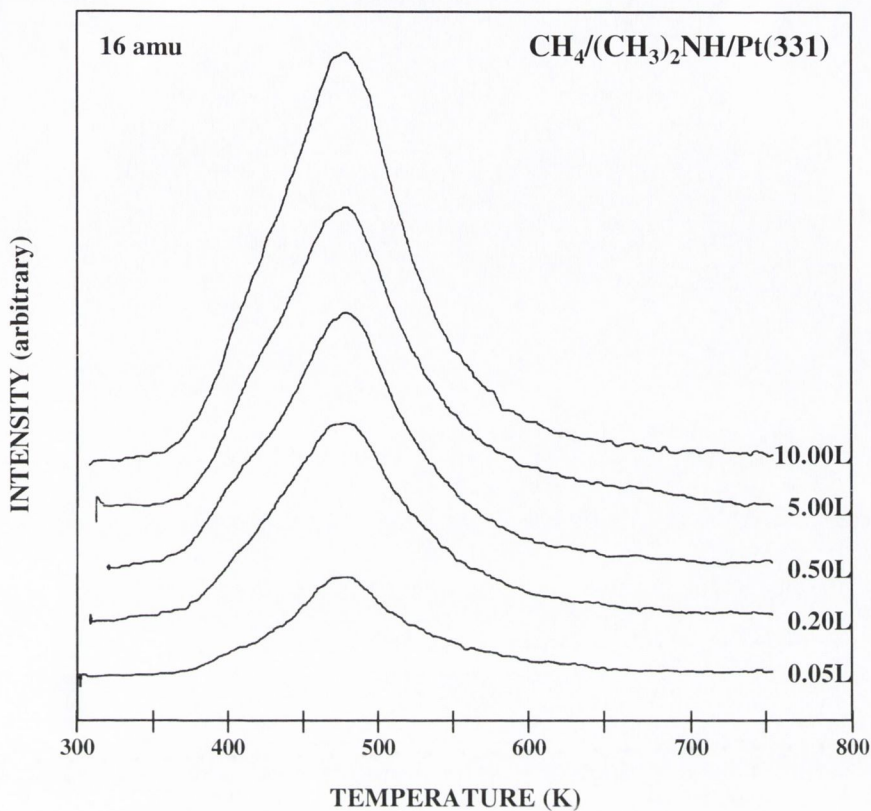


Fig. 4.9 Thermal desorption spectra of CH_4 following exposures of dimethylamine to Pt(331).

Two peaks were detected for H_2 desorption, the main peak at $\sim 460\text{K}$ and a second, lower temperature peak that shifts from $\sim 386\text{K}$ for a 0.2L exposure to $\sim 395\text{K}$ for a 1.0L, becoming a shoulder to the main peak at 10.0L.

Two peaks are present in the spectra recorded at 28 amu, at $\sim 452\text{K}$ and $\sim 491\text{K}$.

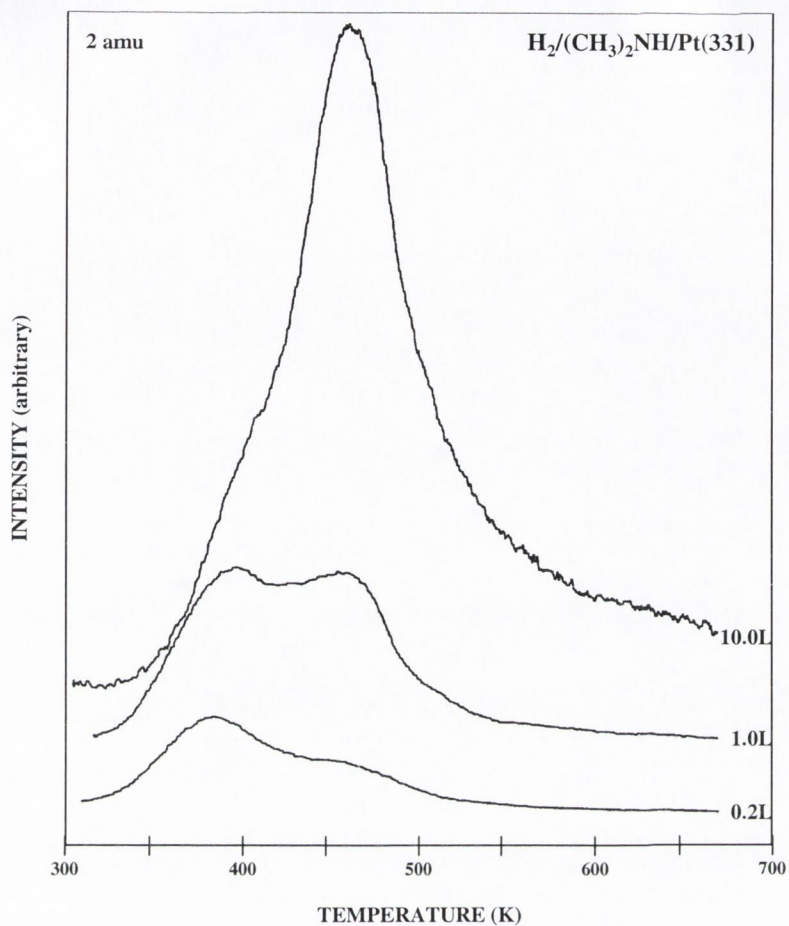


Fig. 4.10 Thermal desorption spectra of H₂ following exposures of dimethylamine to Pt(331).

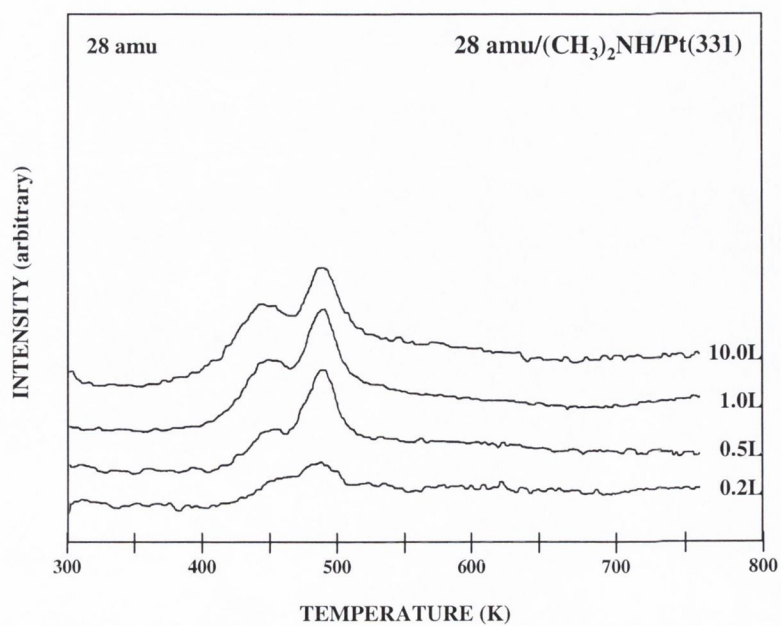


Fig. 4.11 Thermal desorption spectra at 28 amu following exposures of dimethylamine to Pt(331).

XPS spectra for DMA/Pt(331) were collected under the same conditions as outlined in section 3.2. The results are shown in figures 4.12 – 4.14.

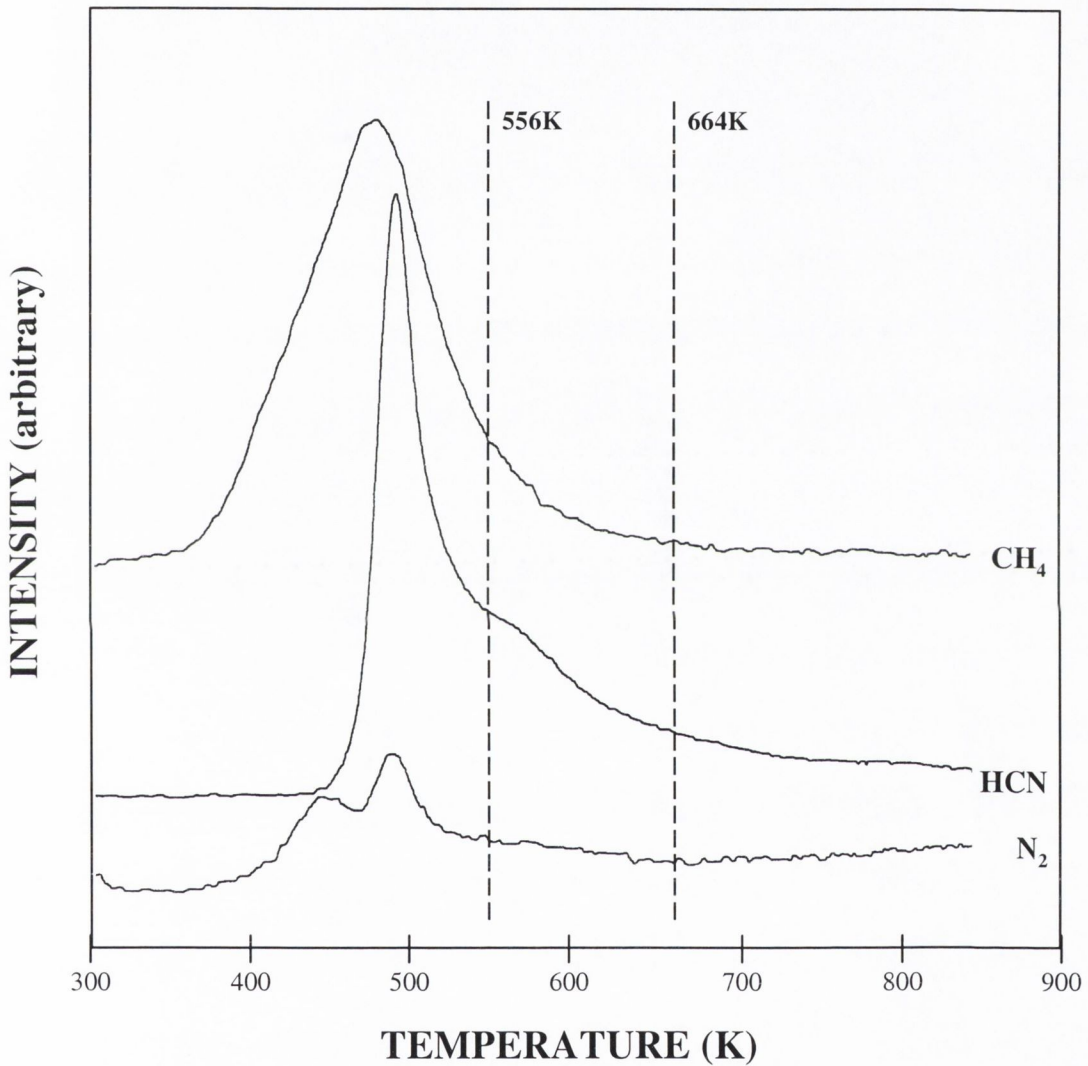
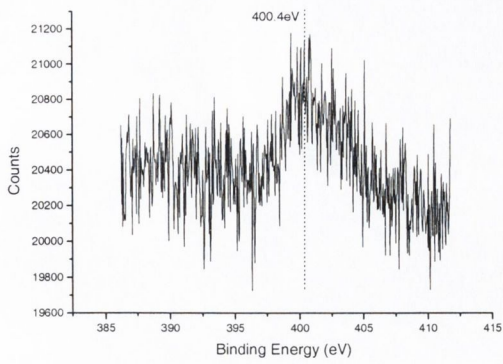
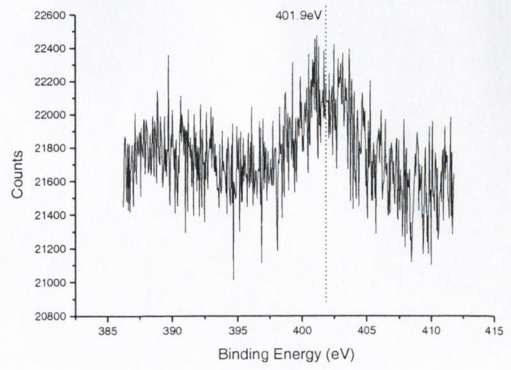


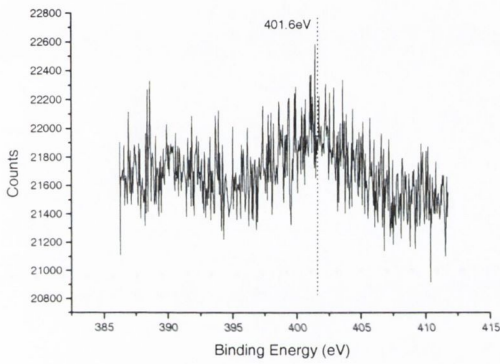
Fig. 4.12 Diagram of annealing temperatures employed during the XPS experiments on Pt(331) following DMA adsorption.



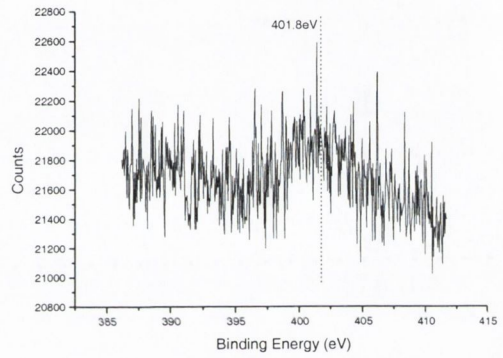
(a)



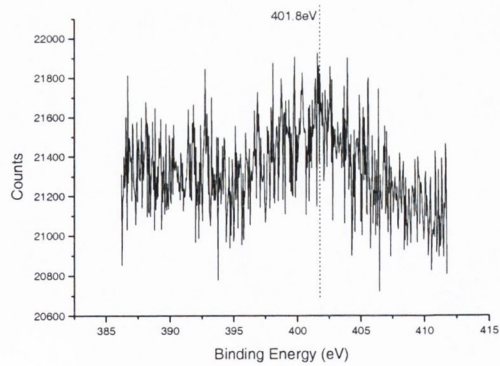
(b)



(c)



(d)



(e)

Fig. 4.13 Pt 4f XPS following DMA adsorption on Pt(331):

(a) 114K; (b) 273K; (c) 553K; (d) 687K; (e) >1000K.

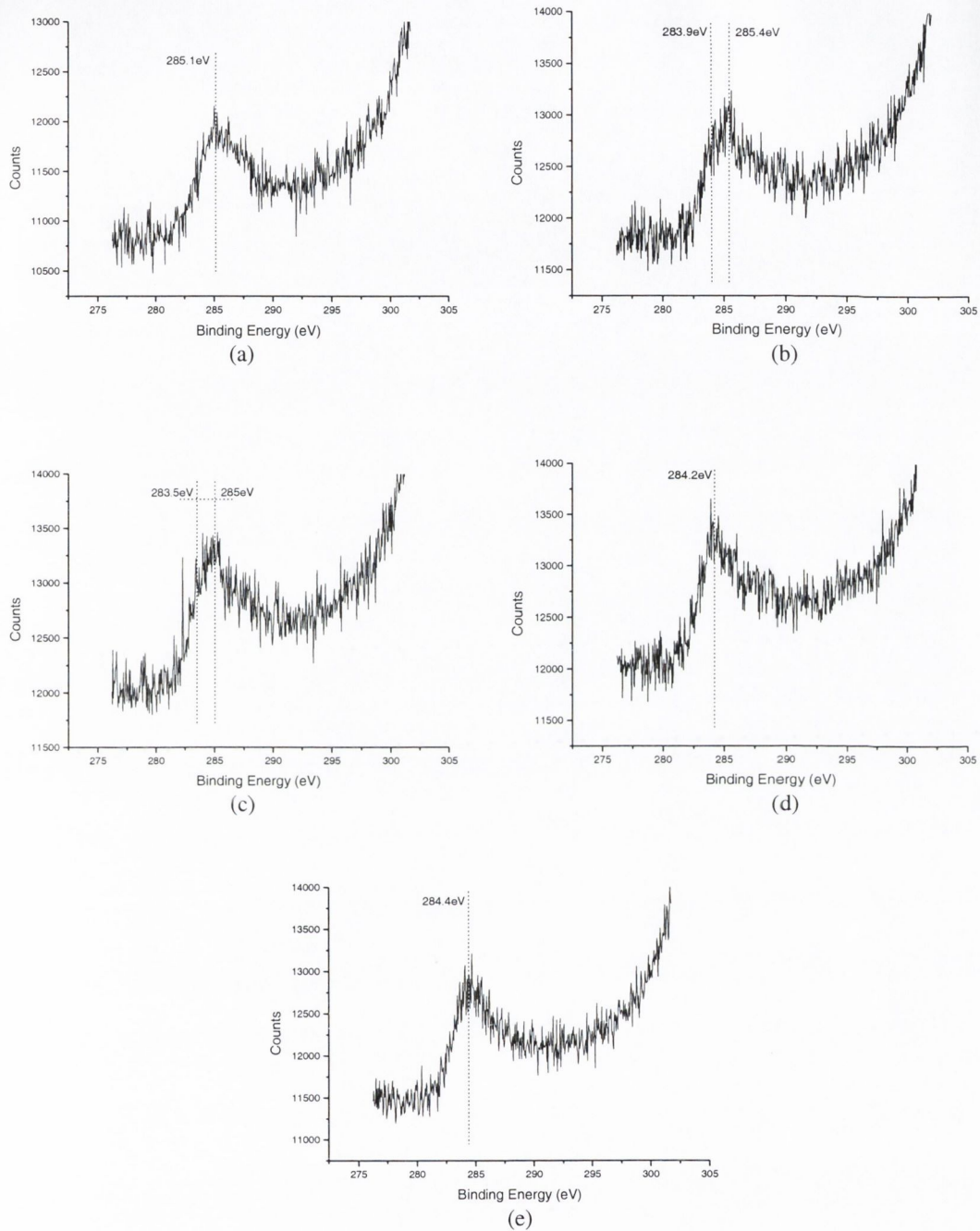


Fig. 4.14 C1s XPS following DMA adsorption on Pt(331):

(a) 114K; (b) 273K; (c) 556K; (d) 687K; (e) >1000K.

4.1.3 Trimethylamine on Pt(111)

Thermal desorption experiments following trimethylamine adsorption on Pt(111) generated the same products as observed for dimethylamine. HCN, CH₄ and H₂ were the main desorption products detected, along with features in the 28 amu spectra. The spectra are shown in figures 4.15 - 4.18.

Spectra taken at 27 amu exhibit a peak at ~574K with a low temperature shoulder between 450 and 500K.

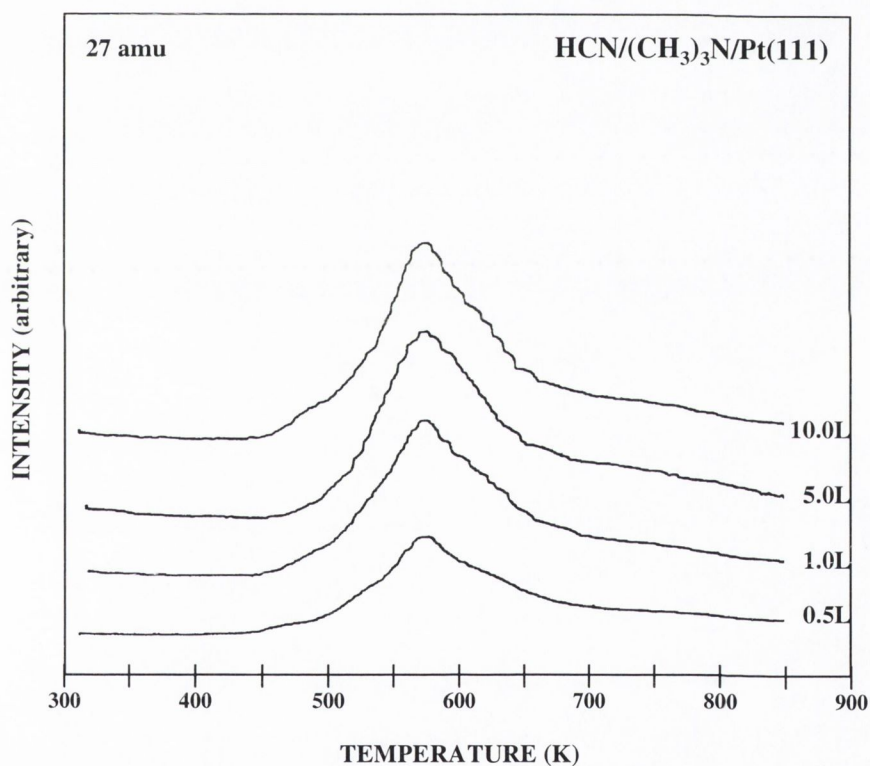


Fig. 4.15 Thermal desorption spectra of HCN following exposures of trimethylamine to Pt(111).

A peak very similar to that obtained from DMA on Pt(111) was detected at ~447K for methane. A sharp peak at ~458K was generated at 28 amu, with a high temperature shoulder at ~570K.

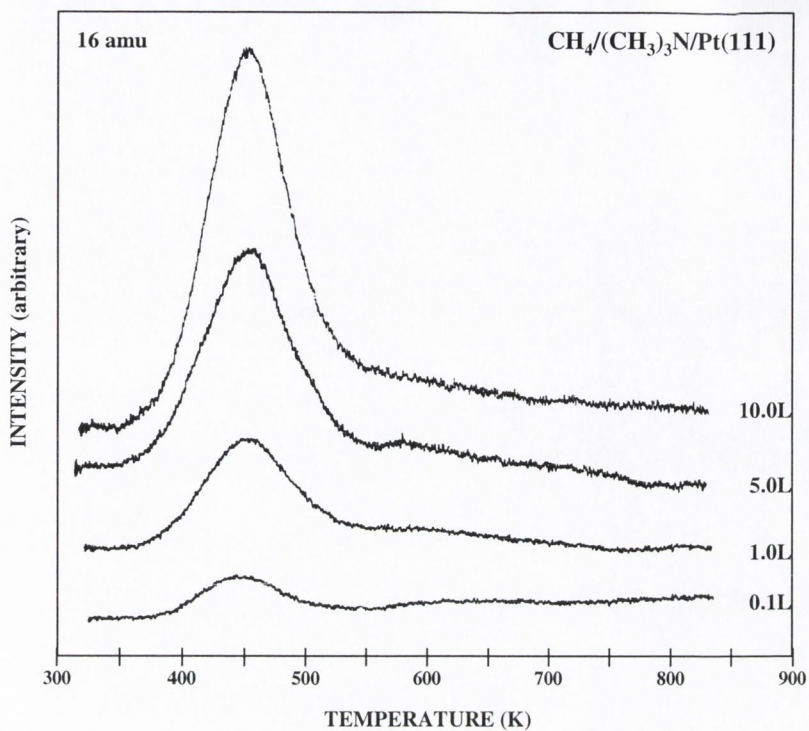


Fig. 4.16 Thermal desorption spectra of CH_4 following exposures of trimethylamine to Pt(111).

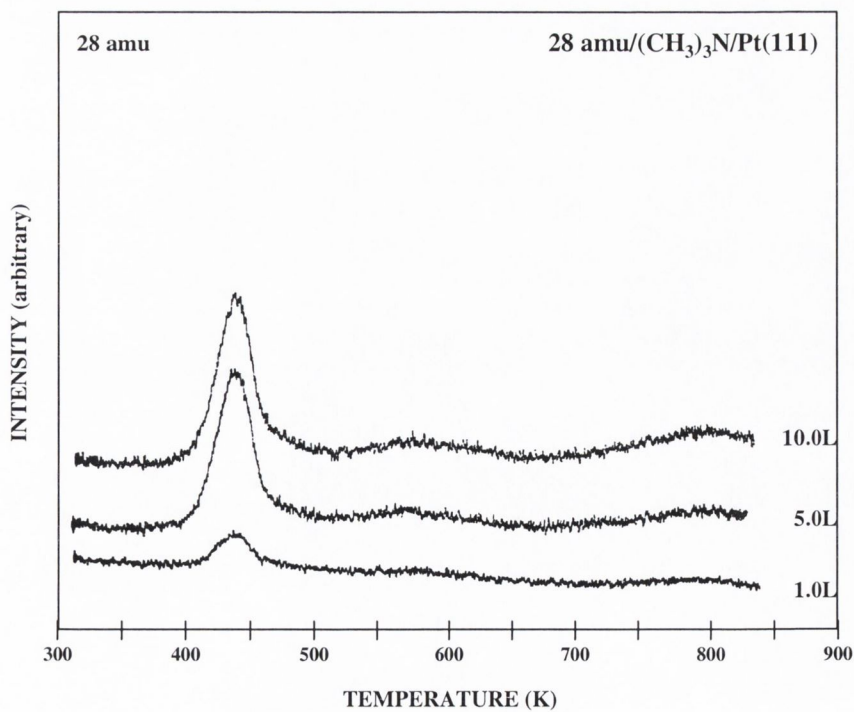


Fig. 4.17 Thermal desorption spectra at 28 amu following exposures of trimethylamine to Pt(111).

Two main peaks at ~413K and ~497K are observed for H₂ desorption. A shoulder on the low temperature side of the 413K peak is present at ~370K.

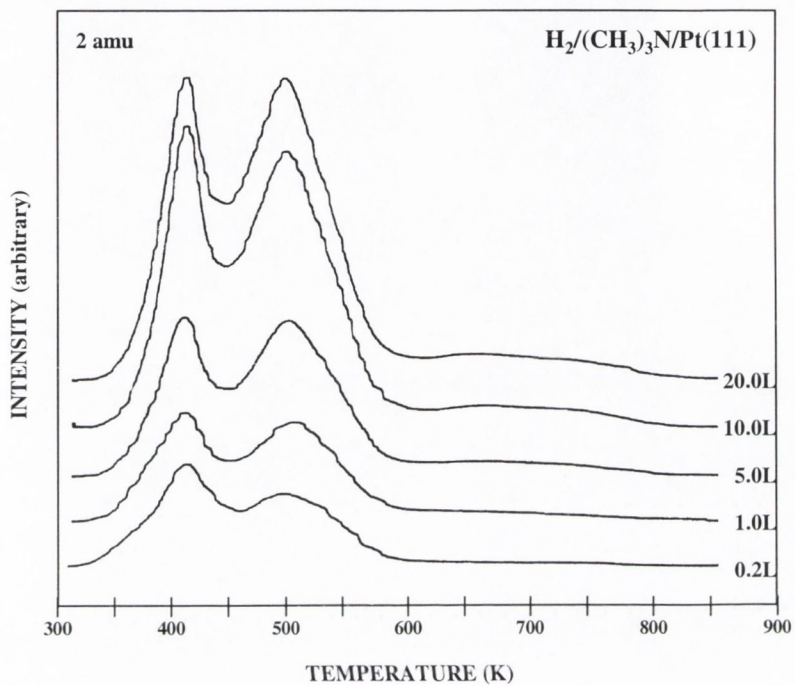


Fig. 4.18 Thermal desorption spectra of H₂ following exposures of trimethylamine to Pt(111).

XPS spectra for TMA/Pt(111) were collected under the same conditions as outlined in section 3.2. The results are shown in figures 4.19 – 4.21.

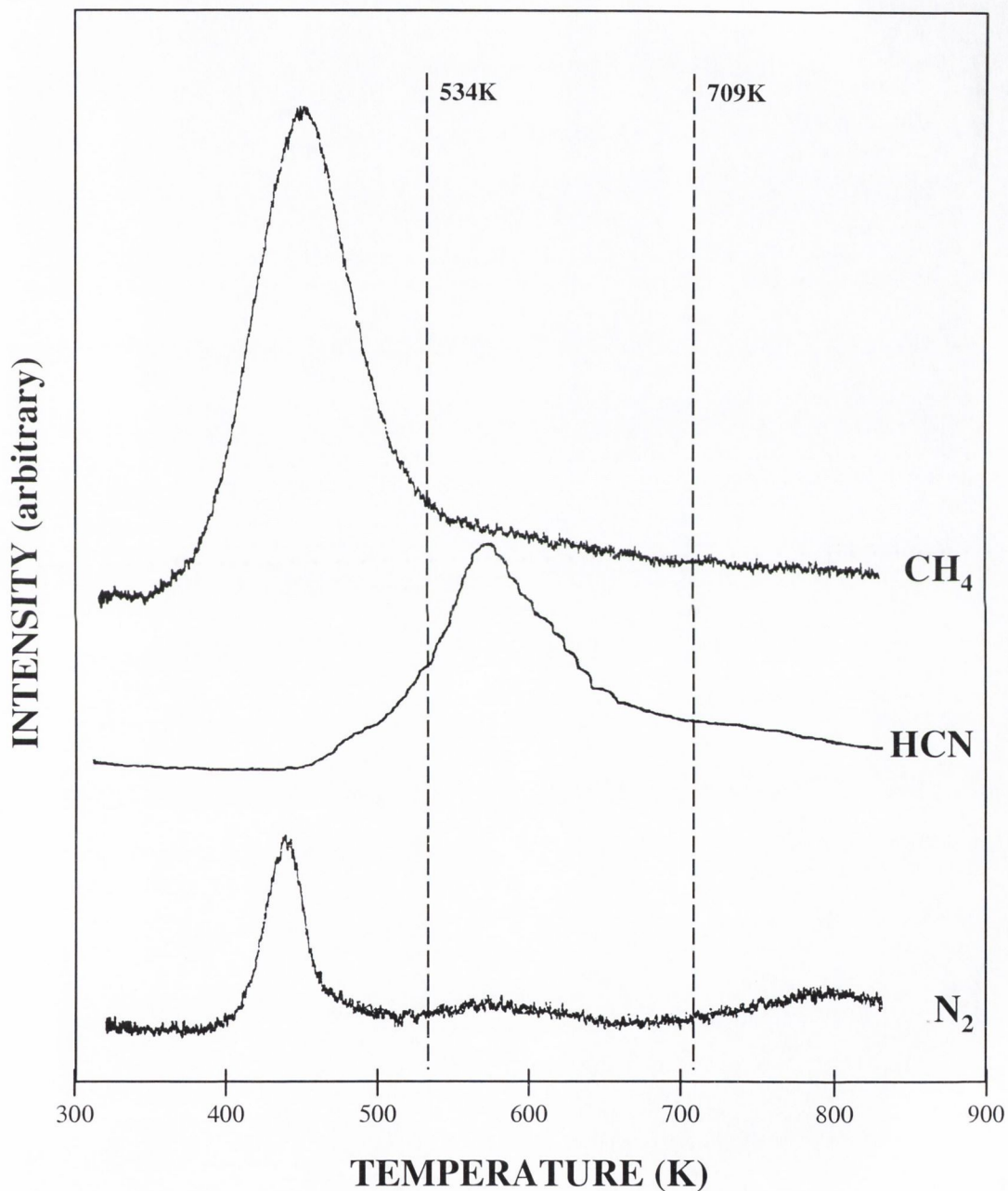
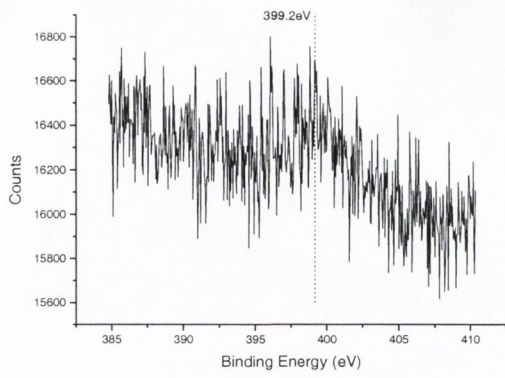
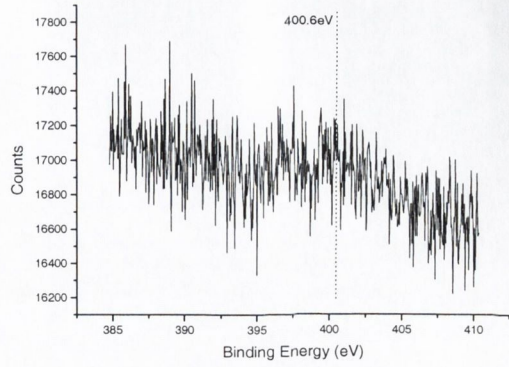


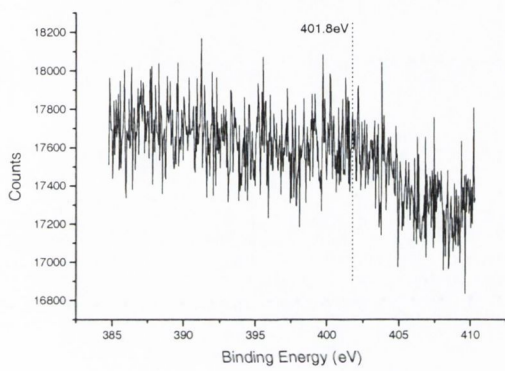
Fig. 4.19 Diagram of annealing temperatures employed during the XPS experiments following TMA adsorption on Pt(111).



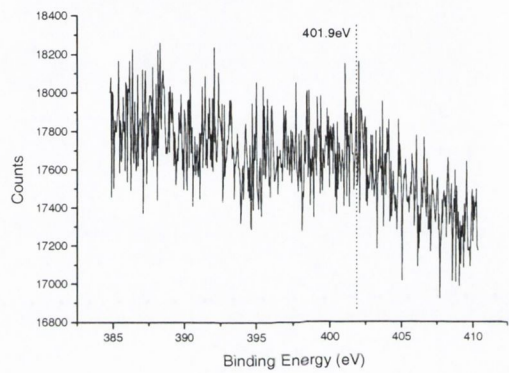
(a)



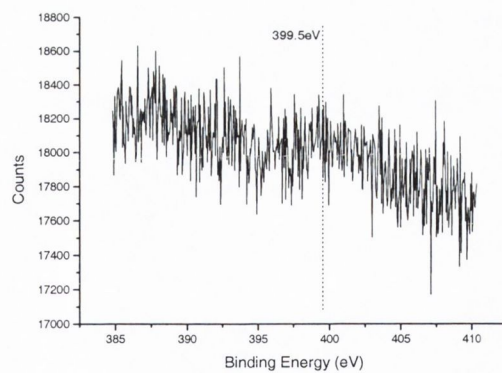
(b)



(c)



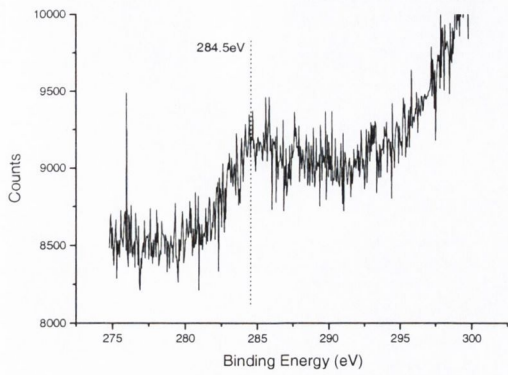
(d)



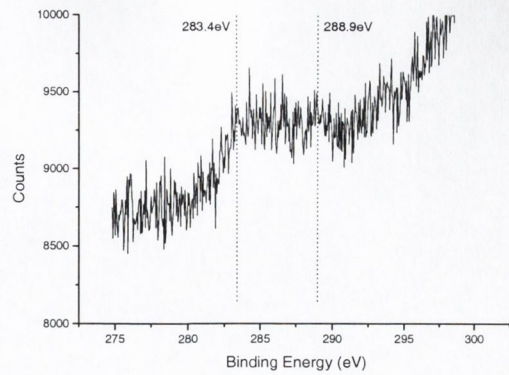
(e)

Fig. 4.20 N1s XPS following TMA adsorption on Pt(111):

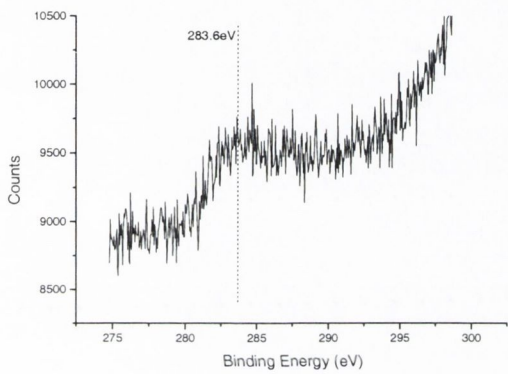
(a) 140K; (b) 273K; (c) 553K; (d) 709K; (e) >1000K.



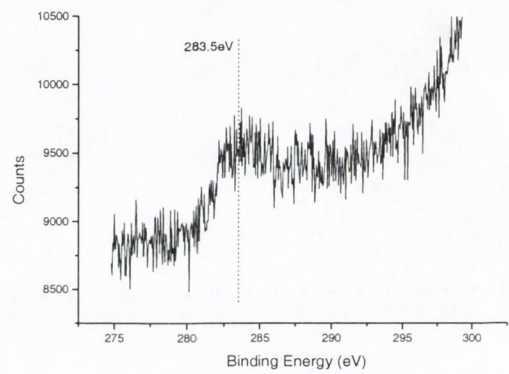
(a)



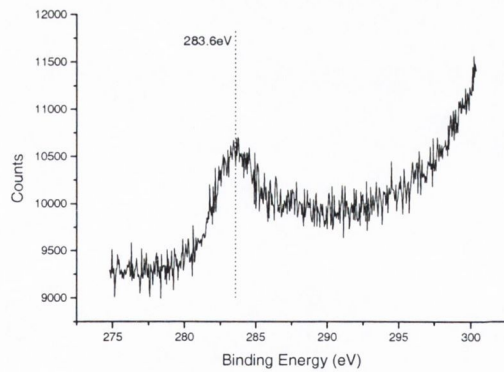
(b)



(c)



(d)



(e)

Fig. 4.21 C1s XPS following TMA adsorption on Pt(111):

(a) 136K; (b) 273K; (c) 534K; (d) 706K; (e) >1000K.

4.1.4 Trimethylamine on Pt(331)

Exposure of the Pt(331) surface to trimethylamine (TMA) produced the thermal desorption products HCN, CH₄, N₂/CO and H₂. They are shown in figures 4.22 - 4.25.

The HCN desorption spectrum has a main peak at ~498K with the suggestion of a second, higher temperature shoulder at ~548K.

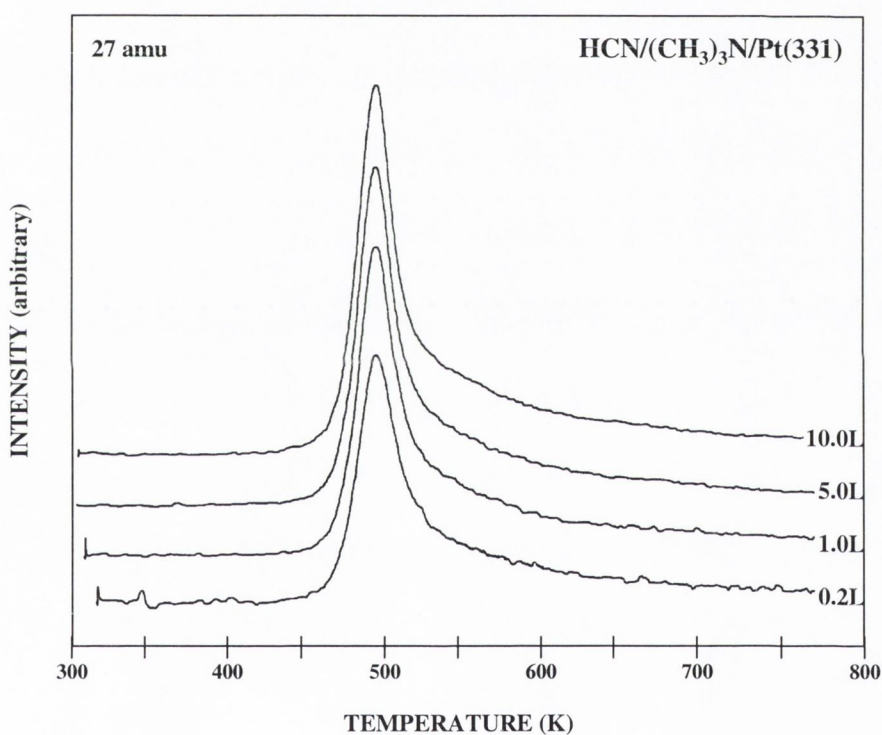


Fig. 4.22 Thermal desorption spectra of HCN following exposures of trimethylamine to Pt(331).

A single broad peak at ~467K is produced for CH₄ desorption whilst N₂ desorption exhibits two peaks; a main peak at ~458K and a high temperature shoulder at ~492K.

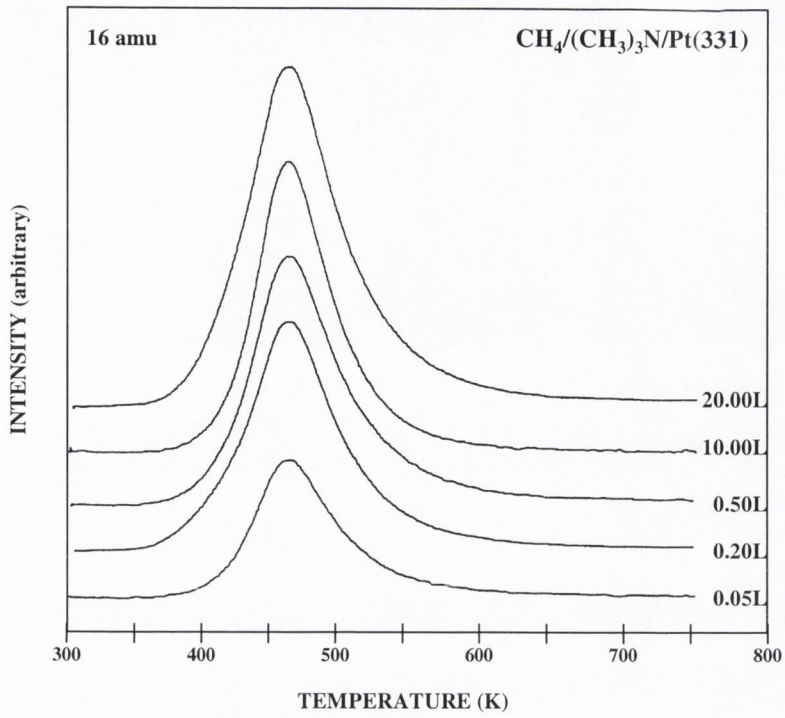


Fig. 4.23 Thermal desorption spectra of CH_4 following exposures of trimethylamine to Pt(331).

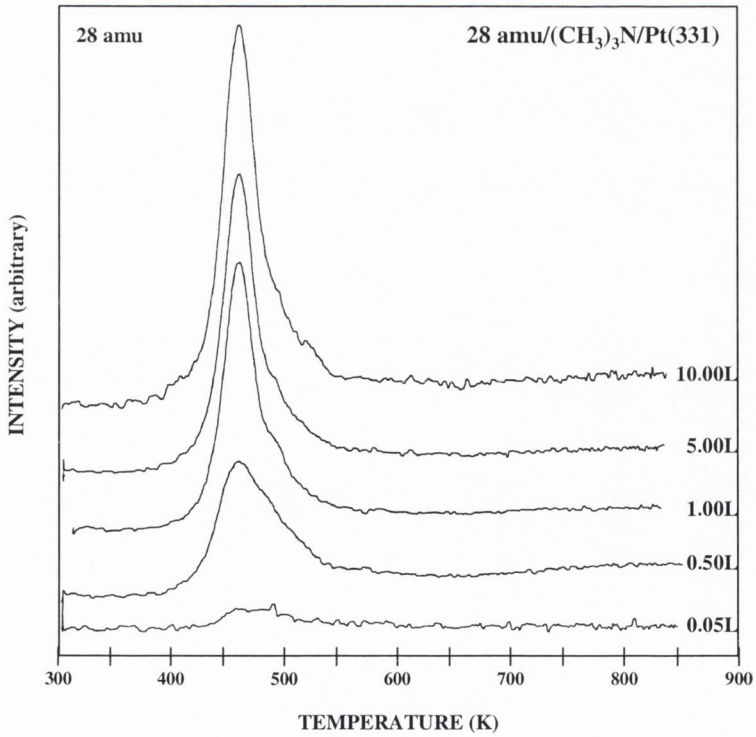


Fig. 4.24 Thermal desorption spectra at 28 amu following exposures of trimethylamine to Pt(331).

Two peaks are observed for H₂, a main peak at ~469K and a lower temperature peak at ~385K.

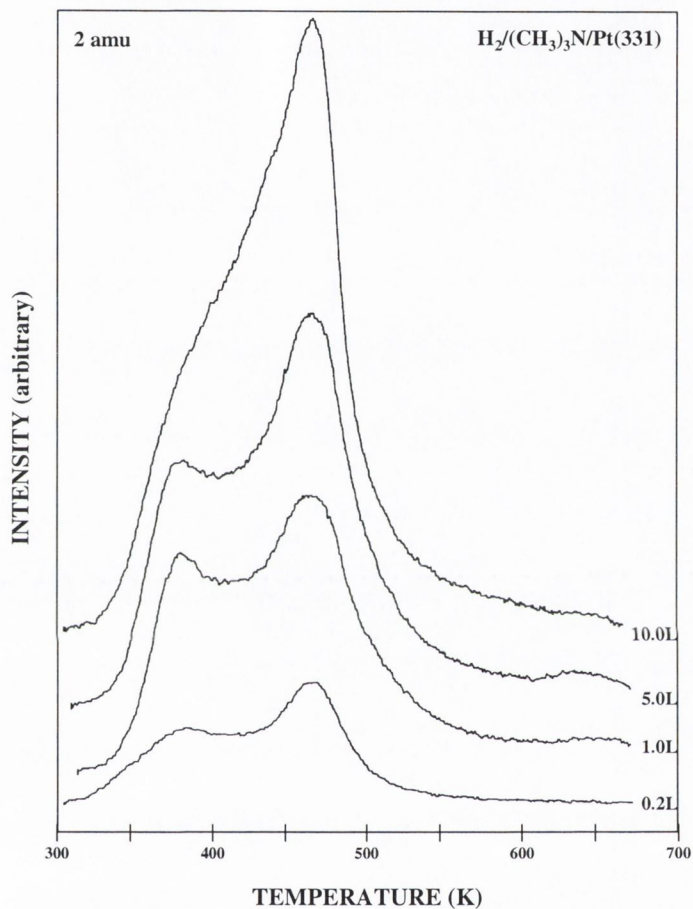


Fig. 4.25 Thermal desorption spectra of H₂ following exposures of trimethylamine to Pt(331).

XPS spectra for TMA/Pt(331) were collected under the same conditions as outlined in section 3.2. The results are shown in figures 4.26 – 4.28.

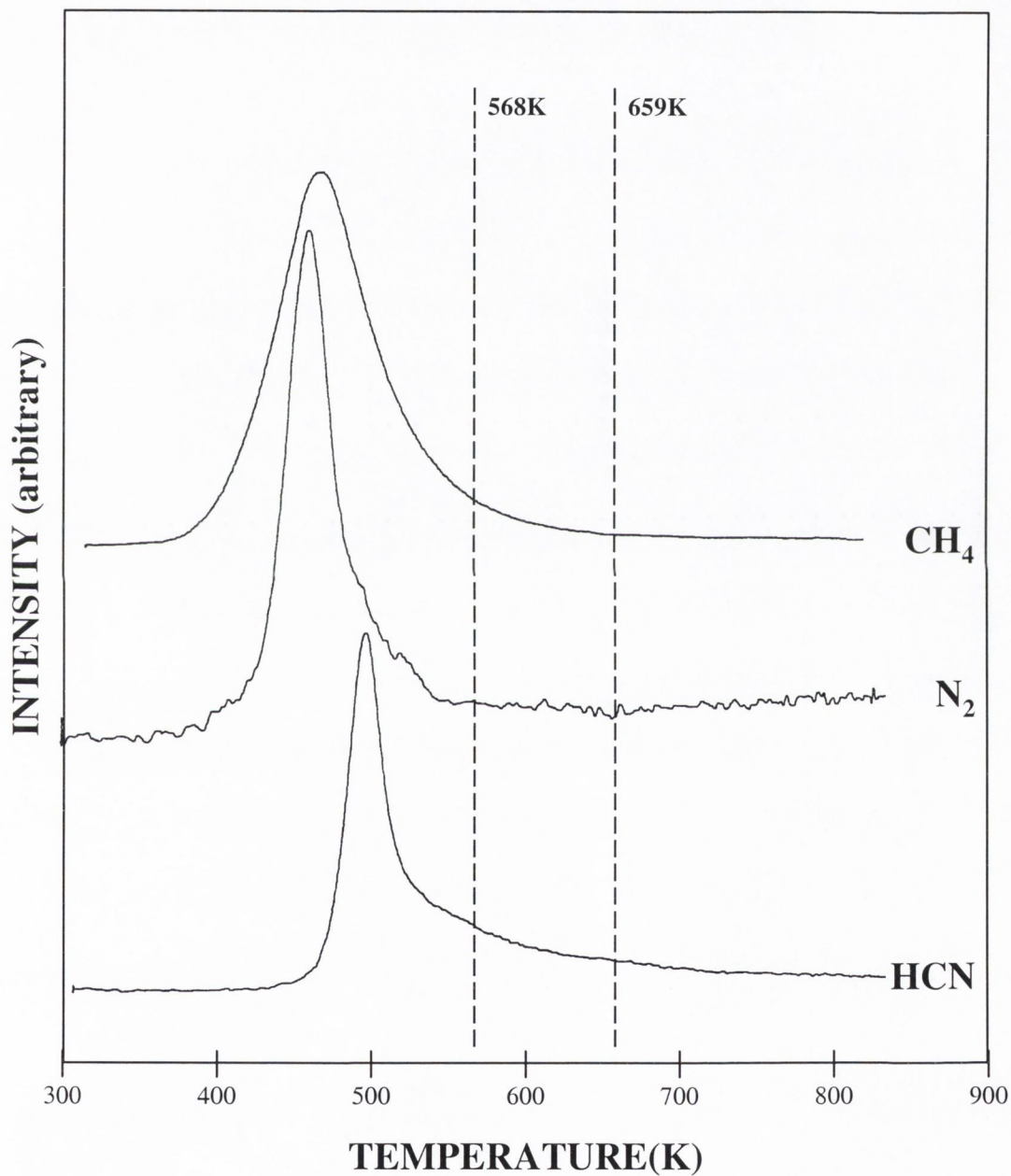
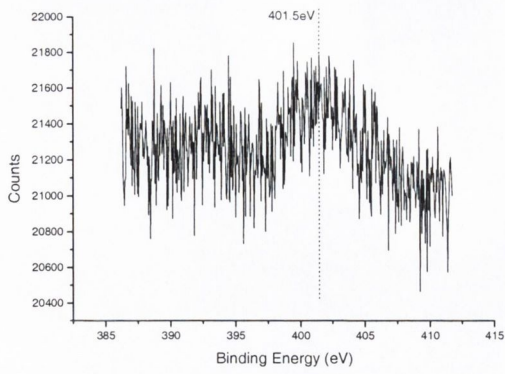
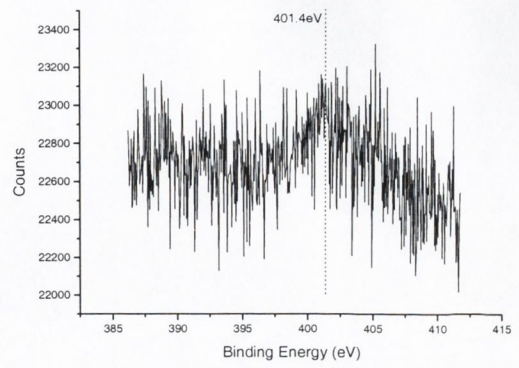


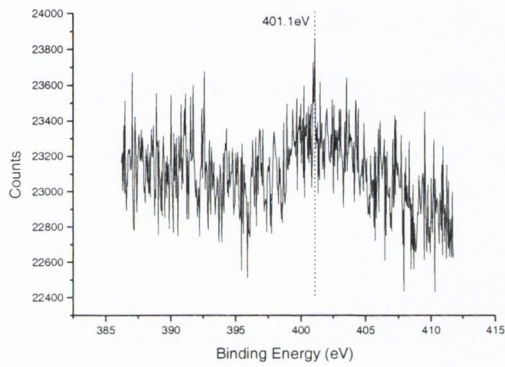
Fig. 4.26 Diagram of annealing temperatures employed during the XPS experiments following TMA adsorption on Pt(331).



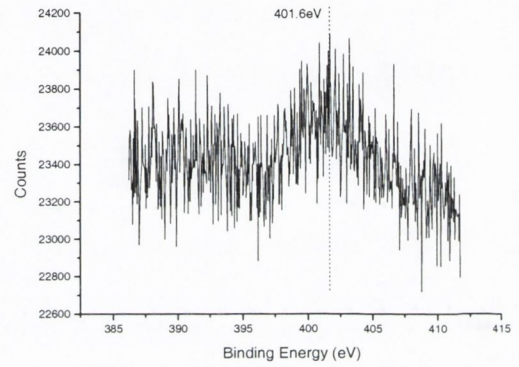
(a)



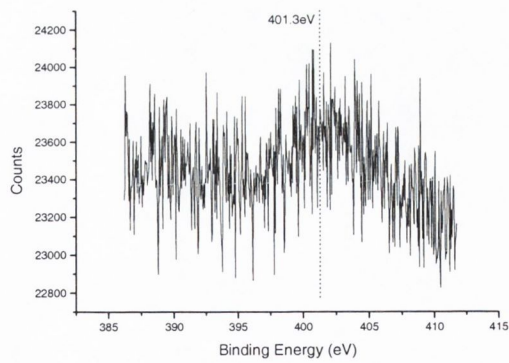
(b)



(c)



(d)



(e)

Fig. 4.27 N1s XPS following TMA adsorption on Pt(331):

(a) 114K; (b) 273K; (c) 568K; (d) 659K; (e) >1000K.

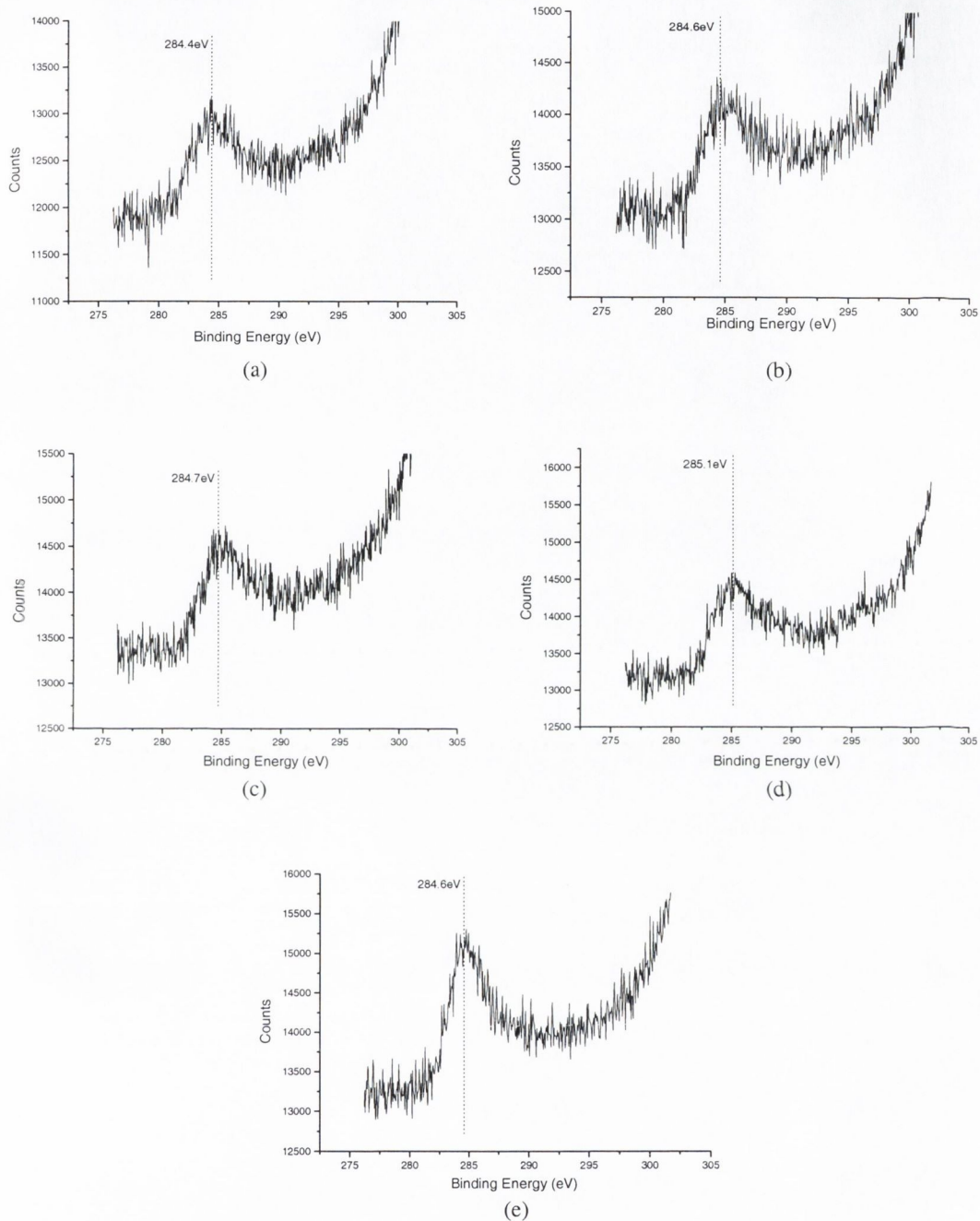


Fig. 4.28 C 1s XPS following TMA adsorption on Pt(331):
 (a) 114K; (b) 273K; (c) 563K; (d) 654K; (e) >1000K.

4.2 DISCUSSION

4.2.1 Trimethylamine on platinum

4.2.1.1 H_2 desorption

The initial step in TMA decomposition appears to be at least partial dehydrogenation of a methyl group. H_2 desorption commences at a temperature below that of all the other desorption products. Close inspection of the low temperature peak at low coverages indicates the presence of a feature on the low temperature side of the peak, which seems to become part of the peak at higher coverages. This feature may represent H_2 desorption following partial dehydrogenation of the first methyl group. It occurs in a temperature range associated with $H_{ads.} + H_{ads.}$ recombination [65, 66]. It is not clear whether initial dehydrogenation occurs upon exposure of the surface to TMA, or early in the thermal process.

The thermal desorption spectra give little information about the manner in which the TMA molecule binds to the surface. Three possibilities were suggested for TMA on molybdenum [51] (see figure 4.29), all of which are possible on the platinum systems. The most likely of these, based on XPS measurements, was considered by Walker and Stair [51] to be (a). However, they acknowledged the possibility that it may be a mixture of the three species, the relative concentrations of each being dependent on the surface temperature.

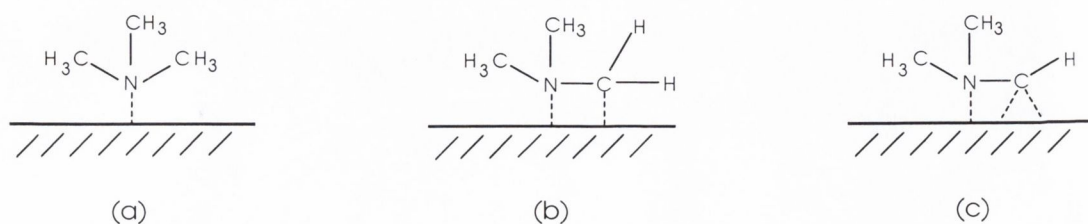


Fig. 4.29 Three possible initial binding states of trimethylamine on platinum.

HREELS and FT-IRAS experiments carried out by Erley *et al.* [49] on TMA/Pt(111) indicated that TMA adsorbs molecularly at 85K in a tilted geometry with at least one of its C-N bonds closer to the surface than the others. They suggested that a methyl-nitrogen bond is broken at 280K forming $(\text{CH}_3)_2\text{N}_{\text{ads}}$ and $\text{CH}_{3\text{ads}}$ species, the methyl group then rapidly dissociating into $\text{C}_{\text{ads}} + 3\text{H}_{\text{ads}}$. In support of this, they note a sharp H_2 peak at 328K and no CH_4 in their TDS spectra. This is in contrast to the TDS results obtained in this work in which CH_4 is a significant product in the decomposition process and the H_2 desorption event below 350K is a minor feature, rather than a significant peak. However, these results followed adsorption at 300K. Furthermore, the XPS spectrum obtained in this work for TMA/Pt(111) adsorbed at 136K and annealed to 273K (figure 4.21 (b), p.87) indicates the presence of two C1s peaks, at 283.4 eV and 288.9 eV. This seems to lend support to the suggestion of a break in the methyl-nitrogen bond. It may be the case that room temperature adsorption results in immediate dehydrogenation of the first methyl group and desorption of H_2 during the adsorption process.

Hydrogen is formed primarily in competition to methane formation. XPS analysis indicates a residual carbon surface species following thermal desorption, so some methyl groups clearly undergo complete dehydrogenation. In the case of Pt(111), the two H_2 desorption features peak at temperatures above that for $\text{H}_{\text{ads}} + \text{H}_{\text{ads}}$ recombination [65,66], indicating that these two peaks are generated as a result of decomposition limited processes. The most probable source of the two hydrogen desorption peaks is consecutive dehydrogenation of the remaining methyl groups. These two peaks were present in the hydrogen desorption spectra obtained by Erley *et al.* [49]. In addition, they noted a peak between these two at 444K which they attributed to the loss of a single hydrogen from the remaining methyl group:



leading finally to complete dehydrogenation at 495K and scission of the C-N bond to give C_{ads} and N_{ads} . The absence of this peak in the hydrogen spectra presented in this work may

be due to the faster heating rate applied. Erley *et al.* used a heating rate of 1Ks^{-1} , whereas a rate of 13Ks^{-1} was applied in this work.

On Pt(331) the low temperature peak saturates at lower coverages. This suggests that the stepped environment inhibits dehydrogenation of the second methyl group at higher coverages. This seems to favour CH_4 production, as would be expected from a competitive process. A chart of relative increase or decrease in products on going from Pt(111) to Pt(331) shows an increase in CH_4 production (figure 4.30).

Despite the lower intensity of the low temperature peak on Pt(331) figure 4.30 shows a moderate overall increase in the relative amount of H_2 produced. This may be explained by the decrease in HCN production, reflecting a greater tendency for the first methyl group to dehydrogenate completely.

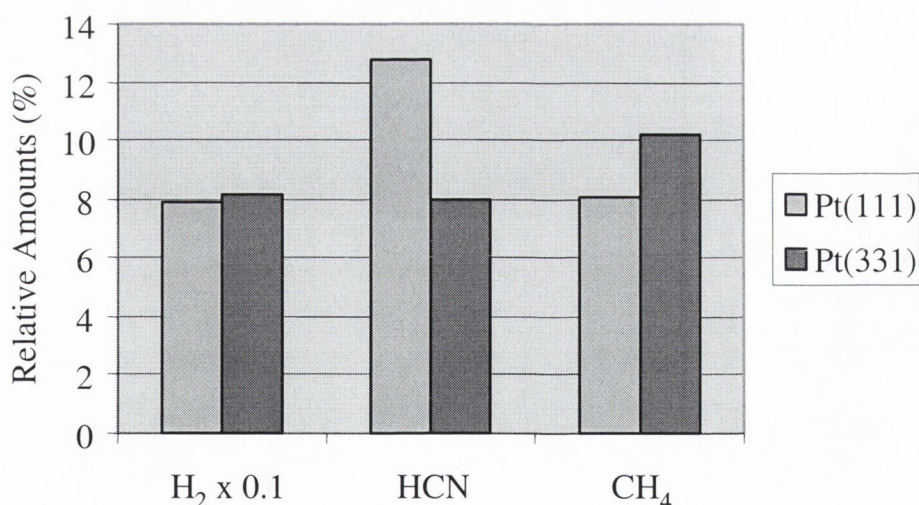


Fig. 4.30 Percentage increase or decrease in products desorbed from Pt(111) and Pt(331). The values presented are uncorrected for mass spectrometer sensitivity, and therefore do not reflect the absolute amounts of each product, but only the relative increase/decrease.

4.2.1.2 HCN desorption

Two possibilities exist for the formation of HCN, either decomposition of the parent molecule or intermediate species, or recombination of H_{ads} and CN_{ads} surface species. In the cases of TMA and DMA adsorption, the thermal desorption data suggest that HCN desorption is the product of decomposition only. There are a number of reasons for this conclusion. Previous studies of C_2N_2 , HCN and MA adsorption on platinum [40, 41, 67-69, 70-74], including the results presented in chapter 3 of this work, have shown that the presence of CN_{ads} species results in the formation of C_2N_2 at temperatures between 600-900K. No C_2N_2 desorption was detected following either DMA or TMA adsorption on platinum. The possibility that all CN_{ads} species are used up in the formation of HCN can be discounted since it would be expected that $H_{ads} + CN_{ads}$ recombination would be in competition with $H_{ads} + H_{ads}$ recombination. However, the bulk of HCN formation occurs at temperatures above that of H_2 formation. It is reasonable to assume therefore that there is no H_{ads} available for recombination at the temperatures at which most of the HCN is formed. Furthermore, it has been shown [32, 75] that $H_{ads} + CN_{ads}$ recombination does not produce HCN to any significant extent on Pt(111). It can therefore be assumed that no CN_{ads} species are formed during decomposition.

HCN desorption occurs at significantly higher temperatures on Pt(111) than on Pt(331). This is a common feature of HCN desorption following adsorption of various CN containing compounds including HCN itself.

4.2.1.3 CH_4 desorption

It is clear from the TDS spectra of methane that the first C-N bonds are broken by 350–370K. Molecularly adsorbed methane desorbs <100K [76]. It has been shown [77, 78] that surface methyl groups on Pt(111) desorb as methane at 250-290K by recombining with background hydrogen and/or from partial decomposition of other methyl moieties, and that further dissociation of CH_x fragments to produce H_2 occurs at 350K and 550K [77]. It is likely, therefore, that in the case of DMA and TMA adsorption methane formation occurs immediately upon scission of the methyl-nitrogen bond, with the methyl group immediately picking up a hydrogen atom. In thermal desorption studies on the adsorption of TMA on Mo(100) Walker and Stair [51] demonstrated, by pre-exposure of the surface to deuterium,

that the methyl groups pick up a hydrogen atom from the surface rather than through intramolecular transfer. It is reasonable to believe that this process is similar on platinum. Hydrogen thermal desorption spectra indicate that H_{ads} species are readily available to the methyl group from the outset of methane desorption to the completion of the desorption process.

4.2.1.4 28 amu desorption

The peak at 435K for 28 amu/TMA/Pt(111) corresponds to the desorption temperature for adsorbed CO on Pt(111) [32, 78, 79]. Likewise, the peak and shoulder for 28 amu/TMA/Pt(331) correspond to the desorption peaks for adsorbed CO on Pt(331) [32] (two desorption peaks for CO are a characteristic of stepped Pt(111) surfaces [79-89], the lower temperature peak associated with desorption from terrace sites, the higher temperature peak with step sites). These peaks are therefore assigned to CO adsorbed from the background.

The small feature between 500K and 600K in the 28 amu spectra of TMA on Pt(111) corresponds to three peaks observed by Erley *et al.* [49] at 500K, 548K, and 595K following TMA adsorption on Pt(111). Since they also observed identical peaks following $(CD_3)_3N$ adsorption, the formation of ethylene was discounted as a source of these peaks. Appearing above the desorption temperature established for CO [32, 78, 79], they were consequently assigned to N_2 formation [90]. A small amount of TMA must, therefore, completely decompose into atomic species on Pt(111). No corresponding features are visible in the desorption spectra for Pt(331).

4.2.1.5 XPS Experiments

The N1s spectra for TMA on both Pt(111) and Pt(331) are very similar, and exhibit an almost constant binding energy of 399.5eV for Pt(111) and 401.4eV for Pt(331). The results are preliminary in nature. The peaks are broad and of low intensity making them difficult to interpret. Further experiments using ARUPS are currently being designed for the TMA/platinum system. It is hoped that more useful information may be obtained from this technique.

4.2.2 Dimethylamine on platinum

Three desorption features are present in the H_2 desorption spectra for DMA on Pt(111). The small, low temperature peak at 371K may be due to recombination of H_{ads} species originating on the nitrogen atom. It is not clear whether the H-N bond is broken upon adsorption or whether it is initiated by the heating process.

This is followed by a competitive process between methane formation and methyl group dissociation to form H_2 and C_{ads} . It is likely that the H_2 peaks at 446K and 527K represent dehydrogenation of consecutive methyl groups. HCN production requires only partial dehydrogenation of one of the methyl groups. It is not clear from the H_2 spectra which peak represents partial dehydrogenation, but the lower intensity of the 527K peak and the fact that it corresponds in temperature to the onset of HCN desorption suggests that this may be the HCN forming process.

The process of methane production is identical to that for TMA decomposition. The peak shape and temperature matches that of $CH_4/TMA/Pt(111)$. This process is one in which the rate limiting step is scission of the C-N bond. The methyl group then immediately picks up a surface hydrogen [51]. It is possible to detect a slight shoulder to the low temperature side of the methane peak, particularly on the Pt(331) spectra. There are two possible sources for the fourth hydrogen atom, the amine hydrogen and the hydrogens initially bonded to a methyl group. Since H-N bond cleavage is the likely initial step in DMA decomposition it is possible that this low temperature shoulder represents CH_4 formed by picking up the amine hydrogen.

The peak at 442K in the 28amu spectra corresponds to the desorption temperature for adsorbed CO on Pt(111) [32, 78, 79], and is therefore assigned to background CO adsorption. The feature between 550K and 650K corresponds to N_2 formation [90] and indicates that complete dissociation occurs to a small degree.

Adsorption and thermal decomposition of DMA on Pt(331) produces the same desorption products as on Pt(111). As in the case of TMA on Pt(331), the HCN and H_2 desorption features peak at lower temperatures than on Pt(111), whilst CH_4 peaks at a higher temperature.

The stepped surface favours CH_4 and HCN production over H_2 , as is evidenced by a decrease in intensity of the 395K peak relative to the corresponding peak on Pt(111). A chart of relative change in the amounts of products between Pt(111) and Pt(331) (figure 4.31) clearly shows a relative increase in CH_4 and HCN production and decrease in H_2 production on Pt(331).

The two peaks present in the 28 amu spectra on Pt(331) can be assigned to CO adsorbed from the background [80, 89].

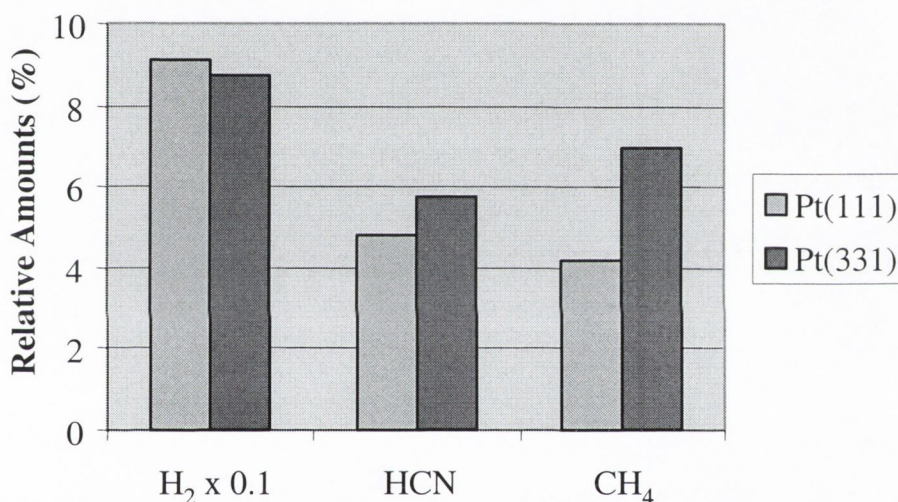


Fig. 4.31 Relative increase or decrease in products desorbed from Pt(111) and Pt(331). The values presented are uncorrected for mass spectrometer sensitivity, and therefore do not reflect the absolute amounts of each product, but only the relative increase/decrease.

The XPS results obtained for DMA on platinum are similar to those for TMA. The N1s binding energy remains constant throughout the annealing cycles.

4.3 CONCLUSIONS

4.3.1 Dimethylamine on platinum

Dimethylamine decomposes on platinum to form H_2 , HCN , CH_4 and small quantities of N_2 . The initial step in DMA decomposition is removal of the amine hydrogen. The first methyl group then undergoes C-N bond cleavage followed either by hydrogen take-up to form CH_4 or dehydrogenation to form C_{ads} and $^{3/2}H_2 g$. The final step involves partial dehydrogenation of the remaining methyl group to give HCN and H_2 (see figure 4.32). In addition to this pathway, some of the DMA experiences cleavage of all the C-N bonds to produce a small amount of N_2 .

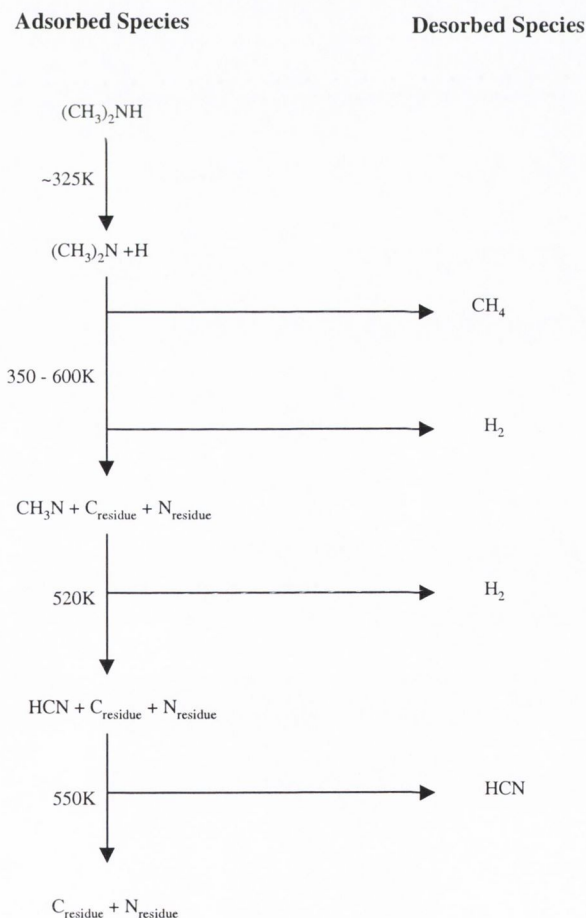


Fig. 4.32 Schematic of reaction pathway of dimethylamine on Pt(111).

Adsorption on Pt(331) does not alter the desorption products. However, the stepped surface favours HCN and CH₄ formation over complete decomposition to form C_{ads.} + N_{ads.} + H_{2g.}

4.3.2 Trimethylamine on platinum

Trimethylamine produces the same desorption products as dimethylamine. It initially undergoes limited C-H bond breaking on one of the methyl groups. This is followed by C-N bond cleavage on the other methyl groups forming either methane, by picking up a surface hydrogen, or decomposing to form hydrogen and C_{ads.}, as indicated in figure 4.33.

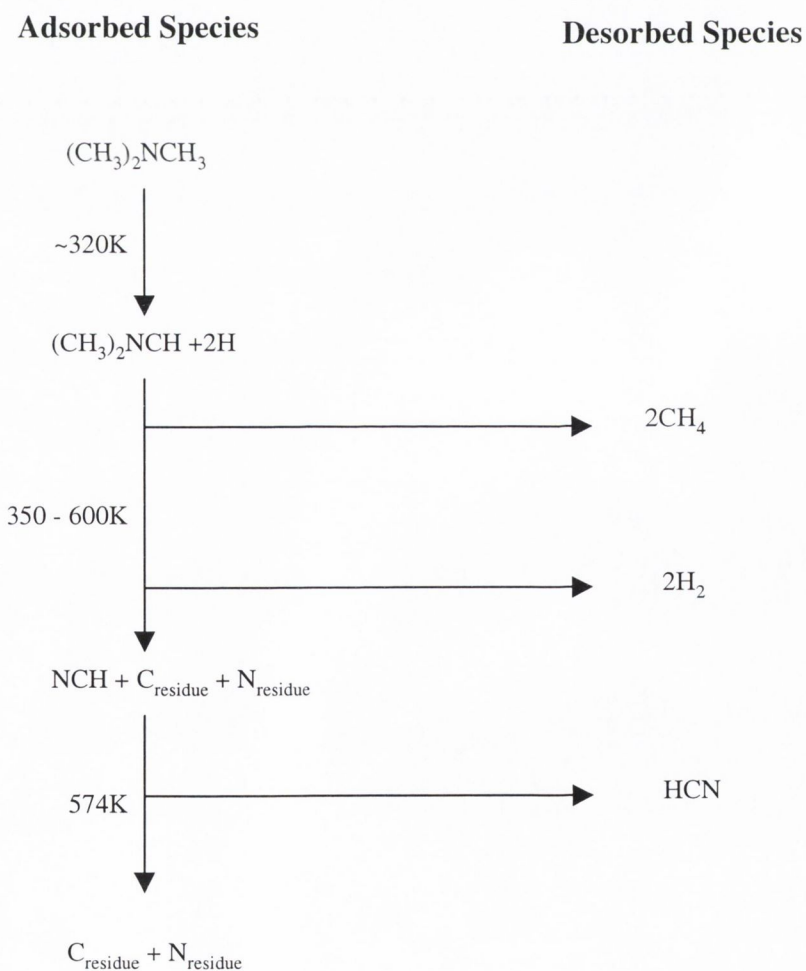


Fig. 4.33 Schematic of reaction pathway of trimethylamine on Pt(111).

Pt(331) favours CH_4 production over H_2 formation. In contrast to DMA on Pt(331), HCN production decreases on the stepped surface.

CHAPTER FIVE

ETHYLENEDIAMINE ON Pt(111) AND Pt(331)

CHAPTER 5 ETHYLENEDIAMINE ON Pt(111) AND Pt(331)

5.1 RESULTS

5.1.1 Ethylenediamine on Pt(111)

Following exposure of the Pt(111) surface to ethylenediamine (EDA) at 300K, the thermal desorption products detected were C_2N_2 , HCN, NH_3 , CH_4 , H_2 and 28 amu. A set of thermal desorption spectra for each of these products is shown in figures 5.1 - 5.6.

The C_2N_2 desorption spectra (52 amu) display a narrow, well-defined peak at $\sim 425K$, with high temperature shoulder between 450K and 540K consisting of two features.

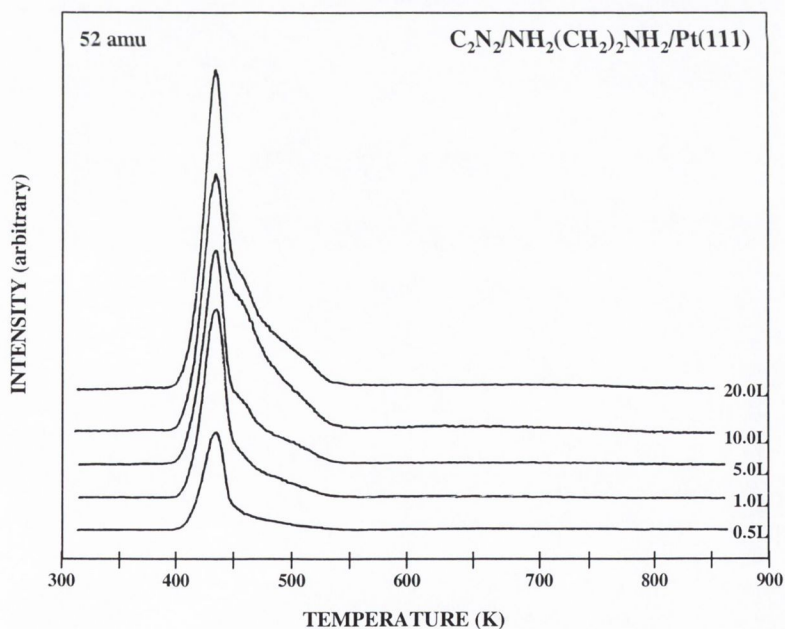


Fig. 5.1 Thermal desorption spectra of C_2N_2 following exposures of ethylenediamine to Pt(111).

The spectra for HCN (27 amu) exhibit three features - a peak at ~470K; a peak at ~520K; and a high temperature shoulder between 540K and 660K.

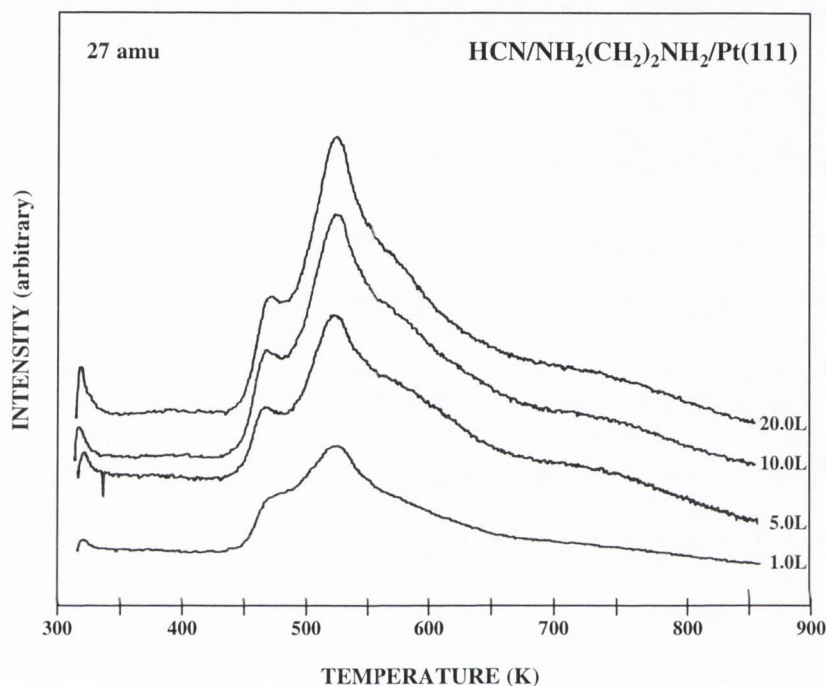


Fig. 5.2 Thermal desorption spectra of HCN following exposures of ethylenediamine to Pt(111).

The thermal desorption spectra for 16 amu and 17 amu both show a major peak at ~420K and ~425K respectively, with a lower temperature peak on both at ~385K.

The H₂ spectra show a main peak at ~375K with a broad, high temperature shoulder, which appears to consist of four desorption features.

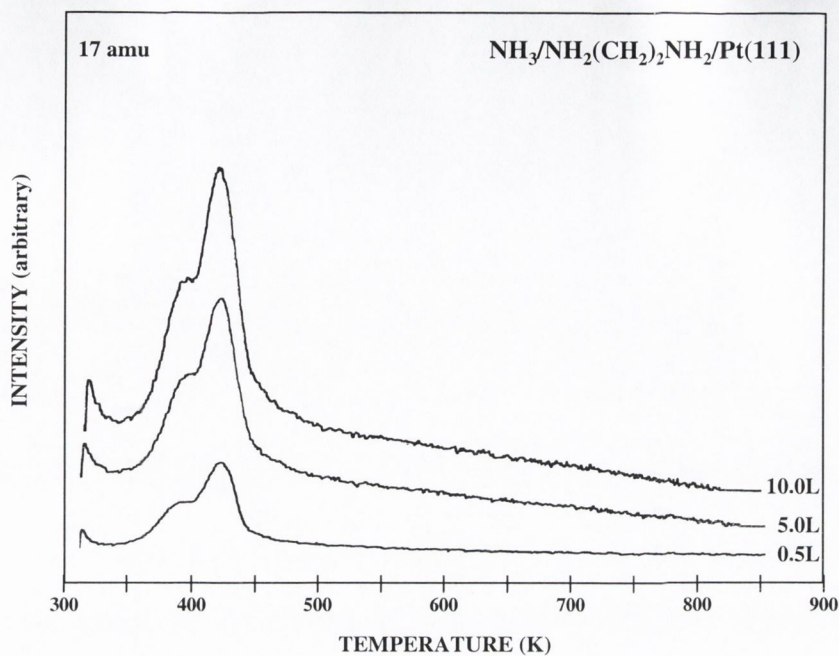


Fig. 5.3 Thermal desorption spectra of NH_3 following exposures of ethylenediamine to Pt(111).

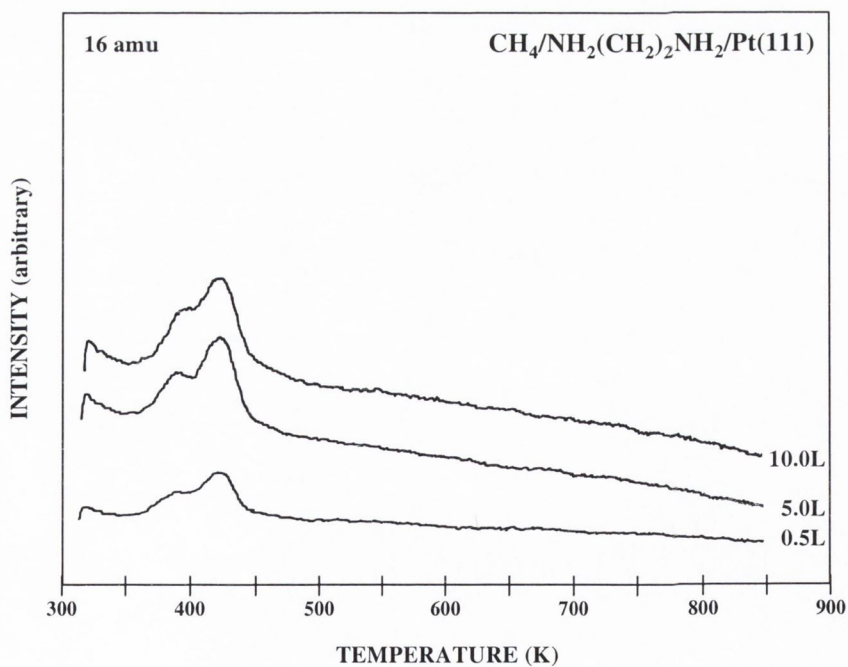


Fig. 5.4 Thermal desorption spectra of CH_4 following exposures of ethylenediamine to Pt(111).

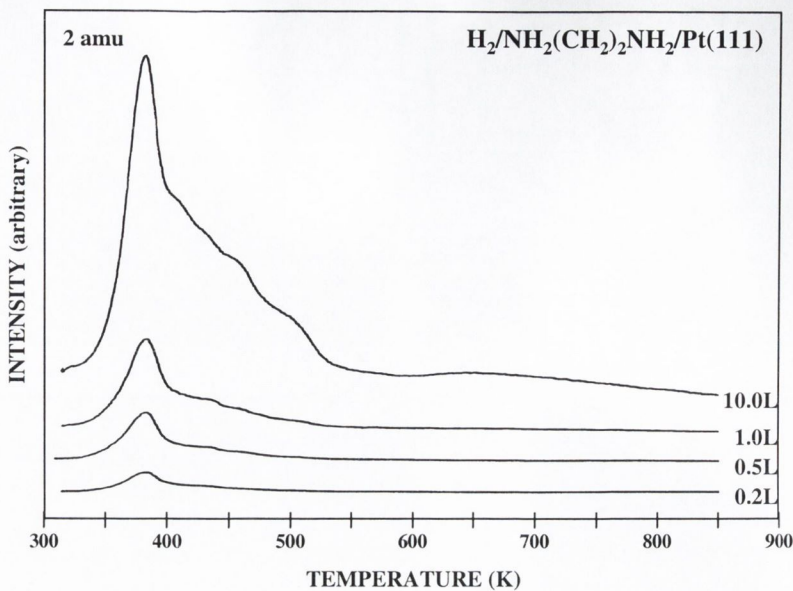


Fig. 5.5 Thermal desorption spectra of H_2 following exposures of ethylenediamine to Pt(111).

At 28 amu a peak was observed which shifts to lower temperatures from $\sim 442\text{K}$ to $\sim 423\text{K}$ with increasing exposures. A small feature was also noted at 526K .

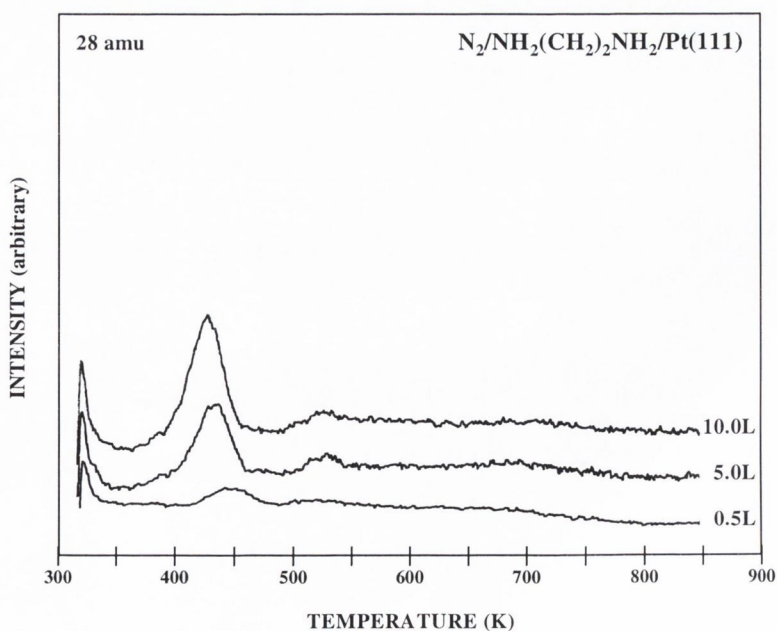


Fig. 5.6 Thermal desorption spectra of 28 amu following exposures of ethylenediamine to Pt(111).

XPS spectra for EDA/Pt(111) were collected under the same conditions as outlined in section 3.1.1. The results are shown in figures 5.7 – 5.9.

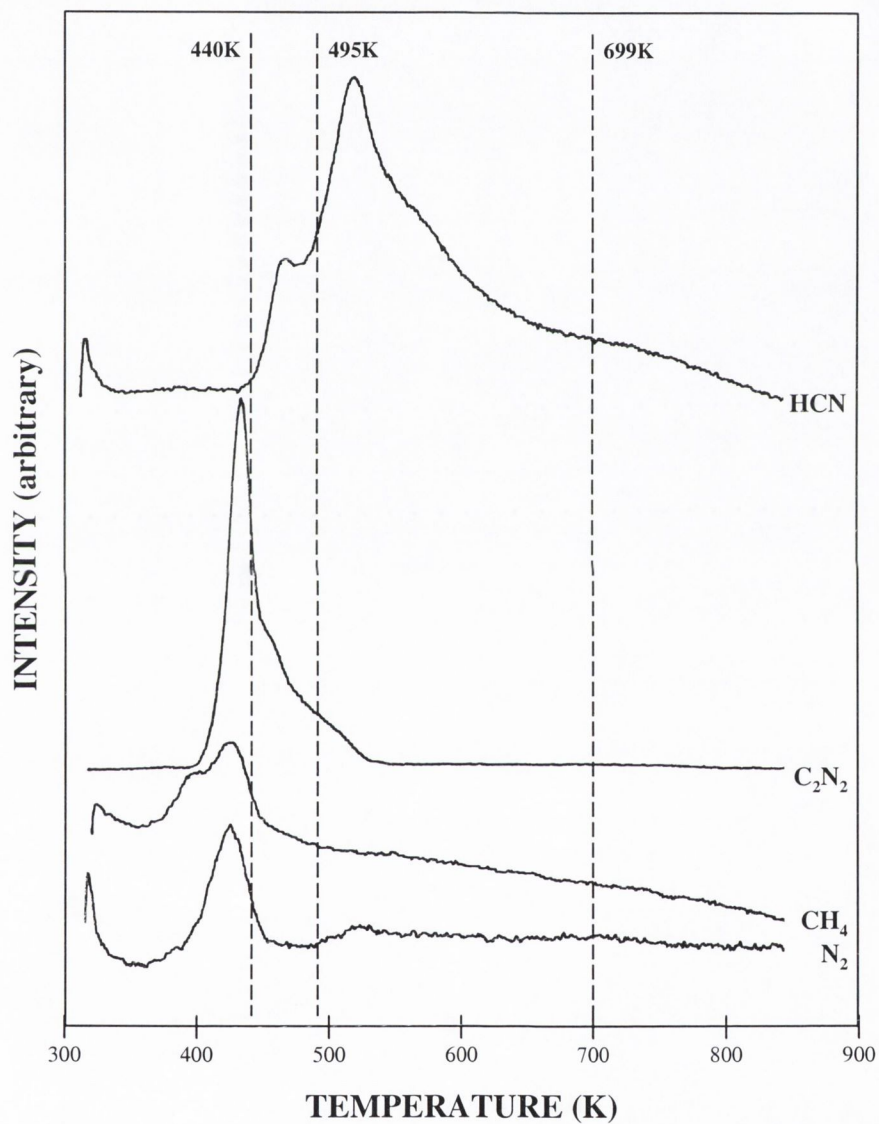


Fig 5.7 Diagram of annealing temperatures employed during the XPS experiments following EDA adsorption on Pt(111).

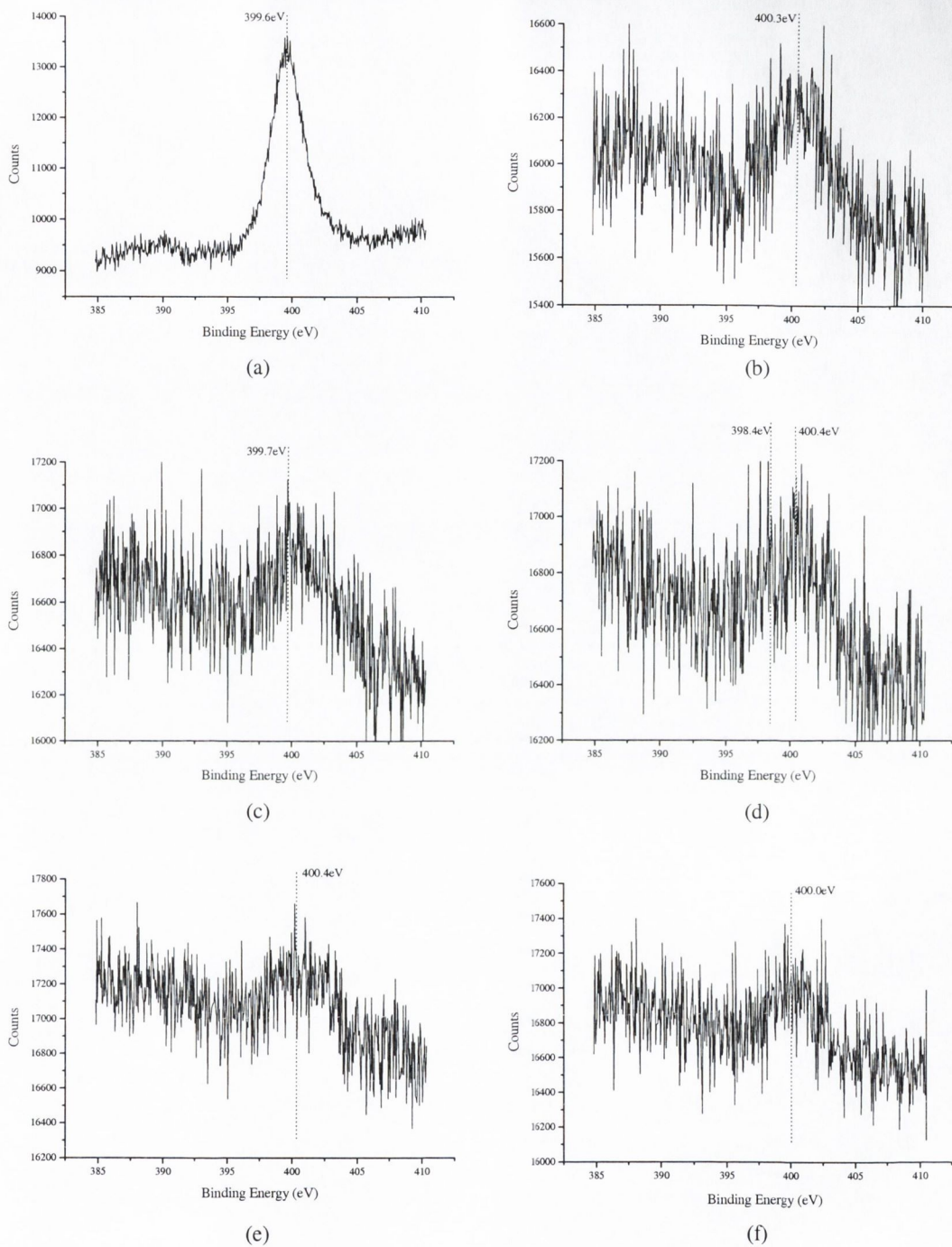
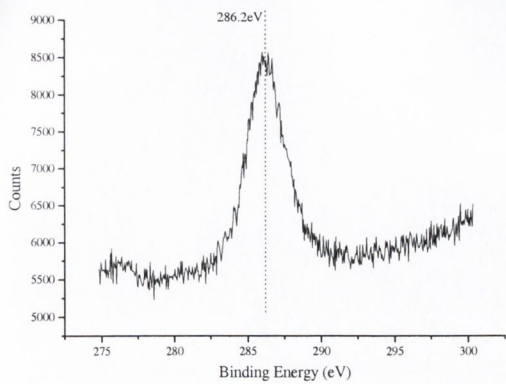
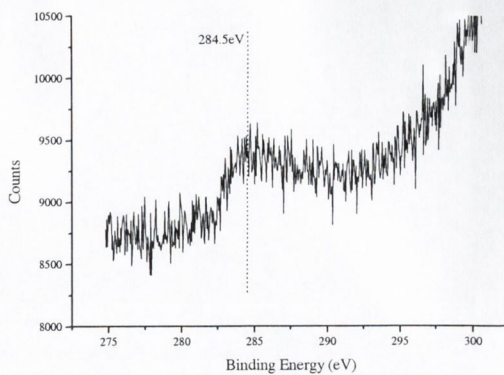


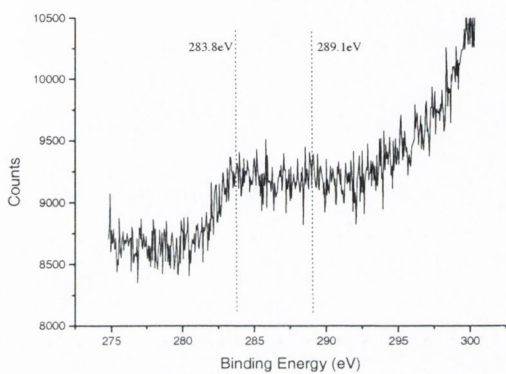
Fig. 5.8 N1s XPS following EDA adsorption on Pt(111):
 (a) 140K; (b) 273K; (c) 440K; (d) 495K; (e) 699K; (f) >1000K.



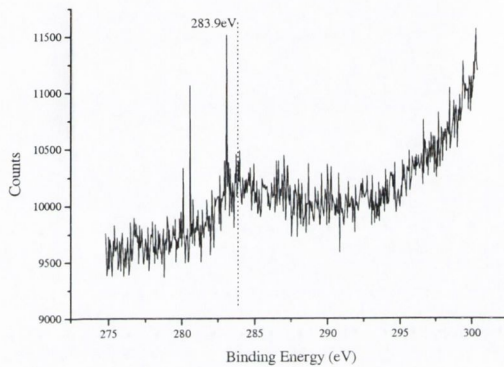
(a)



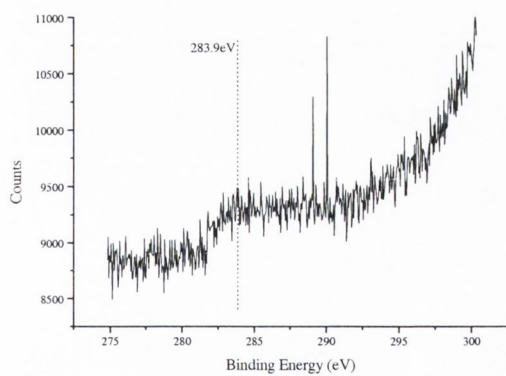
(b)



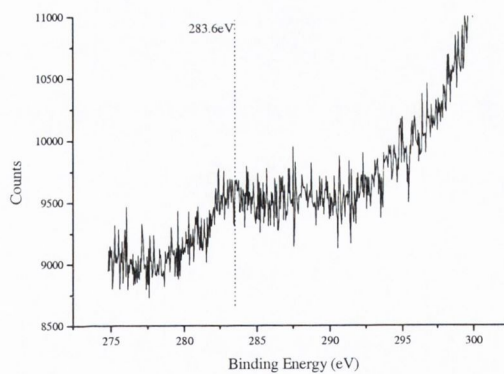
(c)



(d)



(e)



(f)

Fig. 5.9 C1s XPS following EDA adsorption on Pt(111):

(a) 136K; (b) 273K; (c) 435K; (d) 470K; (e) 735K; (f) >1000K.

5.1.2 Ethylenediamine on Pt(331)

Following exposure of the Pt(331) surface to ethylenediamine (EDA) at 300K, the main thermal desorption products detected were C_2N_2 , HCN, NH_3 , CH_4 and H_2 . A set of thermal desorption spectra for each of these products is shown in figures 5.10 - 5.14.

A peak at $\sim 456K$ is observed at 52 amu corresponding to C_2N_2 . At the lower coverages two additional features are observed at $\sim 810K$ (0.5L exposure) and $\sim 728K$ (1.0L exposure).

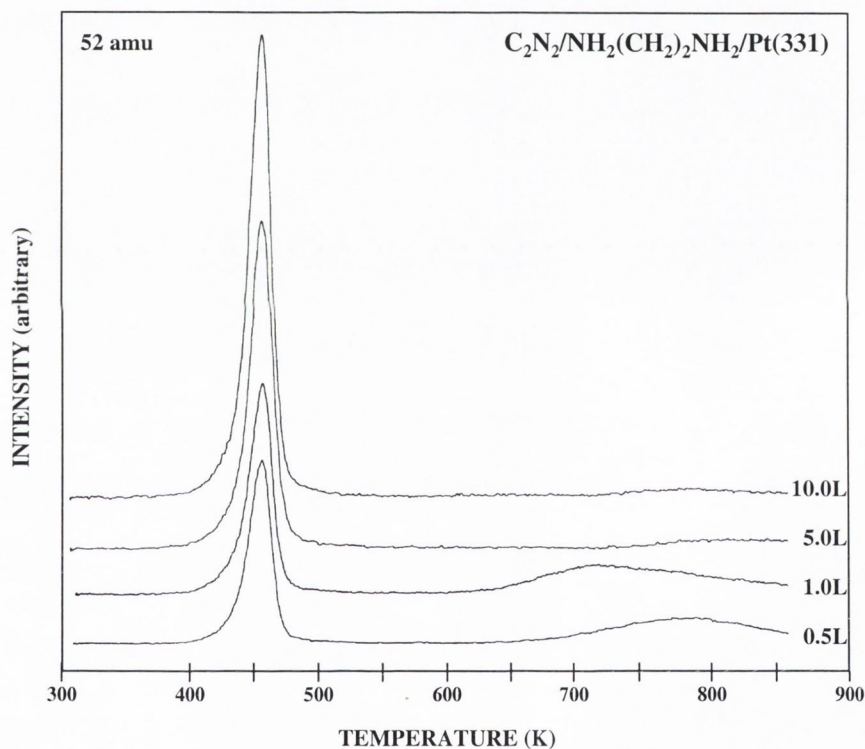


Fig. 5.10 Thermal desorption spectra of C_2N_2 following exposures of ethylenediamine to Pt(331).

The HCN desorption spectra show a sharp peak at $\sim 467K$ with a high temperature shoulder developing at higher EDA exposures at $\sim 520K$.

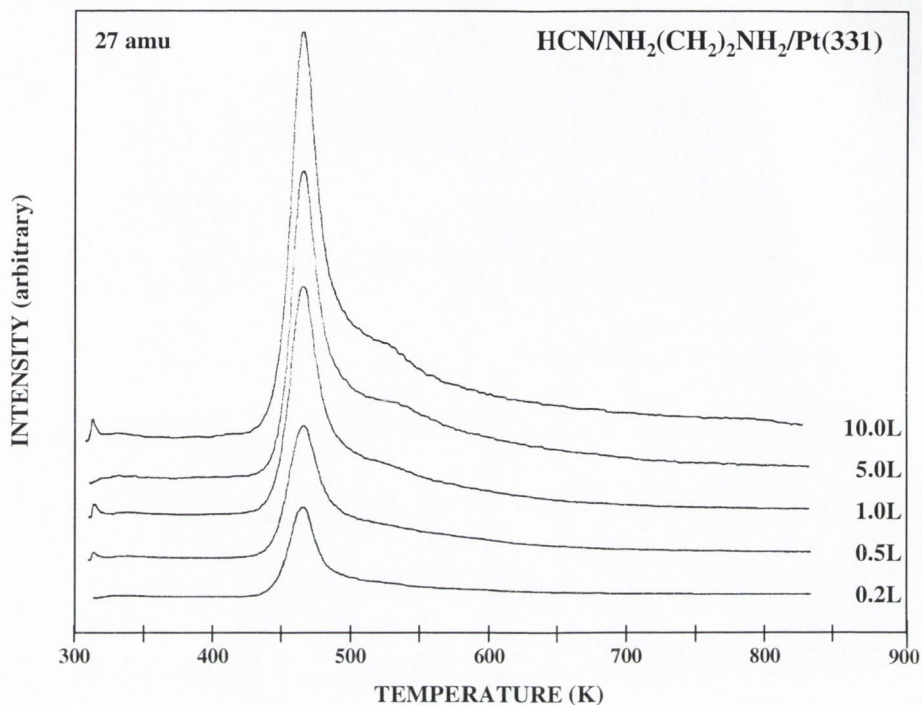


Fig. 5.11 Thermal desorption spectra of HCN following exposures of ethylenediamine to Pt(331).

A single low intensity, broad desorption peak appears at ~446K for NH₃ (17 amu) and ~441K for CH₄ (16 amu).

The H₂ desorption spectra exhibit a sharp peak at ~460K and a broad feature between ~410K to ~441K. This broad peak appears to consist of more than one component, with a feature at 410K dominating at low EDA exposures and another feature at 440K which dominates at higher exposures.

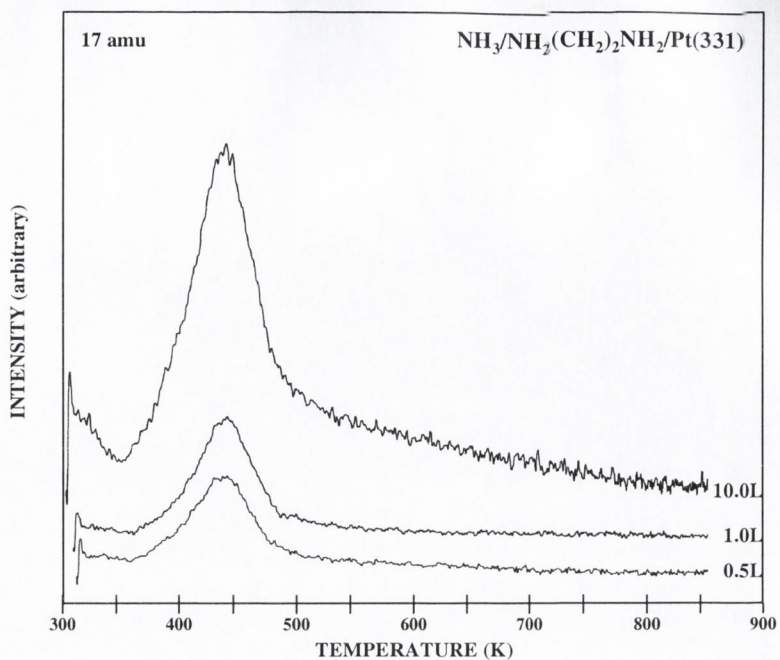


Fig. 5.12 Thermal desorption spectra of NH₃ following exposures of ethylenediamine to Pt(331).

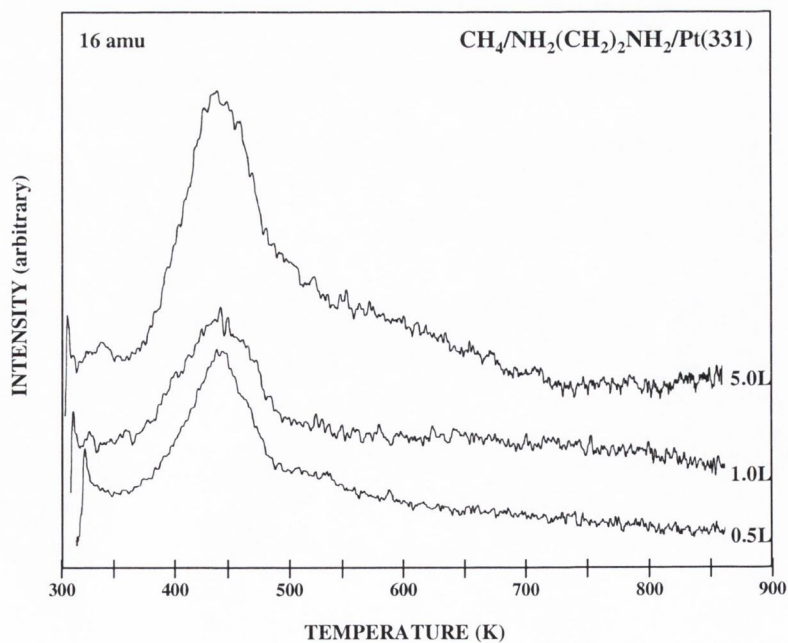


Fig. 5.13 Thermal desorption spectra of CH₄ following exposures of ethylenediamine to Pt(331).

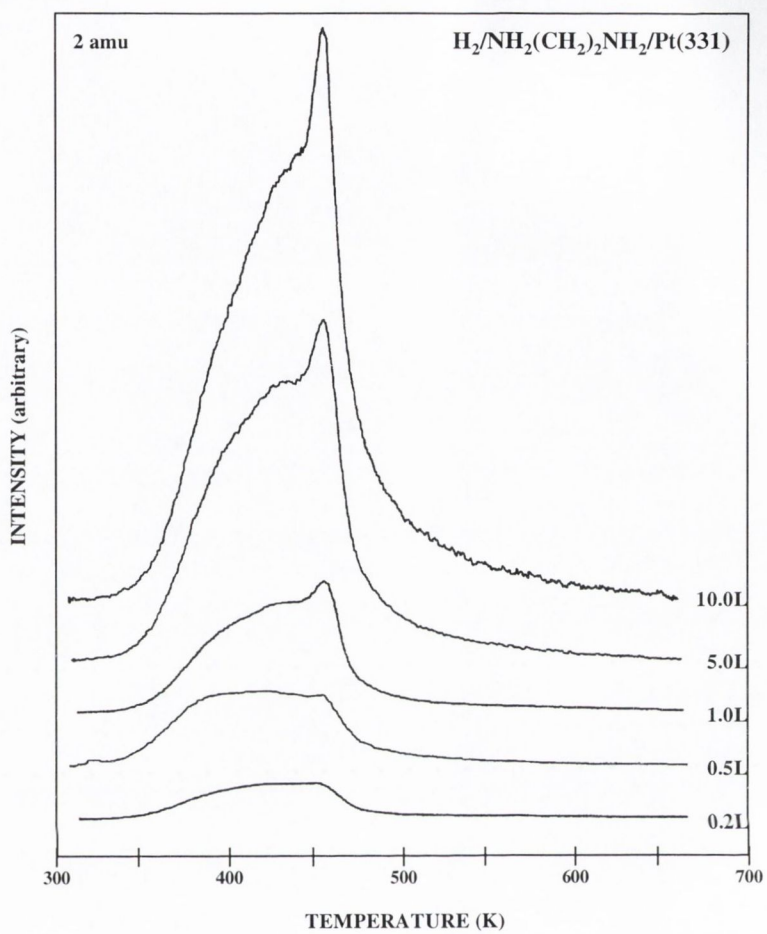


Fig. 5.14 Thermal desorption spectra of H_2 following exposures of ethylenediamine to Pt(331).

XPS spectra for EDA/Pt(331) were collected under the same conditions as outlined in section 3.1.1. The results are shown in figures 5.15 – 5.17.

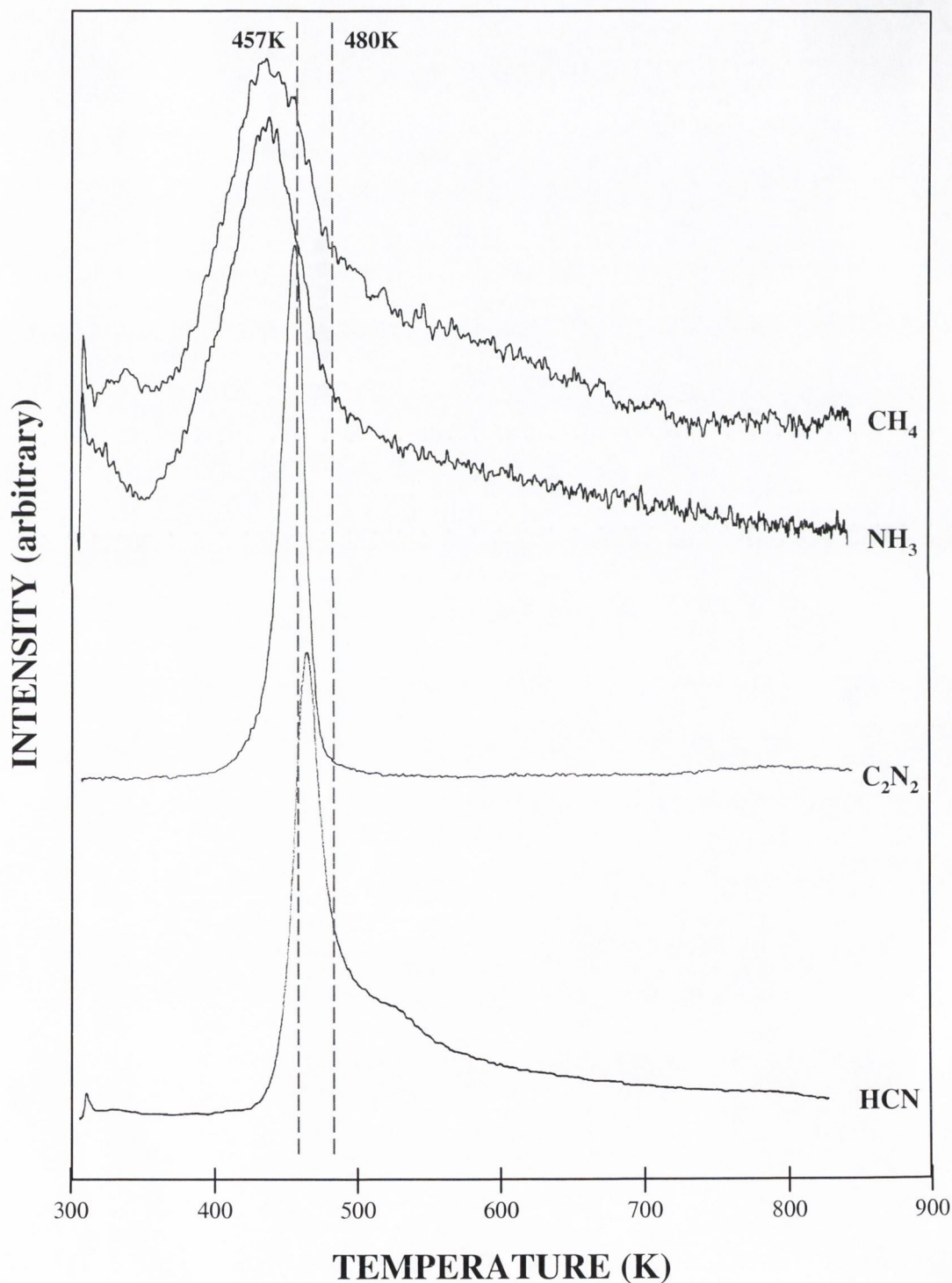
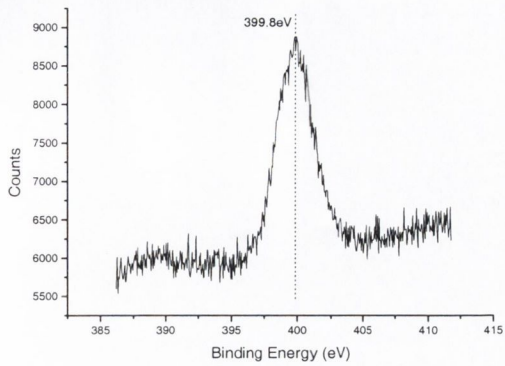
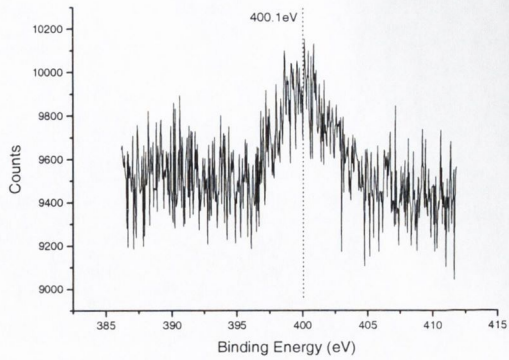


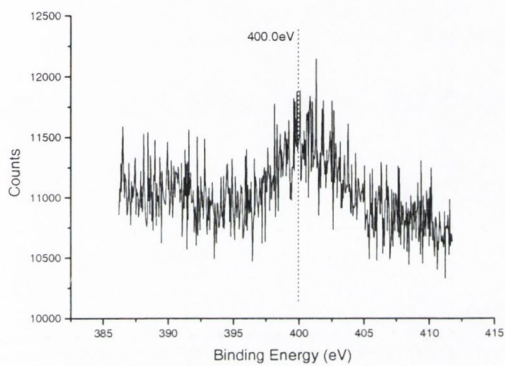
Fig 5.15 Diagram of annealing temperatures employed during the XPS experiments following EDA adsorption on Pt(331).



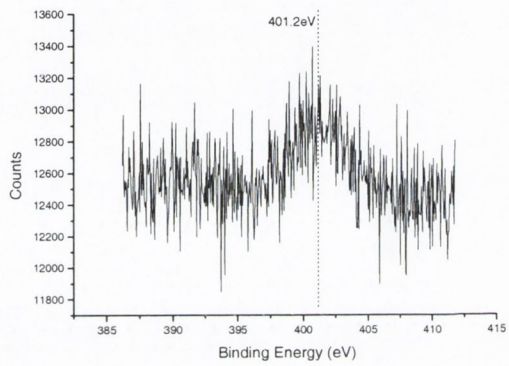
(a)



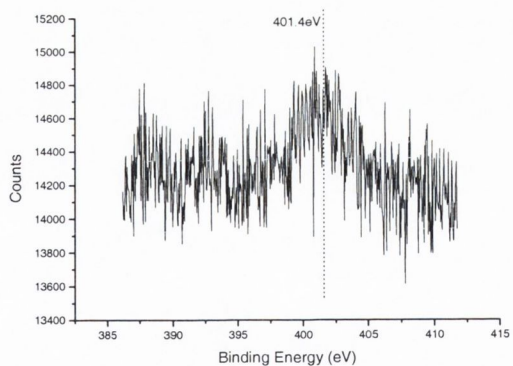
(b)



(c)



(d)



(e)

Fig. 5.16 N1s XPS following EDA adsorption on Pt(331):

(a) 110K; (b) 200K; (c) 273K; (d) 457K; (e) 480K.

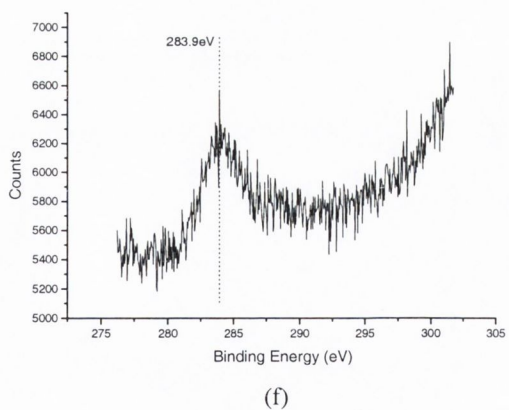
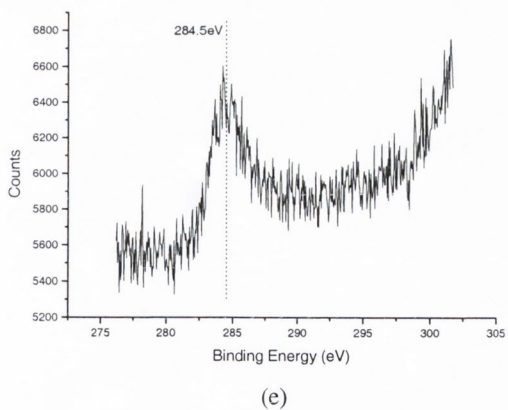
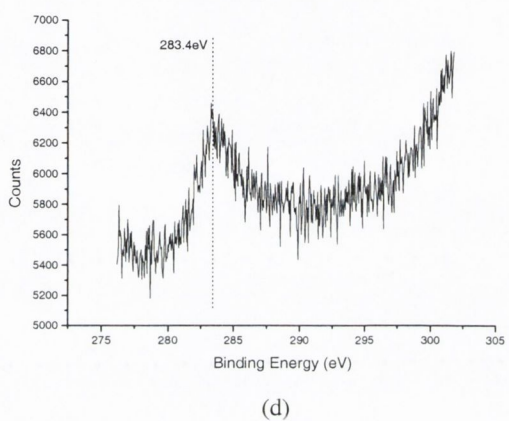
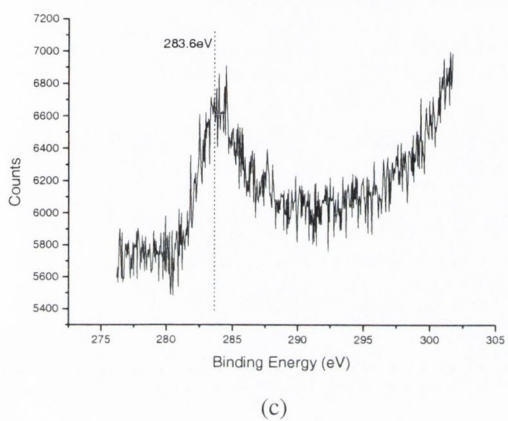
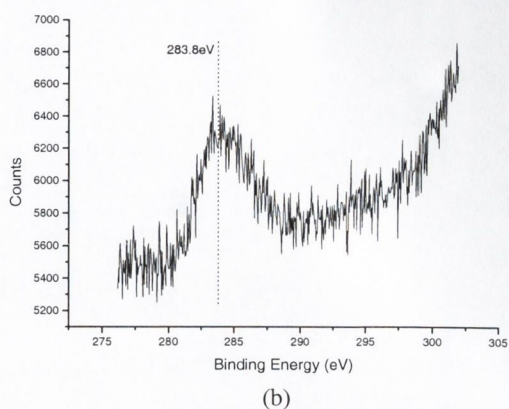
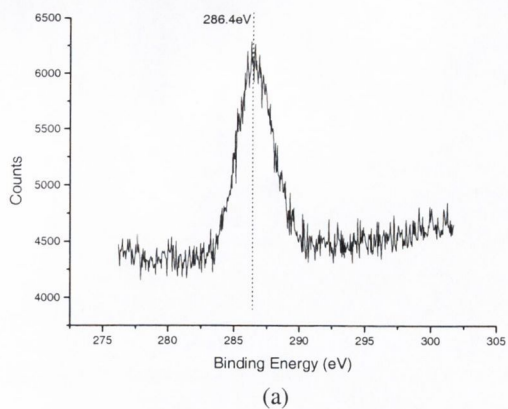


Fig. 5.17 C1s XPS following EDA adsorption on Pt(331):

(a) 114K; (b) 200K; (c) 273K; (d) 457K, (e) 470K; (f) >1000K.

5.2 DISCUSSION

5.2.1 C_2N_2 desorption

The C_2N_2 thermal desorption spectra following ethylenediamine adsorption on Pt(111) reveals three desorption features – a sharp, dominant peak at 425K, and a high temperature shoulder consisting of two features. The dominant peak has previously been designated γ in order to distinguish it from the α and β desorption states that correspond to molecular and recombinative desorption respectively of cyanogen [40, 91, 92]. This peak was first detected following H_2/C_2N_2 co-adsorption experiments [40] and assigned to dehydrogenation of hydrogenated C_2N_2 species.

A high temperature shoulder on Pt(111) has been a feature in previous $C_2N_2/EDA/Pt(111)$ desorption studies [40-42]. A striking difference between these desorption spectra on Pt(111) and the $C_2N_2/EDA/Pt(331)$ spectra is the absence of any shoulder in the C_2N_2 spectra of Pt(331). Two possibilities for the source of this shoulder are defect sites or binding sites present on the (111) surface but absent on the (331) surface. Examination of the desorption spectra following methylamine adsorption on Pt(111) and Pt(331) indicated that the Pt(111) crystal used in this work did indeed have defect sites (see section 3.3.1). These defect sites had the effect of producing desorption features similar to those produced by the stepped Pt(331) surface. Comparing the desorption spectra of C_2N_2 from both crystals, it can be seen that the first of the two features in the high temperature shoulder corresponds in temperature to C_2N_2 desorption from Pt(331) and to the main H_2 desorption peak from Pt(331). It is quite probable therefore that this feature represents C_2N_2 desorption from step-like defect sites. As will be seen in sections 5.2.2 and 5.2.3, minor features in the desorption spectra of H_2 and HCN on Pt(111) also correlate to the main desorption features for these products on Pt(331).

The second feature in the high temperature shoulder of C_2N_2 spectra on Pt(111) does not have a corresponding feature on Pt(331). It is not clear whether this peak is the product of defect sites or alternative binding sites.

Turning specifically to C_2N_2 desorption from Pt(331), the absence of either low or high temperature shoulders that can be assigned to desorption from the (111) terraces suggests that EDA adsorption/decomposition takes place entirely at step sites on Pt(331).

5.2.2 H_2 desorption

The hydrogen desorption spectra obtained in this work show a number of features not previously detected [40-42]. The main desorption peak matches that obtained by Kingsley *et al.* [40], which they attributed to dehydrogenation of the amine groups of EDA, following experiments on ethylene- d_4 -diamine ($NH_2-CD_2-CD_2-NH_2$). These experiments also revealed that the high temperature shoulder on the H_2 peak corresponds to HD and D_2 desorption, HD desorption commencing at a lower temperature than D_2 . The high temperature shoulder previously obtained [40-42] corresponds to the second and third features of the H_2 /EDA/Pt(111) spectra in this work. Therefore, these features can be attributed to dehydrogenation of the methylene groups of the EDA molecule, the second feature predominantly $H_{amine} + H_{methylene}$ recombination, the third feature $H_{methylene} + H_{methylene}$ recombination. These two features correspond in temperature to the main C_2N_2 desorption peak. C_2N_2 desorption is a decomposition process in which the rate limiting step is dehydrogenation of the methylene groups. Lloyd and Hemminger [41] noted, however, that the tail of the H_2 desorption peak in the ethylene- d_4 -diamine experiment extends into the temperature range of the D_2 desorption phase. This coupled with HREELS studies carried out by the same group on the intermediate of H_2/C_2N_2 coadsorption led to the conclusion that the amine groups do not undergo complete dehydrogenation to form a dinitrene intermediate species ($N-CH_2CH_2-N$) as originally suggested by Kingsley *et al.* but rather that the intermediate formed is a di-imine ($NH=CH-CH=NH$) (see figure 5.18).

The fourth and fifth features of the H_2 desorption process correspond to the second and third desorption features of C_2N_2 . Examination of the spectra for EDA decomposition on Pt(331) reveals that the fourth feature on H_2 /EDA/Pt(111) coincides in temperature to the main H_2 and C_2N_2 desorption peaks from Pt(331). As has been suggested in section 5.2.1, this desorption event is a product of step-like defects on the Pt(111) surface. Whether the

fifth feature is a product of defect sites or alternative binding sites on Pt(111) cannot be ascertained from the results in this work. There are no corresponding features on the Pt(331) spectra.

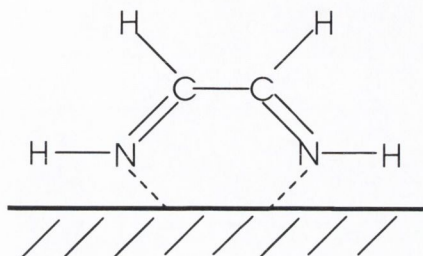


Fig. 5.18 Ethylenedi-imine intermediate proposed by Lloyd and Hemminger [41].

On Pt(331), the mechanism of EDA decomposition appears to be similar to that on Pt(111). The low temperature peak of H_2 can be associated with dehydrogenation of the amine groups [40], whilst the high temperature peak represents a combination of amine and methylene group dehydrogenation.

5.2.3 HCN desorption

HCN desorption following EDA adsorption on Pt(331) produces a sharp peak at 467K with a high temperature shoulder at about 520K. On Pt(111), an initial peak appears at 470K followed by the main peak at 520K and a high temperature tail. It is clear that the first peak on Pt(111) coincides in temperature with the main peak on Pt(331), and the main peak on Pt(111) coincides with the high temperature shoulder on Pt(331). Since the Pt(111) crystal used in this work has already been established to contain step-like defect sites, the low temperature peak on the (111) spectra of HCN can be identified as desorption from these sites. The high temperature shoulder to the HCN peak on Pt(331) seems to represent a desorption process similar to that from Pt(111). It is possible that this feature is a product of

decomposition on the (111) terrace sites. HCN desorption from Pt(111) occurs at elevated temperatures due to the formation of some hydrogen-bonded intermediate [32, 93]. The main peak of the HCN/EDA/Pt(111) spectra exhibits this elevated desorption temperature. However, as already mentioned in section 5.2.1, no features are present in the C₂N₂ spectra on Pt(331) which correlate to desorption from Pt(111). It would seem likely, therefore, that the HCN shoulder is not due to terrace adsorption/decomposition, but may represent a situation in which some of the HCN_{ads.} species from step site decomposition form the intermediate complex suggested for Pt(111).

H_{ads.} + CN_{ads.} recombinative desorption on Pt(331) has been found [32, Chapter 3] to occur between 430K and 440K (see Table 3.2). The desorption temperature for HCN following EDA adsorption on Pt(331) is significantly higher, at 467K. Clearly, this is not a H_{ads.} + CN_{ads.} process, but rather a decomposition process in which the rate limiting step is likely to be C-C bond cleavage.

5.2.4 XPS experiments

The transition from multilayer to monolayer EDA resulted in a shift to higher binding energy for N1s at 273K, giving a value 400.3eV. A single peak at this energy is consistent with molecular adsorption of EDA through the lone pair electrons on both nitrogens [42]. Heating to 440K results in a shift to 399.7eV. This corresponds to the desorption of the main C₂N₂ peak. A similar shift was noted by Lindquist et al. [42] for this temperature. Heating to 495K removes the low temperature HCN peak and C₂N₂ shoulder that are both associated with defect sites. The resulting spectrum indicates the presence of two peaks, one at 398.4eV and one at 400.4eV. The lower binding energy peak can be associated with HCN [42]. The high binding energy peak remains upon heating beyond HCN desorption, and is associated with some nitrogen surface species that persists on the surface to temperatures in excess of 800K. Heating to 699K results in the loss of the 398.4eV feature, with just the peak centred at 400.4eV remaining. At this stage HCN has desorbed. This result is in contrast to the spectra obtained by Lindquist *et al.* upon heating to temperatures of 440K and above. They observed a peak at 397.0eV which is associated with cyanogen β states. Their C₂N₂ thermal

desorption spectrum indicates a β C_2N_2 desorption event. However, no such peak was observed in the TDS spectra in this work, and it is assumed, therefore, that no CN_{ads} species are present on the surface. The absence of the 397eV peak provides further evidence of this. The spectrum following heating above 1000K is unreliable, since some desorption from the probe occurred, which may have resulted in gas re-adsorption onto the surface.

Analysis of the C1s spectra is complicated by the possibility of background CO adsorbing at low temperatures.

The XPS data for EDA on Pt(331) follow the same trend as Pt(111), indicating the similarity in the decomposition process. Again, no peak at 397eV in the N1s spectra was observed.

5.3 CONCLUSIONS

Ethylenediamine decomposition on Pt(111) is essentially a dehydrogenation process, in which the EDA molecule is systematically stripped of hydrogen to produce H_2 and C_2N_2 , with C-C bond scission to produce HCN providing a competitive process. The decomposition process is represented schematically in figure 5.19.

In addition to this pathway is one in which C-N bonds are broken to form NH_3 and carbon residue. No such process has been observed on Pt(111), suggesting this reaction occurs at step sites, and is in competition with CN_{ads} formation.

XPS results do not indicate the presence of the β C_2N_2 desorption states.

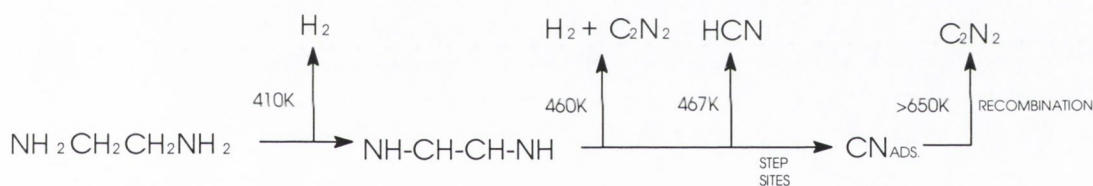


Fig. 5.19 Schematic of principal reaction pathway of ethylenediamine on Pt(331).

EDA decomposes on Pt(331) in a manner similar to that on Pt(111). However, adsorption and decomposition occurs at step sites, with only a minor contribution from the (111) terraces.

CHAPTER SIX

CONCLUSIONS AND FURTHER WORK

CHAPTER 6 CONCLUSIONS AND FURTHER WORK

6.1 METHYLAMINE ON Pt(111) AND Pt(331)

The results of this work on methylamine suggest that HCN formation is a result of recombination of H_{ads} and CN_{ads} on Pt(331), whilst on Pt(111) HCN formation is the result of a decomposition process. Valuable information may be gained by undertaking D_2/MA co-adsorption experiments on Pt(331). Detection of DCN as a desorption product in a similar temperature range should confirm recombination as the source of HCN on this crystal. D_2/MA co-adsorption experiments on Pt(111) should also be of value as a means of confirming whether recombination is the source of any of the HCN peaks, in particular the peak at ~447K obtained for the particular crystal used in this work.

6.2 DIMETHYLAMINE AND TRIMETHYLAMINE ON Pt(111) AND Pt(331)

Trimethylamine and dimethylamine share a similar decomposition process following room temperature adsorption on Pt(111) and Pt(331), in which C-N bonds are broken to form CH_4 , and C-H bonds are broken to form HCN and H_2 . Initial bonding to the surface appears to be via the nitrogen lone pair. The symmetrical TMA and DMA molecules may be well suited to ARUPS analysis, which may provide confirmation of this initial binding state mechanism, as well as providing information about changes in the bonding environment as these molecules thermally decompose.

The results obtained by Erley *et al.* [49] suggest that a different decomposition mechanism may occur following adsorption of TMA at low temperatures. Repetition of these thermal desorption experiments should confirm their results, whilst thermal desorption studies of DMA adsorbed at low temperatures should demonstrate whether or not DMA undergoes a similar change in its decomposition mechanism.

Quantitative LEED studies of molecularly bound TMA and DMA may yield information on the absolute position of these molecules relative to the surface unit mesh for both Pt(111) and Pt(331).

6.3 ETHYLENEDIAMINE ON Pt(111) AND Pt(331)

Ethylenediamine decomposes in a similar manner on both Pt(111) and Pt(331). The absence of high temperature C_2N_2 suggests that no CN_{ads} species are formed, and by extension, that HCN is a decomposition rather than a recombination product. Measurement at 28 amu in search of DCN as a desorption product following D_2 /EDA co-adsorption should provide further evidence that this is the case.

REFERENCES:

- [1] P. Auger, *Surface Sci.* **48** (1975) 1
- [2] L.A. Harris, *J. Appl. Phys.* **39** (1968) 1419
- [3] C.C. Chang, *Surface Sci.* **25** (1971) 53
- [4] G. Ertl and J. Küppers, “Low Energy Electrons and Surface Chemistry”, VHC (1985)
- [5] M.W. Roberts, in: *Specialist Periodical Reports – Surface and Defect Properties of Solids*, vol. 1, eds. M.W. Roberts and J.M. Thomas (The Chemical Society, 1971) 177
- [6] P.J. Estrup and E.G. McCrae, *Surface Sci.* **25** (1971) 1
- [7] J.B. Pendry, “Low Energy Electron Diffraction”, (Academic Press, 1974)
- [8] D.G. Castner and G.A. Somorjai, *Chem. Rev.* **79** (1979) 233
- [9] M.A. Van Hove and S.Y. Tong, “Surface Crystallography by LEED”, in: *Springer Series in Chemical Physics*, vol. 2, ed. R. Gomer, (Springer - Verlag, 1979)
- [10] F. Feuerbacher, B. Fitton and R.F. Willis, *Electron Spectroscopy and the Electronic Properties of Surfaces* (Wiley, 1978)
- [11] C.R. Brundle and A.D. Baker, *Electron Spectroscopy: Theory, Techniques and Applications* (Academic Press, 1977)
- [12] H. Ibach, H. Hopster and B.A. Sexton, *Appl. Surface Sci.* **1** (1977) 1
- [13] A.M. Bradshaw, *Appl. Surface Sci.* **11-12** (1982) 712
- [14] J. Pritchard, in: *Specialist Periodical Reports – Surface and Defect Properties of Solids*, vol. 7, eds. M.W. Roberts and J.M. Thomas (The Chemical Society, 1978)
- [15] A.M. Bradshaw, *Surface Sci.* **158** (1985) 624

- [16] D.A. King and M.G. Wells, *Surface Sci.* **29** (1972) 454
- [17] G.A. Somorjai, *Acc. Chem. Res.* **9** (1976) 248
- [18] D.P. Woodruff and T.A. Delchar, "Modern Techniques of Surface Science"
(Cambridge University Press (U.K.) 1986)
- [19] D.P. Woodruff and A.M. Bradshaw, *Rep. Prog. Phys.* **57** (1994) 1029
- [20] D.P. Woodruff, *Prog. Surface Sci.* **57** (1998) 1
- [21] P.A. Redhead, *Vacuum* **12** (1962) 203
- [22] D.A. King, *Surface Sci.* **47** (1975) 384
- [23] J.L. Falconer and R.J. Madix, *Surface Sci.* **48** (1975) 393
- [24] C.L. Thomas, "Catalytic Processes and Proven Catalysts",
(Academic Press, 1970)
- [25] J.H. Sinfelt, *Prog. Solid State Chem.* **10** (1975) 55
- [26] F.G Ciapetta and D.N. Wallace, *Catal. Rev.* **5** (1972) 67
- [27] C.C. Chang and L.L. Hegedus, *J. Catal.* **57** (1976) 361
- [28] M. Shelef, *Catal. Rev. Sci. Eng.* **11** (1975) 1
- [29] Y. Cong, V. van Spaendonk and R.I. Masel, *Surface Sci.* **385** (1997) 246
- [30] Y. Seimiya, G. Cao, Y. Ohno, T. Yamanaka, T. Matsushima and K. Jacobi,
Surface Sci. **415** (1998) L988
- [31] M. Sano, Y. Seimiya, Y. Ohno, T. Matsushima, S. Tanaka and M. Kamada,
Surface Sci. **421** (1999) 386
- [32] D. Chrysostomou, PhD thesis, Trinity College, Dublin (1997)
- [33] K. Wandelt, *Surface Sci.* **251/252** (1991) 387
- [34] P. Hollins, *Surface Sci. Rep.* **16** (1992) 51

- [35] K. Wandelt, in: *Physics and Chemistry of Solid Surfaces VIII*, (Springer, 1990)
- [36] H. Wagner, in: *Springer Tracts in Mod. Phys.*, vol. 85 (Springer – Verlag, 1979)
- [37] S.H. Payne and H.J. Kreuzer, *Surface Sci.* **399** (1998) 135
- [38] G.A. Somorjai, “*Introduction to Surface Chemistry and Catalysis*”, (John Wiley and Sons, Inc. 1994)
- [39] G.C. Bond, “*Catalysis by Metals*”, (Academic Press, 1962)
- [40] J.R. Kingsley, D. Dahlgren and J.C. Hemminger, *Surface Sci.* **139** (1984) 417
- [41] K.G. Lloyd and J.C. Hemminger, *Surface Sci.* **179** (1987) L6
- [42] J.M. Lindquist, J.P. Ziegler and J.C. Hemminger, *Surface Sci.* **210** (1989) 27
- [43] M.E. Bridge and J. Somers, *Vacuum* **38** (1988) 317
- [44] S.Y. Hwang, E.G. Seebauer and L.D. Schmidt, *Surface Sci.* **188** (1987) 219
- [45] W. Erley and J.C. Hemminger, *Surface Sci.* **316** (1994) L1025
- [46] D. Jentz, M. Trenary, X.D. Peng and P. Stair, *Surface Sci.* **341** (1995) 282
- [47] K.A. Pearlstine and C.M. Friend, *J. Am. Chem. Soc.* **108** (1986) 5842
- [48] T.S. Nunney, J.J. Birtill and R. Raval, *Surface Sci.* **427/428** (1999) 282
- [49] W. Erley, R. Xu and J.C. Hemminger, *Surface Sci.* **389** (1997) 272
- [50] B. W. Walker and P.C. Stair, *Surface Sci.* **91** (1980) L40
- [51] B. W. Walker and P.C. Stair, *Surface Sci.* **103** (1981) 315
- [52] P.M. Marcus and F. Jona, *Appl. Surface Sci.* **11/12** (1982) 20
- [53] E.A. Wood, *J. Appl. Phys.* **35** (1964) 1306
- [54] H.E. Bishop and J.C. Riviere, *J. Appl. Phys.* **40** (1969) 1740

- [55] E.H. Burhop, *J. Phys. Radium* **16** (1955) 625
- [56] J.M. Wilson, *Phil. Mag.* **27** (1973) 1467
- [57] P.W. Palmberg, *Surface Sci.* **25** (1971) 598
- [58] K.J. Rawlings, S.D. Foulis, G.G. Price and B.J. Hopkins, *Surface Sci.* **118** (1982) 47
- [59] R.K. Wild, *Vacuum TAIP* **31** (1981) 183
- [60] J. Stohr in: *Emission and Scattering Techniques*, ed. P. Day, (Nato Advanced Institutes, Series C, 1981) p.213
- [61] J.K. Roberts, "Some Problems in Adsorption", (Cambridge University Press, 1939)
- [62] C.G. Goymour and D.A. King, *J.C.S. Faraday I* **69** (1973) 736, 749
- [63] J. Somers, PhD thesis, Trinity College, Dublin (1986)
- [64] P.W. Davies and R.M. Lambert, *Surface Sci.* **110** (1981) 227
- [65] R.W. McCabe and L.D. Schmidt, *Surface Sci.* **65** (1977) 189
- [66] K. Christman, G. Ertl and T. Pignet, *Surface Sci.* **54** (1976) 365
- [67] F.P. Netzer, *Surface Sci.* **61** (1976) 343
- [68] J.R. Kingsley and J.C. Hemminger, *Langmuir* **2** (1986) 460
- [69] W. Hoffman, E. Bertel and F.P. Netzer, *Journal of Catalysis* **60** (1979) 316
- [70] M.G. Ramsey, G Rosina, F.P. Netzer, H.B. Saalfeld and D.R. Lloyd, *Surface Sci.* **217** (1989) 140
- [71] M.E. Kordesch, W. Stenzel and H. Conrad, *J. Spectr. Rel. Phenom.* **39** (1986) 89
- [72] K. Besenthal, G. Chiarello, M.E. Kordesch and H. Conrad, *Surface Sci.* **178** (1986) 667

- [73] F. Solymosi and J. Kiss, *Surface Sci.* **108** (1981) 368
- [74] F.P. Netzer, *Surface Sci.* **52** (1975) 709
- [75] S.Y. Hwang, E.G. Seebauer and L.D. Schmidt, *Surface Sci.* **188** (1987) 219
- [76] C.R. Arumainayagam, M.C. McMaster, G.R. Schoofs and R.J Madix, *Surface Sci.* **222** (1989) 213
- [77] S.K. Jo, X.-Y. Zhou, D. Lennon and J.M. White, *Surface Sci.* **241** (1991) 231
- [78] M.A. Henderson, G.E Mitchell and J.M. White, *Surface Sci.* **248** (1991) 279
- [79] G. Ertl, M. Neumann, and K.M. Streit, *Surface Sci.* **64** (1977) 393
- [80] M.A. Henderson and J.T. Yates, Jr., *Surface Sci.* **268** (1992) 189
- [81] F.P. Netzer and R.A. Willie, *Surface Sci.* **74** (1978) 547
- [82] H. Hopster and H. Ibach, *Surface Sci.* **77** (1978) 109
- [83] D.M. Collins and W.E. Spicer, *Surface Sci.* **69** (1977) 85
- [84] B.E. Hayden, K. Kretzschmar, A.M. Bradshaw and R.G. Greenler, *Surface Sci.* **149** (1985) 394
- [85] D.R. Lambert and R.G. Tobin, *Surface Sci.* **232** (1990) 149
- [86] H.R. Siddiqui, X. Guo, I. Chorkendorff and J.T. Yates, Jr., *Surface Sci.* **191** (1987) L813
- [87] M. Trenary, S.L. Tang, R.J. Simonson and F.R. McFeely, *J. Phys. Chem.* **80** (1984) 477
- [88] M.R. McClellan, J.L. Gland and F.R. Feely, *Surface Sci.* **112** (1981) 63
- [89] J. Xu and J.T. Yates, Jr., *Surface Sci.* **327** (1995) 193
- [90] J.L. Gland and B.A. Sexton, *Surface Sci.* **94** (1980) 355
- [91] M.E. Bridge, R.A. Marbrow and R.M. Lambert, *Surface Sci.* **57** (1976) 415

- [92] M.E. Bridge and R.M. Lambert, *Journal of Catalysis* **46** (1977) 143
- [93] D. Jentz, P. Mills, H. Celio, M. Belyansky and M. Trenary, *J. Chem. Phys.* **105** (No. 8) (1996) 3250
- [94] P.L. Hagans, X. Guo, I. Chorkendorff, A. Winkler, H. Siddiqui and J.T. Yates, Jr., *Surface Sci.* **203** (1988) 1
- [95] C.L. Levoguer and R.M. Nix, *J. Chem. Soc., Faraday Trans.* **92** (No. 23) (1996) 4799
- [96] M.E. Bridge and R.M. Lambert, *Surface Sci.* **63** (1977) 143
- [97] C.L. Levoguer and R.M. Nix, *Surface Sci.* **365** (1996) 672
- [98] J. Somers and M.E. Bridge, *Surface Sci.* **159** (1985) L439
- [99] X. Guo, A. Hoffman and J.T. Yates Jr., *J. Phys. Chem.* **93** (1989) 4253
- [100] D. Jentz, H. Celio, P. Mills and M. Trenary, *Surface Sci.* **341** (1995) 1
- [101] M.E. Kordesch, W. Stenzel, H. Conrad, *Surface Sci.* **186** (1987) 601
- [102] E. Timothy, work in progress
- [103] P.A. Thomas and R.I. Masel, *J. Vac. Sci. Technol. A* **5** (No. 4) (1987) 1106
- [104] T. Nakayama, K. Inamura, Y. Inoue, S. Ikeda and K. Kishi, *Surface Sci.* **179** (1987) 47
- [105] B.A. Sexton and A.E. Hughes, *Surface Sci.* **140** (1984) 227
- [106] D. Chrysostomou, M.E. Bridge, T. McCabe, D.R. Lloyd, E. McCash and M.A. Chesters, to be published

BIBLIOGRAPHY:

- G.A. Ertl and J. Küppers, “Low Energy Electrons and Surface Chemistry” VHC (1985)
- M. Prutton, “Surface Physics” Oxford University Press, 2nd ed. (1983)
- D.P. Woodruff and T.A. Delchar, “Modern Techniques of Surface Science” Cambridge University Press (U.K.) (1986)
- G.A. Somorjai, “Introduction to Surface Chemistry and Catalysis” John Wiley and Sons, Inc. (1994)
- J.C. Vickerman, “Surface Analysis – The Principal Techniques” John Wiley and Sons, Inc. (1997)
- J.F. Moulder, W.F. Stickle, P.E. Sobol and K.D. Bomben, “Handbook of X-ray Photoelectron Spectroscopy”, Physical Electronics, Inc. (1992)
- K. Kimura, S. Katsumata, Y. Achiba, T. Yamazaki and S. Iwata, “Handbook of HeI Photoelectron Spectra of Fundamental Organic Molecules” Japan Scientific Societies Press (1981)
- J.F. Nicholas, “An Atlas of Models of Crystal Surfaces” Gordon and Breach, Science Publishers, Inc. (1965)